

Variability of the recent accumulation rate in coastal Dronning Maud Land, Antarctica

Dissertation zur Erlangung des Grades Dr. rer. nat.
vorgelegt dem Fachbereich Geowissenschaften
der Universität Bremen

von

HELGARD ANSCHÜTZ

Alfred-Wegener-Institut für Polar- und Meeresforschung
Bremerhaven

12. Dezember 2006

Name: Helgard Anshütz

Datum: 12. 12. 2006

Anschrift: Sommerstr. 29
28215 Bremen

ERKLÄRUNG

Hiermit versichere ich, daß ich

1. die Arbeit ohne unerlaubte fremde Hilfe angefertigt habe,
2. keine anderen als die von mir angegebenen Quellen und Hilfsmittel benutzt habe und
3. die den benutzten Werken wörtlich oder inhaltlich entnommenen Stellen als solche kenntlich gemacht habe.

Bremen, den

Helgard Anshütz

NE DUBITA, CUM PETES MAGNA, IMPENDERE PARVA.

M. Porcius Cato maior

Contents

Kurzfassung	iii
Abstract	v
1 Introduction	1
1.1 Antarctica and its mass balance	1
1.2 Mass balance and surface-mass balance	2
1.2.1 Influences on surface-mass balance	3
1.2.2 Overview of measurement methods	4
1.3 Large-scale estimates of (surface-)mass balance	5
1.3.1 Recent estimates of Antarctic surface-mass balance	6
1.3.2 Uncertainties and implications	7
1.4 Satellite-based approaches	8
1.4.1 Determination of ice-mass changes	8
1.4.2 Results and uncertainties	9
1.4.3 The VISA project and this study	11
2 Area of investigation	13
3 Methods	17
3.1 GPR and GPS	17
3.1.1 Application of GPR in glaciology	18
3.1.2 GPR: Data acquisition and processing	19
3.1.3 GPS	21
3.1.4 Combining GPR and GPS data	22
3.2 Firn cores and snow pits	23
3.3 Combination of GPR and firn-core data	25
3.3.1 Conversion of radar layers to depth and cumulative mass	25
3.3.2 Origin of reflecting layers in radargrams	27
3.3.3 Accumulation rates along GPR profiles	28

4	Scope of papers	31
5	PAPER I	33
6	PAPER II	45
7	PAPER III	59
8	Summary and outlook	71
	Acknowledgements	75
	Bibliography	77

Kurzfassung

Im Hinblick auf mögliche zukünftige Änderungen des Meeresspiegels sind Untersuchungen der Oberflächenmassenbilanz der polaren Eisschilde zu einem zentralen Punkt glaziologischer Forschung geworden. Dennoch ist die Massenbilanz des antarktischen Eisschildes nicht hinreichend genau bekannt, wodurch sich große Unsicherheiten in der Abschätzung des Meeresspiegelanstiegs im 21. Jahrhundert ergeben. Die vorliegende Arbeit leistet einen wichtigen Beitrag durch die Analyse neuer Daten von Schneeakkumulation und stellt neue Erkenntnisse über lokale Effekte vor, die die Akkumulationsverteilung beeinflussen. Ziel der Arbeit ist es, ein umfassendes Bild der räumlichen Verteilung der Akkumulation auf der Skala von einigen zehn Kilometern zu erhalten, sowie von zeitlichen Variationen sowohl auf jährlicher als auch auf dekadischer Skala. Zu diesem Zwecke wurde Profile mit einem hochfrequenten Bodenradar gemessen und flache Firnkerne erbohrt. Das Untersuchungsgebiet konzentriert sich auf die gegründeten Küstengebiete des Dronning Maud Landes in der Ostantarktis, die zugleich im Mittelpunkt neuer Satellitenmissionen stehen. Gerade die Küstengebiete reagieren empfindlich auf globale Klimaveränderungen, jedoch ist ihre Akkumulationsrate auf lokaler und regionaler Skala bislang nicht sehr gut durch globale Zirkulationsmodelle oder regionale Klimamodelle repräsentiert. Daher sind Feldmessungen der Akkumulation von entscheidender Bedeutung.

Die Akkumulationsraten auf dem Potsdamgletscher im küstennahen Bereich des zentralen Dronning Maud Landes weisen ein undulierendes Muster und eine hohe räumliche Variabilität auf: Die einfache Standardabweichung beträgt nahezu 50 % des Mittelwertes von $140 \text{ kg m}^{-2} \text{ a}^{-1}$ für den Zeitraum von 1970–2004. Die zeitlichen Variationen auf der Zeitskala von Dekaden betragen lediglich einige Prozent, abgeleitet aus den gebietsweiten Mittelwerten der Akkumulationsraten. Jährliche Schwankungen der Akkumulationsrate fallen deutlich höher aus, da die Firnkernanalysen Standardabweichungen von 30–40 % des Mittelwertes der Akkumulation für die jeweiligen Kerne aufweisen. Eine statistische Analyse der räumlichen Akkumulationsverteilung macht die hohe Periodizität des Akkumulationsmusters mit Wellenlängen von 5 km und Amplituden von 10 m deutlich. Dies lässt den Schluss zu, daß die hier beobachtete Akkumulationsverteilung derjenigen gleicht, wie sie von den Megadünen auf dem ostantarktischen Plateau bekannt ist, auch wenn die Dünen auf dem Potsdamgletscher weder die räumliche Ausdehnung noch die extreme Morphologie der Megadünen aufweisen. Analog zu

den Megadünen lässt sich die Entstehung der auf dem Potsdamgletscher beobachteten Strukturen sehr wahrscheinlich durch ein spezielles Rückkopplungssystem zwischen Atmosphäre und Kryosphäre erklären. Das Auftreten von dünenartigen Undulationen wie die in dieser Arbeit diskutierten ist von Bedeutung für Firnkernbohrungen in küstennahen Gebieten sowie für die Fernerkundung von Eismassenänderungen.

Das zweite Untersuchungsgebiet im westlichen Dronning Maud Land, in der Nähe der Kottasberge am Fusse des polaren Plateaus, weist eine geringere räumliche Variabilität der Akkumulationsrate auf. Hier beträgt die Standardabweichung lediglich 5–10 % des Mittelwertes von $190 \text{ kg m}^{-2} \text{ a}^{-1}$ (1980–2005). Allerdings sind in diesem Gebiet die zeitlichen Variationen höher, sie zeigen Werte von 16 % auf dekadischer Skala, abgeleitet aus den Mittelwerten der Akkumulation im Untersuchungsgebiet. Die jährlichen Schwankungen betragen wie auf dem Potsdamgletscher ca. 30 %, wie sich aus der Firnkernanalyse ergibt. Der Vergleich von räumlichen und zeitlichen Variationen entlang eines Radarprofils auf einer Gletscherfließlinie macht eine schwache Korrelation deutlich, wie sie ebenfalls auf dem Potsdamgletscher zu beobachten ist. Dieses Ergebnis deutet an, daß die zeitlichen Differenzen der Akkumulationsrate auf der Skala von einigen zehn Jahren dort am grössten sind, wo auch die räumlichen Differenzen auf der Skala von einigen 100 Metern bis zu wenigen Kilometern ein Maximum aufweisen.

Die hier vorgestellten Ergebnisse sind wichtig für die Validierung von Eismassenänderungen, die aus Satellitendaten abgeschätzt werden und die daher über mehrere 100 Kilometer gemittelt sind und somit keine kleinräumlichen Einflüsse erfassen. Deutliche räumliche Variationen in der Akkumulationsrate wie diejenigen auf dem Potsdamgletscher beeinflussen sehr wahrscheinlich das Schweresignal z.B. der Satellitenmission GRACE. Dies zeigt die Notwendigkeit der Validierung von Satellitendaten mit bodengestützten Messungen, wie sie in dieser Arbeit diskutiert werden.

Abstract

In light of possible future sea-level change, investigation of surface-mass balance of the polar ice sheets has become a major concern of glaciological research. Yet Antarctica's total surface-mass balance is still not accurately determined, making up for the largest uncertainties of predictions regarding sea-level rise in the 21st century. This study contributes new data sets of recent snow-accumulation rates and provides insight in local features affecting the small-scale distribution of accumulation. The aim of the work is to establish a detailed picture of spatial accumulation variability on the scale of some tens of kilometers and of temporal behaviour on interannual to decadal scales. To this end, high-frequency ground-penetrating radar profiling and analyses of shallow firn cores have been utilized. The area of investigation focuses on coastal regions of Dronning Maud Land, East Antarctica, which are likewise in the focus of new satellite missions. The coastal regions are susceptible to global climate change but the local to regional-scale variability of accumulation is not well addressed by general circulation models or regional climate models, thus making it necessary to obtain and analyze field data.

The accumulation rates on Potsdam Glacier in the coastal part of central Dronning Maud Land have been found to show an undulating pattern, exhibiting a one-fold standard deviation of nearly 50 % around a mean value of some $140 \text{ kg m}^{-2} \text{ a}^{-1}$ for the time period 1970–2004. Temporal variations on decadal scales obtained from the area-wide mean values are only a few per cent, but inter-annual variations derived from dated firn cores are high, showing values between 30–40 % of the core means. Statistical analysis of spatial accumulation series reveals a high periodicity of these undulations with a wavelength of 5 km and amplitudes of 10 m, leading to the conclusion that the features are similar to the megadunes known from the polar plateau, although they lack the spatial extent and the extreme snow morphology of the latter. Thus, the features are likely explicable by a feedback system between atmosphere and cryosphere. The presence of dune-like features as those revealed by this study has implications for firn-core drilling at these coastal sites and for remote sensing of ice-mass changes.

Another test site in western Dronning Maud Land, near Kottasberge at the foot of the polar plateau, shows less spatial variability, only 5–10 % around a mean value of $190 \text{ kg m}^{-2} \text{ a}^{-1}$ (1980–2005), yet the temporal variations are higher with values of 16 % on decadal scales and likewise about 30 % on interannual scales obtained from firn cores. Comparing spatial and temporal vari-

ations on an along-flow radar profile reveals a weak correlation, which is likewise found for the corresponding radar profile on Potsdam Glacier. This observation indicates that the largest temporal differences on decadal scales tend to occur where spatial variability on the scales of some hundreds of meters to several kilometers is highest.

The results presented here are valuable for the validation of satellite-derived ice-mass changes, which are usually averaged over several hundreds of kilometers and do not capture small-scale variability. Spatial variations in accumulation rates as those reported from Potsdam Glacier are likely sensed by gravity missions like GRACE, emphasizing the necessity of ground-truthing, as provided by this study.

Chapter 1

Introduction

This chapter comprises a short general description of Antarctica, focusing on the continent's mass balance. Relevant terms are introduced and methods for their measurement are given, followed by recent results and implications.

1.1 Antarctica and its mass balance

Albeit remote, Antarctica is capable to significantly influence the Earth's climate and is itself very sensitive to global-climate change. It is not only the coldest, but also the driest and the highest continent, with precipitation of some 50 mm a^{-1} in the vast interior [Monaghan *et al.*, 2006a] and elevations up to 4000 m above sea level (a.s.l.). The thickness of the ice cover in the interior is about 2500 m, reaching a maximum of 4800 m [Lythe *et al.*, 2001]. Antarctica is surrounded by the global oceans, influencing their salinity and circulation on global scales [Goosse and Fichefet, 1999, and references therein].

The Antarctic ice sheet holds about 90 % of the Earth's ice, equivalent to 70 % of the fresh water reservoir. If completely melted, this would rise sea level by some 60 m [e.g. Alley *et al.*, 2005]. Due to the obvious environmental and societal impacts, monitoring of Antarctica's ice mass and its changes plays a crucial role in glaciological research [among others Wingham *et al.*, 1998; van der Veen, 2002; Thomas *et al.*, 2004; Alley *et al.*, 2005; Church and White, 2006]. Projected sea-level rise by the end of the 21st century is $0.5 \pm 0.4 \text{ m}$ in response to additional global warming [Alley *et al.*, 2005, and references therein] with the largest errors arising from the uncertain Antarctic contribution. Thus, a modest imbalance of the Antarctic ice sheet may cause a major change in sea level and an acceleration of sea-level rise which currently amounts to $1.5\text{--}2 \text{ mm a}^{-1}$ [Bamber, 2004]. Moreover, it could also determine the sign of future sea-level change.

The last years have therefore seen increasing efforts to examine the possible contribution of the Antarctic ice sheet to global sea-level change. Unfortunately, today neither the net Antarctic

mass gain nor its loss can be determined accurately enough to derive clear predictions [Vaughan, 2005], although several regions have been reported to be significantly out of balance [van den Broeke et al., 2006]. In light of these uncertainties and their impacts on global sea-level change, knowledge of the variability of the Antarctic surface-mass balance on different spatial scales is of major importance.

1.2 Mass balance and surface-mass balance

Mass balance (MB) refers to the net ice-mass gain or loss by biasing all input and output contributors of snow or ice mass with a MB of zero referring to equilibrium conditions. Thus, MB is generally calculated as difference between input and output mass fluxes [Rignot and Thomas, 2002]. However, accurate determination of the mass fluxes is still largely difficult [Zwally et al., 2005].

Mass is mainly gained by freezing water beneath the ice shelves and by precipitation, most of which falls as solid snow. Only in small stripes along the coasts and on the Antarctic Peninsula occasional rain fall occurs. In the Antarctic interior, clear-sky precipitation, or diamond dust, the mechanism of which is not fully understood yet [van de Berg et al., 2006], may contribute significantly to mass gain. The main contribution to mass removal stems from ice-flow across the margins of Antarctica and subsequent basal melting underneath the ice shelves as well as from iceberg calving at their ice fronts.

Surface-mass balance (SMB) can be written as [van de Berg et al., 2005; King, 1996]

$$SMB = P_s - SU - M - ER_{ds} - SU_{ds} \quad (1.2.1)$$

where P_s denotes solid precipitation, SU sublimation from the surface (sometimes also referred to as evaporation, since evaporation largely consists of surface sublimation in Antarctica [Déry and Yau, 2002]), M melt (i.e., surface melt) and runoff, ER_{ds} erosion due to divergence in horizontal snow transport, and SU_{ds} snowdrift sublimation. Note that only P_s adds mass, whereas the other terms remove mass and are therefore negative in Equation (1.2.1). All terms are usually given in mm w.e. (water equivalent) a^{-1} , which is equivalent to the unit $kg\ m^{-2}\ a^{-1}$. The terms MB and SMB are not used concisely in literature. Here, SMB denotes the sum of all *surface* processes, as given above. If not mentioned otherwise, it refers to the entire Antarctic ice sheet. On the other hand, MB addresses the sum of *all* ice-mass changes, including dynamic effects from glacier flow and subsurface processes.

Snow accumulation, hereinafter referred to as *accumulation*, denotes all processes adding snow mass to the surface in a certain area, i.e., precipitation and redistribution of freshly fallen snow by wind influence [Paterson, 1994]. Accumulation can be determined locally by in-situ measurements - see chapter 3. Note that the term accumulation as used in the publications of

this study (Paper I–III) and in several others refers to the in-situ determined accumulation rates, meaning *net* accumulation averaged over a certain time period in the respective study area.

Ablation is defined as the sum of all processes removing mass from the surface, consisting of the negative terms in Equation (1.2.1), as explained above. Sublimation is mainly controlled by temperature, which depends strongly on elevation. Regionally, katabatic winds also influence sublimation. In Dronning Maud Land, sublimation reaches up to $200 \text{ kg m}^{-2} \text{ a}^{-1}$ [van de Berg *et al.*, 2005], thus significantly contributing to the SMB. Snowdrift sublimation has been reported to remove about 10–20 % of the annual accumulation in coastal regions [Bintanja, 1998]. The Antarctic interior experiences much less snowdrift sublimation, due to lower temperatures and less intense winds. Surface melt occurs only locally in Antarctica, mainly in regions adjacent to the coast, on ice shelves, and on the Antarctic Peninsula [Torinesi *et al.*, 2003]. In Dronning Maud Land, surface melt plays generally a minor role and can thus be neglected [Zwally and Fiegles, 1994]. Some authors even restrict surface melt and runoff to the northernmost parts of the Antarctic Peninsula only [van den Broeke and van Lipzig, 2003]. Divergence from horizontal snow transport is difficult to quantify, but has been reported to contribute locally to SMB, particularly in the coastal areas. Déry and Yau [2002] estimate that surface sublimation and snowdrift together remove 17–20 % of the annual precipitation over Antarctica.

1.2.1 Influences on surface-mass balance

SMB as well as accumulation rates have been shown to vary locally to regionally in Antarctica [e.g. Richardson-Näslund, 2001; Spikes *et al.*, 2004; Eisen *et al.*, 2005; Frezzotti *et al.*, 2005]. In general, accumulation decreases with distance from the coast and with decreasing temperature [e.g. Giovinetto *et al.*, 1990; Richardson-Näslund, 2001]. The interior parts of Antarctica receive less moisture than the areas in the vicinity of the ocean. In the interior, katabatic (i.e., gravity driven) winds dominate the wind regime, following the surface slopes [Parish and Bromwich, 1991]. In coastal areas, katabatic winds also follow the steep slopes, but these regions are characterized by the occasional presence of nunataks, that are capable to modify wind flow locally [Jonsson, 1995]. Furthermore the coastal areas are influenced by synoptic weather systems which do not penetrate far inland enough to reach the polar plateau. In Dronning Maud Land coastal areas are marged by mountain chains at the transition to the polar plateau. Precipitation is higher at the foot of those mountains, therefore these parts experience more accumulation, whereas the plateau region receives far less precipitation.

Yet accumulation is not only influenced by precipitation and thus by general weather systems but also by the interaction between near-surface wind pattern and surface topography [King *et al.*, 2004]. Accumulation maxima tend to be located in local surface-elevation troughs and on the windward sides of surface-elevation undulations [e.g. Black and Budd, 1964; Goodwin,

1990; *Frezzotti et al.*, 2005]. Local hills and their leeward sides experience far less accumulation, sometimes even ablation. This pattern is attributed to wind influence from a prevailing wind direction. Over large areas of the East Antarctic plateau a specific feedback system between atmosphere and cryosphere results in highly regular undulations of accumulation pattern, leading to the formation of so-called megadunes [*Frezzotti et al.*, 2002a]. These features are characterized by wavelengths of a few kilometers and amplitudes of a few meters, covering areas of roughly 500 000 km² [*Fahnestock et al.*, 2000], their subparallel crests extending over hundreds of kilometers.

Thus, accumulation is a complex function of such parameters as continentality, moisture source, precipitation regime, temperature, surface slope and structure, surface elevation, and glacier flow. As outlined above, climatic conditions at coastal sites tend to be more complicated than on the rather smooth and homogeneous regions of the Antarctic plateau, leading to the higher variability of accumulation features reported in several studies [e.g. *Richardson-Näslund*, 2001]. Since the coastal parts contribute significantly to the pattern and the total amount of Antarctica's SMB, they are in the focus of several new satellite missions and the respective ground-truthing campaigns, involving this study.

In principle, bedrock topography is also capable to influence the accumulation pattern, since large-scale surface-elevation features have been reported to mirror bedrock topography [e.g. *Welch and Jacobel*, 2005]. However, in the investigation areas of this study ice thickness is generally much larger than 1000 m and the bedrock topography is generally rather smooth [*Lythe et al.*, 2001; *Meyer et al.*, 2005], thus it can be assumed that bedrock influences do not contribute significantly to the small-scale accumulation variability reported in this study.

1.2.2 Overview of measurement methods

Methods to determine SMB or MB can be divided in large-scale approaches comprising the whole Antarctic continent or at least large drainage basins [e.g. *Giovinetto and Bentley*, 1985] and in-situ measurements naturally providing local to regional-scale values.

The latter consist of point measurements such as firn cores, snow pits, or stake readings. Additional ground-penetrating radar (GPR) profiling is often used to connect firn-core drilling sites [among others *Richardson et al.*, 1997; *Spikes et al.*, 2004; *Eisen et al.*, 2005]. Such in-situ measurements consisting of shallow firn cores and GPR profiling are performed in this study and will be addressed in section 3 and in the accompanying papers (Paper I–III).

Large-scale estimates of SMB can be carried out by modeling, e.g., using general circulation or regional atmospheric models [*Genthon and Krinner*, 2001; *Genthon*, 2004; *van de Berg et al.*, 2005]. Interpolation of widespread in-situ data has been used to derive maps of distribution of SMB over the entire ice sheet (see next section). Satellite-derived changes in ice-sheet elevation allow determination of large-scale MB, when accompanied by gravity measurements.

Atmospheric models and large-scale compilations from interpolation are introduced in section 1.3, followed by recent results, satellite-based approaches are discussed in section 1.4.

1.3 Large-scale estimates of (surface-)mass balance

Rignot and Thomas [2002] give three methods to determine Antarctica's MB:

- The mass-budget method:
This method is valid for the grounded ice sheet and compares net input from snow accumulation with melt and ice discharge. The difference between these contributors describes the mass budget. Accumulation is usually inferred from ice-core analyses. Melt rates can be estimated by positive degree-day models or from satellite-derived brightness temperatures [*Torinesi et al., 2003*]. Ice discharge across the grounding line is derived from ice-flow velocities obtained by interferometric analysis of synthetic aperture radar (SAR) data [*Dietrich et al., 1999; Joughin and Tulaczyk, 2002*] or by GPS measurements.
- Elevation change:
Detection of changes in ice-sheet elevation over time became possible by satellite altimetry, like ERS-1/2, Geosat, and ICESat. Elevation changes can be translated into volume changes, provided that the vertical motion of the underlying ground due to isostatic adjustment and postglacial rebound is known. More information about this method is given in section 1.4. A detailed discussion of recent mass changes of Antarctica as well as Greenland using ERS-1/2 data is given by *Zwally et al. [2005]*.
- Weighing of ice sheets:
This approach is carried out likewise by satellite-borne measurements. The GRACE mission, maintained by NASA and DLR (Deutsches Zentrum für Luft- und Raumfahrt), provides measurements of the time-variable gravity field. Combination with elevation data yields estimates of the MB [*Wahr et al., 2000*]. This method will likewise be discussed further in section 1.4.

The distribution of SMB over the entire ice sheet is generally estimated from large-scale approaches utilizing modeling and interpolation of field data. Modeling usually involves usage of general circulation models (GCMs) [e.g. *Genthon and Krinner, 2001*] or regional atmospheric climate models [e.g. *van de Berg et al., 2005*], both deriving SMB from the modelled distribution of precipitation and melt over Antarctica.

1.3.1 Recent estimates of Antarctic surface-mass balance

Large-scale compilations of SMB have been given by *Vaughan et al.* [1999] and *Giovinetto and Zwally* [2000]. Prior to these more recent studies, *Giovinetto and Bentley* [1985] published a map of SMB distribution, based on several in-situ studies and the delineation of major ice-drainage basins. They obtain distribution of SMB by positioning isopleths of SMB considering parameters like surface slope, surface elevation, and regional estimates of atmospheric variables like condensation levels and directions of lower tropospheric flow. Thus they derive an average of $124 \text{ kg m}^{-2} \text{ a}^{-1}$ for the grounded ice sheet, $263 \text{ kg m}^{-2} \text{ a}^{-1}$ for the ice shelves, and $143 \text{ kg m}^{-2} \text{ a}^{-1}$ for the whole of Antarctica. Accuracy is reported to be $\pm 10 \%$. *Giovinetto and Zwally* [1995] derive accumulation distribution from passive microwave data, relating firn emissivity and accumulation rates. Their results suggest that the former compilation of *Giovinetto and Bentley* [1985] underestimates SMB by 12 % for West Antarctica and by 39 % for East Antarctica.

Vaughan et al. [1999] interpolate more than 1800 in-situ measurements from firn cores and snow pits. They use passive microwave brightness temperature to control the interpolation. A new elevation model derived from ERS-1 satellite altimetry is employed to delineate the boundaries of the drainage basins more precisely than before. Thus, they report net surface accumulation of 2288 Gt a^{-1} or $166 \text{ kg m}^{-2} \text{ a}^{-1}$ for the entire Antarctic ice sheet and 1811 Gt a^{-1} or $149 \text{ kg m}^{-2} \text{ a}^{-1}$ for the grounded ice sheet with an estimated accuracy of $\pm 5 \%$. *Giovinetto and Zwally* [2000] use practically the same data set as *Vaughan et al.* [1999] yet a different interpolation scheme by utilizing visual interpolation of isopleths. Compared to the previous compilation of *Giovinetto and Bentley* [1985] they also account for deflation and ablation adjustment, i. e., mass loss due to wind influence and due to evaporation and runoff. The implementation of these adjustments affects the coastal areas only, constrained to a zone stretching about 50–100 km inland from the grounding line. *Giovinetto and Zwally* [2000] thus derive 2020 Gt a^{-1} or $149 \text{ kg m}^{-2} \text{ a}^{-1}$ on average net accumulation for the entire ice sheet (or $159 \text{ kg m}^{-2} \text{ a}^{-1}$ without adjustment). The difference between this and the older compilation of *Giovinetto and Bentley* [1985] in overall net accumulation amounts to $6 \text{ kg m}^{-2} \text{ a}^{-1}$, however, some of the drainage basins exhibit much larger differences. Hence, although the derived overall SMB has not changed much due to more accurate compilations, results for individual areas become significantly more precise the more in-situ data are available and included.

The difference between the calculations of *Vaughan et al.* [1999] and *Giovinetto and Zwally* [2000] considering the entire ice sheet amounts to 268 Gt a^{-1} , equivalent to about $\sim 0.7 \text{ mm a}^{-1}$ global sea-level change, demonstrating that the same data set may lead to different conclusions, thus affecting predictions of possible future climate changes.

Arthern et al. [2006] utilize satellite observations of microwave emission and in-situ measurements to obtain an map of Antarctic accumulation rates. Their general accumulation pattern

agrees well with the results of *Vaughan et al.* [1999] and *Giovinetto and Zwally* [2000], yet regionally differences exceed $100 \text{ kg m}^{-2} \text{ a}^{-1}$. *Arthern et al.* [2006] derive an average value of $143 \pm 4 \text{ kg m}^{-2} \text{ a}^{-1}$ over the grounded ice sheet with an accuracy of some 10 %. *van de Berg et al.* [2005] use a regional atmospheric climate model (RACMO2/ANT), comprising the components precipitation, sublimation/deposition, and melt. Mass loss by snowdrift or snowdrift sublimation is not accounted for in their model. Integrated over the grounded ice sheet, their derived average SMB results as $153 \text{ kg m}^{-2} \text{ a}^{-1}$, agreeing within 5 % with the measurement compilations from *Vaughan et al.* [1999]. Moreover, *van de Berg et al.* [2006] calibrate the results of *van de Berg et al.* [2005] with the in-situ measurements used by *Vaughan et al.* [1999], thus obtaining a calibrated mean SMB of $171 \pm 3 \text{ kg m}^{-2} \text{ a}^{-1}$.

This overview shows that from the earlier compilation given by *Giovinetto and Bentley* [1985] estimates of mean SMB generally increased over the years as more in-situ data became available. Although the accuracy of the estimates increased likewise, interpolations still suffer from data sparsity. Therefore, continuing efforts in field work enlarge the available data base and contribute to constraining future large-scale models.

1.3.2 Uncertainties and implications

Generally, the large-scale compilations neglect small-scale variability and present results averaged horizontally over 50 to some 100 km. As explained before, accumulation is subject to local and regional variations, especially in the coastal areas. Interpolation of point measurements for large-scale maps therefore requires some knowledge of the spatial representativity of the values, which is likely rather small [*Richardson-Näslund*, 2001]. Implementation of measurements covering different time periods may obstruct the results of large-scale compilations since long-term trends and short-term temporal variability are mixed. Recent studies revealed that interannual variability of precipitation is considerable, with common fluctuations of $\pm 20 \text{ kg m}^{-2} \text{ a}^{-1}$ [*Monaghan et al.*, 2006b]. Inclusion of accumulation records covering very short time periods therefore might likely lead to biases in the derived compilation.

Moreover, the large-scale approaches have been shown to overestimate SMB in coastal areas [*van de Berg et al.*, 2006], where the GCMs likewise show biases [*Genthon*, 2004]. Yet these regions are especially sensitive to global climate change [*Genthon and Krinner*, 2001], therefore accurate knowledge of accumulation pattern in the coastal areas is relevant for climatological research.

Large-scale compilations do not capture the variability of local climatic influences sufficiently due to their grid-cell size. Satellite-based approaches (discussed in the next section) likewise suffer from averaging over large areas. In light of the biases in GCMs and other large-scale approaches in-situ measurements are required for validation.

1.4 Satellite-based approaches

This section describes the satellite-based approaches to determine Antarctica's MB, comprising a short description of methods and recent results as well as uncertainties and implications. Furthermore the VISA project, forming the framework of this study, is introduced, followed by the outline of the specific goals of this study.

1.4.1 Determination of ice-mass changes

Satellite-based approaches to derive changes in ice mass include altimetry and gravity missions. ESA's European Remote Sensing (ERS)-1/2 mission (ERS-1: 1991–2000, ERS-2: launched 1995), carries among other devices a synthetic aperture radar and a radar altimeter. ERS yields information about the ice-sheet elevation and its changes [e.g. *Wingham et al.*, 1998], however, these satellites cover only areas up to latitudes of 80° S/N and do not give reliable results over the steep slopes that widely dominate the grounded coastal areas. [*Vaughan*, 2005; *Zwally et al.*, 2005]. NASA's ICESat (Ice, Cloud, and Land Elevation Satellite), launched in 2002, carries on board the Geoscience Laser Altimeter System (GLAS), measuring the surface elevation by laser altimetry. GLAS's footprint is small, only 60 m on average, and spaced at 172 m along-track, enabling an averaged accuracy of 15 cm [*Zwally et al.*, 2002]. Thus, high-resolution monitoring of surface-elevation changes is possible. Surface-elevation changes are equivalent to ice-thickness changes minus the vertical motion of the underlying bedrock due to postglacial rebound. Furthermore, short-term changes introduced by variations in near-surface firn compaction must be taken into account [*Zwally and Li*, 2002]. The ICESat mission is dedicated to give a temporal and spatial coverage of ice-sheet surface elevation such that interannual and long-term elevation changes can be obtained with an accuracy of $< 1.5 \text{ cm a}^{-1}$ for spatial averages over areas of 100 km x 100 km. Vertical resolution resolves changes of about 10 % of the accumulation rate [*Zwally et al.*, 2002]. ICESat data provide coverage up to at least 86° S/N of the polar regions but does not penetrate cloud covers, which are particularly present near the coasts.

The upcoming CryoSat-2 mission, which is scheduled to be launched in 2009 after the failure of CryoSat-1 in 2005, will cover latitudes up to 88° S/N, monitoring precise changes in thickness of polar glaciers and floating sea ice using a special radar altimeter. More information about CryoSat and its deliverables can be found in *Wingham et al.* [2006]. Together, ICESat and CryoSat-2 will provide detailed data sets of ice-sheet elevation. Thus, data sets already available from ERS-1/2 are expected to be extended by the ICESat and CryoSat-2 missions. However, from satellite altimetry alone one cannot distinguish between changes in elevation or in density of the firn column, as firn compaction influences the signal sensed by the satellites. Furthermore, postglacial rebound also affects the ice-elevation changes derived from satellite

observations [*Huybrechts and Le Meur, 1999*]. Thus, additional information is mandatory.

Another approach to yield ice-mass changes involves gravity measurements, as gravity is linked directly to mass. Time-variable gravity data are provided by the Gravity Recovery and Climate Experiment (GRACE) mission [*Tapley et al., 2004a*], continuously mapping the gravity field up to latitudes of 89°S/N. Monthly solutions are provided by Geoforschungszentrum (GFZ) Potsdam, Germany, and Center for Space Research (CSR) Texas, USA, consisting of spherical harmonics, the Stokes coefficients. GRACE actually comprises two identical satellites, separated from each other by ~ 220 km along-track and linked by a highly accurate intersatellite microwave ranging system [*Tapley et al., 2004b*]. This concept is referred to as satellite-to-satellite tracking at low-low mode [*Bentley and Wahr, 1998*]. A change in distance, extracted from the phase measurement of the signal transmitted between the satellites, implicitly contains the influence of the globally integrated mass distribution and its movements within the Earth [*Tapley et al., 2004b*]. GRACE delivers only data of resolution of some 400 km [*Tapley et al., 2004b*], hence, the derived ice-mass changes are averaged over several hundred kilometers [*King et al., 2006*].

Unfortunately, major ambiguities arise for the interpretation of gravity changes over the ice sheets, comprising postglacial rebound as well as interannual variations in snow-accumulation rates and in mean atmospheric pressure [*Bentley and Wahr, 1998*]. Concerning isostatic rebound, GRACE-derived parameters enable the improvement of models regarding the viscosity of the Earth's mantle, yet a certain amount of GRACE solutions has to be available for this method, as well as information about surface elevation from altimetry. Groundborne observations of elevation using GPS receivers also add valuable data for model constraints of isostatic rebound effects. Moreover, interannual changes of snow accumulation can likewise be addressed by GRACE [*Bentley and Wahr, 1998*], however, they are also averaged over several hundreds of kilometers. Additional field measurements will thus be necessary. The contribution from the atmosphere can be estimated from atmospheric data and models [*Swenson and Wahr, 2002*]. Increasing the number of automatic weather stations employed in Antarctica further helps to diminish the errors caused by fluctuations of atmospheric pressure.

1.4.2 Results and uncertainties

Combination of the results from gravity and altimetry missions yields ice-mass changes. Recent results from the gravity method are given by *Velicogna and Wahr* [2006]. They estimate Antarctic mass loss to be about $-152 \pm 80 \text{ km}^3 \text{ a}^{-1}$, equivalent to $0.4 \pm 0.2 \text{ mm a}^{-1}$ sea-level rise. Separated for West and East Antarctica, they derive mass rates of $-148 \pm 21 \text{ km}^3 \text{ a}^{-1}$ for the West Antarctic ice sheet (WAIS) and $0 \pm 56 \text{ km}^3 \text{ a}^{-1}$ for the East Antarctic ice sheet (EAIS). Uncertainties are introduced by postglacial rebound and the so-called leakage effect, i. e., the fact that the gravity signal is affected also by mass outside of the Antarctic ice sheet. The un-

certainties from postglacial rebound dominate the error, showing an even larger magnitude than the uncorrected trend from GRACE. Thus, independent models have to be employed in order to decontaminate the GRACE signal from postglacial rebound and leakage effects. A significant ice-mass trend does only appear after removal of postglacial rebound from the GRACE solutions, implying that ice-mass variability and postglacial rebound are closely related, yet with opposite signs [Velicogna and Wahr, 2006]. Long-term postglacial rebound rates will remain constant over the mission duration (projected for five years, but expected to yield eight years), hence, it should be possible to resolve long-term changes in the rate of mass loss, as more GRACE data become available.

Chen et al. [2006] likewise utilize GRACE data to determine regional ice-mass changes of West and East Antarctica. They conclude that the WAIS is losing mass at a rate of $-77 \pm 14 \text{ km}^3 \text{ a}^{-1}$ whereas EAIS shows mass gain of $+80 \pm 16 \text{ km}^3 \text{ a}^{-1}$. Other studies report approximate ice-mass balance of East Antarctica [e.g. *Rignot and Thomas*, 2002]. Comparison of the results presented by *Chen et al.* [2006] with those from *Rignot and Thomas* [2002] indicate that either snow accumulation increased significantly after 2002 (i.e., the launch of GRACE) in this region in comparison to earlier studies, or an unmodeled contribution of postglacial rebound obscures the results. *Chen et al.* [2006] argue that the latter is more probable, demonstrating that models of postglacial rebound need to be improved over Antarctica. Using yet another correction for postglacial rebound, *Ramillien et al.* [2006] derive an ice-mass change of $-107 \pm 23 \text{ km}^3 \text{ a}^{-1}$ for WAIS and $+67 \pm 28 \text{ km}^3 \text{ a}^{-1}$ for EAIS. The entire Antarctic ice sheet is in their study reported to contribute to sea-level rise by $0.11 \pm 0.09 \text{ mm a}^{-1}$. This is significantly less than the results presented by *Velicogna and Wahr* [2006], again demonstrating the necessity for a reliable model of postglacial rebound as well as detailed ground-truthing of satellite-based approaches.

Horwath and Dietrich [2006] demonstrate that errors are likely even larger than given above. They address errors in the GRACE solution itself (the Stokes coefficients), of which regional mass variations arise as linear combinations using adapted filter techniques [*Swenson and Wahr*, 2002]. Thus, errors in the solution linearly propagate into the derived mass variations. For this reason current estimates of Antarctic ice-mass trends like those published by *Velicogna and Wahr* [2006] and other studies very likely underestimate errors and uncertainties.

Concludingly, although the aforementioned new satellite missions yield a better coverage of Antarctica and more accurate estimates of MB and ice-mass changes, it still cannot be determined at present whether Antarctica as a whole is in or out of balance. It is currently agreed that the WAIS is out of balance with a negative mass budget [e.g. *Thomas et al.*, 2004], whereas the EAIS is believed by some authors to be in balance [e.g. *Rignot and Thomas*, 2002; *Velicogna and Wahr*, 2006]. Others report increase in elevation and snow accumulation on the EAIS [*Davis et al.*, 2005; *Chen et al.*, 2006]. Yet as a result of data sparsity the mass balance of

the EAIS is largely uncertain and subject to errors, especially due to the uncertain contribution of postglacial rebound affecting the gravity signal. *Chen et al.* [2006] state that the uncertainties arising from the postglacial-rebound model adopted may be on the order of 100 %. Thus, ground-based studies of accumulation variability help to establish a more complete picture of (East) Antarctic mass balance.

1.4.3 The VISA project and this study

This study is part of the so-called VISA project: *Validation, densification, and interpretation of satellite data in Antarctica using airborne and groundborne measurements for the determination of gravity field, magnetic field, ice-mass balance, and crustal structure*. In Dronning Maud Land, the Atlantic sector of Antarctica, information about the gravity field, magnetic field, and ice-sheet elevations derived from satellite missions like GRACE, GOCE (Gravity Field and steady-state Ocean Circulation Explorer, <http://www.goce-projektbuero.de>), and ICESat shall be validated with the help of groundborne and airborne measurements. Variations of accumulation and density on temporal and spatial scales influence the relation of elevation changes and changes in gravity and mass. *Velicogna and Wahr* [2002] show from analysis of simulated GLAS and GRACE data that the main error source in the combined signal arises from the unknown time-variable accumulation and its effect on the density of the sensed firn or ice column. Thus, the knowledge of spatial and temporal patterns of ice-mass changes provides key information especially for the validation of the time-varying gravity field as sensed by GRACE [*Scheinert et al.*, 2005]. For this reason small-scale variations of the accumulation rate play a significant role and need to be investigated closely by groundborne operations.

This study uses geophysical and glaciological methods to investigate the recent accumulation rate and analyze its spatial and temporal distribution in selected grounded coastal areas of Dronning Maud Land. It thus serves, together with results from adjacent study regions, as a base for ground-truthing of satellite-based approaches. The accompanying papers discuss local-scale accumulation features and yield new insight in small-scale variability of accumulation rates, providing important information for the detailed validation of ice-mass changes derived from GRACE and ICESat.

Chapter 2

Area of investigation

Dronning Maud Land (DML) makes up the Atlantic sector of Antarctica (Figure 2.1a), comprising the area between 20° W and 45° E, in some studies only up to 20° E. The Northern and Southern boundaries are not clearly defined [Näslund, 1998], but mostly seen as the coast line in the North.

Following the description of *Richardson-Näslund* [2001], DML can be divided into three main parts, consisting of ice shelves, grounded coastal areas, and the inland-ice plateau. The ice shelves (Riiser-Larsenisen, Ekströmisen, Fimbulisen, Nivlisen etc.) are afloat on the ocean, at rather low elevations. They are separated by the grounding line from the grounded coastal areas. The latter ascend from near sea level to elevations of about 1500–2000 m a.s.l., stretching up to the coastal mountain ranges (Heimefrontfjella, Kirwanveggen, Mühlig-Hoffmanngebirge, Wohlthat Massif, etc.), south of which the inland-ice plateau starts, consisting of the Amundsenisen in the West and the Wegenerisen in the East. The plateau areas exhibit elevations of 2500–3000 m a.s.l. and a generally smooth surface with small sastrugis, owed to the generally less intense winds [Noone *et al.*, 1999]. Accumulation on the plateau shows values on the order of 45–90 kg m⁻² a⁻¹ [Karlöf *et al.*, 2005, and references therein], with some 64 kg m⁻² a⁻¹ at the German Kohnen station (75°00' S, 00°04' E, 2892 m a.s.l.) [Oerter *et al.*, 1999], whereas on the ice shelves and the grounded coastal parts values up to nearly 800 kg m⁻² a⁻¹ are reported [Melvold *et al.*, 1998].

Ice thickness varies between about 1000 to 2000 m in the grounded coastal parts, with the exception of some nunataks and the mountain chains protruding through the ice sheet. On Amundsenisen and Wegenerisen plateau ice thickness reaches some 3000 m [Lythe *et al.*, 2001; Steinhage *et al.*, 2001].

Expeditions started in the 1920s and in the early 1930s, lead by Norway, and followed in 1938/39 by the German Schwabenland expedition under Ritscher. From 1949–1952 the Norwegian-British-Swedish expedition undertook detailed airborne photographic mapping of the area. Most of the geographical names stem from these latter two expeditions [Näslund,

1998, and references therein]. The American South Pole Queen Maud Land Traverse (SPQMLT) was conducted 1964–1968, drilling firn cores in the southern part of DML [Piciotto *et al.*, 1971]. The last decades have seen increasing efforts of field work in DML, especially in the western part and on the plateau region. Apart from seismic investigations, studies consisted mainly of firn-core drilling of shallow (some 10–30 m) to medium-depth cores (up to about 150 m deep), carried out among others by expeditions from Germany [Schlosser *et al.*, 1999; Oerter *et al.*, 1999, 2000], Sweden [Isaksson and Karlen, 1994; Isaksson *et al.*, 1999], and Norway [Melvold *et al.*, 1998; Karlöf *et al.*, 2005]. Additional GPR profiles from the coast to the plateau regions [Richardson-Näslund, 2004] and near the German Kohnen station [Rotschky *et al.*, 2004; Eisen *et al.*, 2005] complemented the activities. The European Project for Ice Coring in Antarctica (EPICA) is dedicated to retrieve a deep ice core at the Kohnen station in DML and another one at Dome C (75°06'S, 123°21'E, 3233 m a.s.l.), both serving as a valuable climate archive [EPICA community members, 2004]. The DML core is furthermore supposed to give useful insights in climatic effects related to the Northern hemisphere and the Greenland ice cores, e.g. NorthGRIP [Dahl-Jensen *et al.*, 2002]. Prior to the drilling activities at Kohnen station, which started in the season 2001/2002 and ended in 2005/2006, intensive pre-site surveys have been carried out on Amundsenisen [among others Steinhage *et al.*, 1999; Oerter *et al.*, 1999, 2000; Rotschky *et al.*, 2004; Hofstede *et al.*, 2004; Eisen *et al.*, 2005; Karlöf *et al.*, 2005].

Despite all these research activities there are still large areas of DML uncovered, mainly in the central and eastern parts. Rotschky *et al.* (submitted), present an accumulation map from all available firn-core and snow-sample data, uncovering regions suffering from data sparsity, including particularly large areas in eastern DML as well as the coastal parts of central DML. The coastal areas are less well captured by large-scale compilations or resolved by atmospheric models, as outlined before. Their generally higher accumulation, the influence of synoptic weather systems, and the fact that glaciers drain through the coastal areas into ice shelves and oceans, makes the coastal parts sensitive to global climate change. Therefore close coverage of these areas by in-situ measurements is of vital importance.

Within this work two selected areas have been investigated (Figure 2.1b): the Potsdam Glacier in central DML and the region around Kottas Camp, located about 10 km north of Kottasberge/Heimefrontfjella in western DML, hereinafter referred to as Kottasberge. Potsdam Glacier is a comparatively small outlet glacier (when compared to e.g. Jutulstraumen) coming down from Wegenerisen and meandering through the mountains of Wohlthat Massif before finally feeding Nivlisen, north of the Russian station Novolazarevskaya. The area of investigation comprises the region between 11–12° E and 71–71.3° S. Although the accumulation data presented in this study cover only a small region, they are the first detailed groundborne accumulation values from Potsdam Glacier. Korth and Dietrich [1996] report accumulation data from stake readings, however, they do not provide density measurements but rely on general

empirical field data for conversion of snow height to accumulation. Since this region is characterized by a complicated orography and undulations of surface elevation, the accumulation pattern exhibits large variability over small distances which is not captured sufficiently by *Korth and Dietrich* [1996].

Additional data from the second study area, Kottasberge, complement the accumulation values discussed in this study. The latter area is more inland than Potsdam Glacier, on Ritscherflya at the foot of Amundsenisen plateau. Apart from an older GPR profile [*Richardson-Näslund*, 2004] there are only sparse point measurements published from this region so far. Thus, this study closes some data gaps and may be used together with other results of adjacent regions for the enhancement of regional accumulation maps of DML in future work. Detailed maps of accumulation distribution are valuable for validation of satellite-derived ice-mass changes.

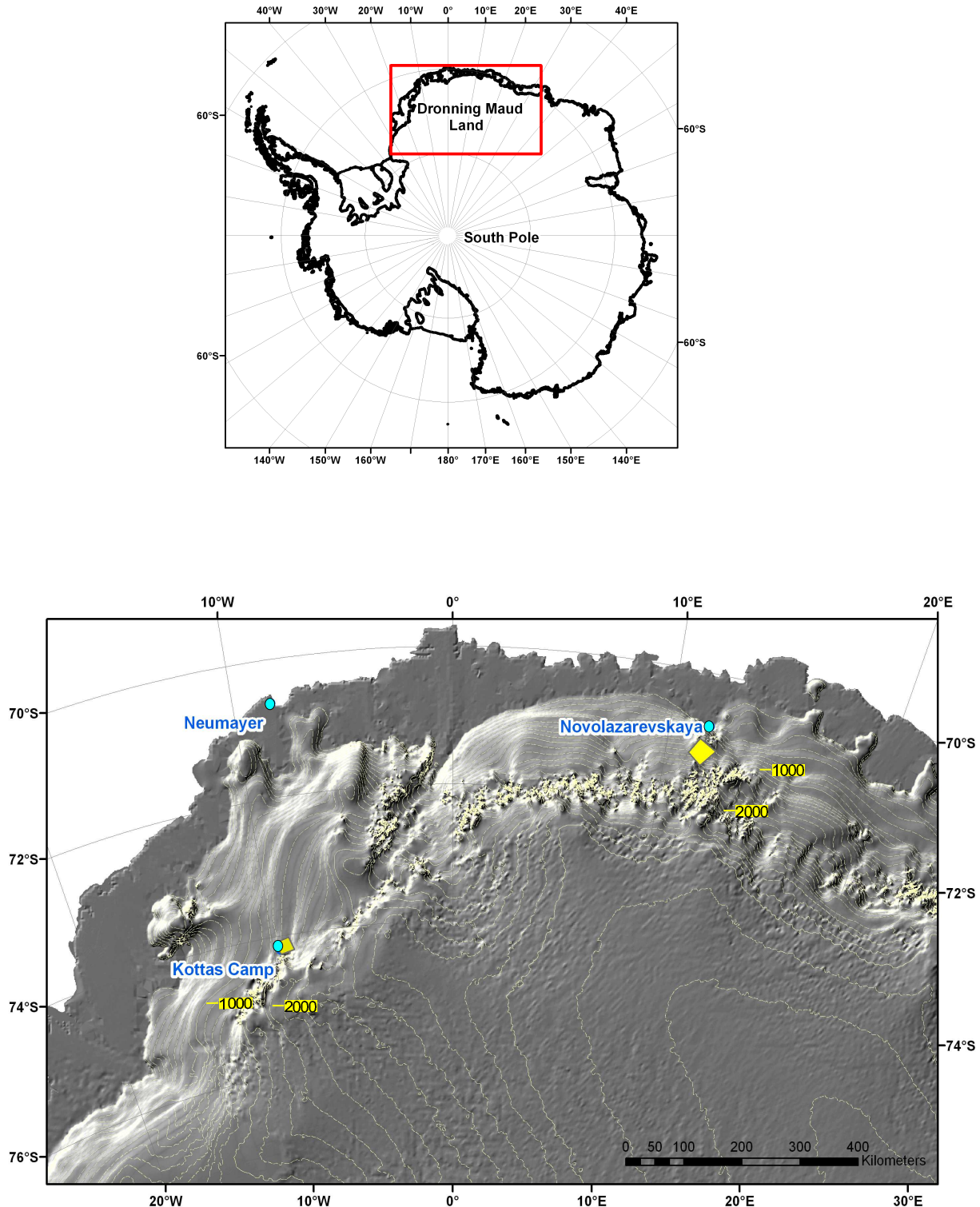


Figure 2.1: a) Above: Antarctica with Dronning Maud Land. (b) below: Dronning Maud Land: the part marked in (a) is depicted. Blue circles: stations relevant to this study; yellow areas: areas of investigation in this study; light yellow lines: elevation contour lines at 100 m spacing. Map source: Antarctic Digital Database 4.0. Satellite image: RAMP (provided by National Snow and Ice Data Center, Boulder, USA, <http://nsidc.org/data/ramp>). Figure courtesy of C. Wesche, 2006.

Chapter 3

Methods

This section briefly introduces ground-penetrating radar as a geophysical device used in glaciology and describes the most important theoretical background. A short overview of glaciological applications of Global Positioning System (GPS) is given likewise. Acquisition and processing of GPR and GPS data are explained as well as the analyses of firn cores and the determination of accumulation rates from GPR and firn-core data. The chronological order of this chapter follows the procedure of data acquisition in the field, starting with GPR and GPS and their deliverables, followed by firn-core studies and the combination of these data sets, yielding accumulation rates on spatial and temporal scales.

3.1 GPR and GPS

Ground-penetrating radar (GPR) has been widely applied in geophysical investigations. It is based on propagation of electromagnetic (EM) waves in the radio frequency range through the subsurface. A GPR device typically consists of a control unit and a transmitter (TX) and receiver (RX) antenna, transmitting EM waves and recording the EM response of the subsurface. A GPR antenna is called monostatic if one antenna is used to transmit and record the response, and bistatic if two separate antennae are used as transmitter and receiver. Typical antenna frequencies for GPR applications are in the range of 10 MHz–1 GHz.

GPR can be used in several modes of data acquisition. For profiling usually the method of common offset (CO) is used, meaning that receiver and transmitter are kept at constant distance (or offset) and towed along the GPR profile. The recorded radargram typically shows distance along the profile or trace number versus two-way travel time (TWT) and provides information about subsurface structures. The common-midpoint (CMP) technique is utilized to determine a velocity profile of the EM waves in the subsurface, similar to seismic techniques. In this case, the offset between the antennae is increased symmetrically to the central point. In this study the CO method was used throughout.

3.1.1 Application of GPR in glaciology

The theory of EM wave propagation is given in literature, see e.g. *Jackson* [1996]; *Ulabay et al.* [1982]. Here, only a brief outline of the most important parameters and equations for application in glaciology will be given. GPR is sensitive to changes in the dielectric parameters of the subsurface. EM waves are reflected from layer boundaries exhibiting different dielectric properties. In soils, propagation speed of EM waves is mainly ruled by the content of liquid water and by conductivity, provided that only non-magnetic material is present. Both parameters decrease the velocity and the penetration depth significantly with increasing water content and conductivity, respectively.

The material electric properties of ice (and other media) are described by the complex relative dielectric permittivity ε which is given by:

$$\varepsilon = \varepsilon' - i\varepsilon'' = \varepsilon' - i \frac{\sigma}{\omega\varepsilon_0} \quad (3.1.1)$$

where σ is electrical conductivity, ω the angular frequency, and $\varepsilon_0 = 8.85 \cdot 10^{-12} \text{ F m}^{-1}$ the dielectric constant. Generally ε depends on the frequency of the EM wave, however, in ice the real part ε' is nearly frequency-independent in the frequency range of GPR applications [*Fujita et al.*, 2000]. Since ice absorbs EM energy, Equation (3.1.1) can also be written as:

$$\varepsilon = \varepsilon'(1 - i \tan \delta) \quad (3.1.2)$$

$$\tan \delta = \frac{\varepsilon''}{\varepsilon'} \quad (3.1.3)$$

The loss tangent $\tan \delta \ll 1$ for glacial ice [*Bogorodsky et al.*, 1985]. Thus, the wave speed in low-loss media as ice is given by

$$v = \frac{c_0}{\sqrt{|\varepsilon|}} \approx \frac{c_0}{\sqrt{\varepsilon'}} \quad (3.1.4)$$

with $c_0 = 2.998 \cdot 10^8 \text{ m s}^{-1}$ the speed of EM waves in vacuum. Magnetic permeability $\mu = 1$, since ice is a non-magnetic material.

For a plane reflecting interface the reflection coefficient, ruling the power of the reflected signal, can be determined by the dielectric permittivities ε_1 and ε_2 of layer no. 1 and no. 2:

$$R = \frac{\sqrt{\varepsilon_2} - \sqrt{\varepsilon_1}}{\sqrt{\varepsilon_2} + \sqrt{\varepsilon_1}} \quad (3.1.5)$$

In the case of one narrow layer ε_2 embedded in a material with ε_1 , Equation (3.1.5) must be written as:

$$R = \frac{\sqrt{\varepsilon_2} - \sqrt{\varepsilon_1}}{\sqrt{\varepsilon_2} + \sqrt{\varepsilon_1}} 2 \sin \frac{2\pi l}{\lambda_m} \quad (3.1.6)$$

[*Kanagaratnam et al.*, 2001], where l is the thickness of the embedded layer and λ_m the wavelength in it. Note that this applies to monochromatic waves only. Thus, the magnitude of the

reflection coefficient increases with increasing dielectric contrast, yet it is modulated by a sinusoidal term related to layer thickness and wavelength. Considering glaciological conditions, Equation (3.1.6) applies to narrow ice lenses, arising e.g. from melt events, and to volcanic ash layers embedded in firn or ice.

In glaciological research, GPR has been used to map bedrock topography as well as internal layering of the ice sheet. For mapping the bedrock and for inferring layering of the deeper parts of the ice sheet, low frequencies of typically 5–200 MHz have to be utilized, yielding a larger penetration depth at the expense of vertical resolution. Contrarily, for investigation of internal layering in the upper 10–100 m higher frequencies are used, usually between 400–1000 MHz, resulting in a higher resolution of closely spaced layers. In firn and ice these internal layers arise from changes in density or in conductivity. The latter affect the imaginary part ϵ'' of the dielectric permittivity, occurring mainly in deeper parts of the ice sheet, whereas density changes affect the real part ϵ' [e.g. Kovacs *et al.*, 1995] and tend to dominate in the upper hundreds of meters [Fujita *et al.*, 1999]. As a third mechanism changes in crystal-orientation fabrics have been discussed, which mainly affect the deeper parts of the ice sheet [Matsuoka *et al.*, 2003].

Horizons with different densities are due to depositional stratigraphy, e.g., separating winter- and summer-layers. Single high-density layers occur after surface melt or intense winds, resulting in a glazed surface with higher density than the underlying snow or firn. When fresh snow falls onto this glazed surface, the layer is preserved in the subsurface, exhibiting a higher density which is seen as a reflection horizon in the radargram. In the dry-snow zone density changes are due to firn compaction from the pressure of the overlying snow column and due to depositional stratigraphy. Layers with different conductivities arise from acidic impurities mainly after major volcanic eruptions [Hammer, 1980]. The origin of radar layers in this study will be discussed in section 3.3.2.

The processes forming the observed layers in GPR records take place at the surface at approximately the same time, where the submergence rate of the isochronal surface is determined by interaction of the flow field and the surface accumulation rate [Gudmandsen, 1975]. Thus, these layers can be regarded as isochrones [among others Eisen *et al.*, 2004; Vaughan *et al.*, 2004].

3.1.2 GPR: Data acquisition and processing

In this study a commercial RAMAC (Malå Geoscience, Sweden) radar unit transmitting a monopulse was used. The parameters used for recording are listed in Table 3.1. The bistatic, shielded antenna with a center frequency of 500 MHz, housed in a plastic box, was mounted to a Nansen sledge pulled by a snow vehicle at an average speed of 5 km h⁻¹. Traces were recorded every 0.5 m triggered by an odometer, and the antenna was connected to the central unit via

fibre-optic cables. GPR data were stored on a Husky Px5 personal computer and after the survey saved on CD-ROM, together with GPS data. The acquisition allows for a theoretical vertical resolution in firm of ~ 0.1 m (i.e., $\frac{\lambda}{4}$ with λ the wavelength in firm, assuming $v_{firm} = 2 \cdot 10^8$ m s⁻¹). Actual accuracy can decrease to ± 0.2 m ($\pm \frac{\lambda}{2}$) due to noise present in the radargrams [Eisen *et al.*, 2004]. Simultaneously with the GPR data differential GPS data were collected at a sampling interval of one second. The roving station was mounted to the snow vehicle and the reference station was located at the respective field camp during the expeditions.

Table 3.1: Acquisition parameters of GPR surveys in this study

Parameter	Value
Center frequency	500 MHz
Time window	400 ns
Samples per trace	2048
Sample frequency	5120 MHz
Stacks	8
Trace increment	0.5 m
Offset TX–RX	0.18 m

GPR data were processed using Paradigm Geophysical Software FOCUS, applying the following steps:

- Time offset:
Data were corrected for the arrival of the direct wave (i.e., the wave travelling through the air from the transmitter to the receiver). The time offset was calculated by dividing the offset between TX–RX by the wave speed in air. Thus, the arrival time of the direct wave was taken as zero reference for the subsequent reflections.
- Stacking:
In order to increase signal-to-noise ratio, 10-fold horizontal stacking was applied, thus averaging out noise and enhancing the signal.
- Automatic gain control:
Automatic gain control (AGC) was applied to account for energy loss due to spherical divergence in the deeper parts of the radargram. This technique norms the energy of each trace according to the mean energy of the time window in which AGC is applied. Here, time windows between 20–30 ns were chosen.
- Filtering:
Filtering made use of a bandpass butterworth filter of sixth order. The lower cut-off

frequency was set to 350 MHz and the higher cut-off frequency to 850 MHz. These values have been obtained after testing several combinations of filters and cut-off frequencies.

Figure 3.1 exemplarily depicts a processed radargram together with the corresponding surface-elevation plot of the data obtained in the Antarctic summer season 2003/2004 on Potsdam Glacier. From the processed GPR data internal reflection horizons (IRHs) were tracked throughout the profiles where possible, using Landmark Open-Works release 2003 software and REFLEXW (Sandmeier Scientific Software, Karlsruhe, Germany). Tracking was done semi-automatically by exploiting the coherency of the signal (minimum, maximum, or zero amplitude), with manual correction in the parts of low signal-to-noise ratio. Despite the use of the automatic tracking algorithm, not all IRHs could be traced throughout the GPR profiles but are lost within the time window of the direct wave or where layers are spaced too closely to resolve them individually. In order to convert the tracked IRHs from TWT to depth, information about the velocity in the subsurface is needed. Due to the lack of CMP data in this study, firn-core parameters have been used to establish a model yielding TWT versus depth. More information will be given in section 3.3.1, after the introduction of firn-core studies required to obtain a velocity-depth distribution for the radar waves.

3.1.3 GPS

Here, kinematic GPS (Global Positioning System) measurements have been carried out simultaneously with GPR profiling. GPS was also used for accurate determination of the positions of firn-core drill sites. In principle, GPS utilizes a receiver sensing the signals of at least four GPS satellites and measuring the travel time from the respective satellite to the receiver. Thus, the position of the receiver in space and time is obtained. Details are given in literature, e.g. *Hofmann-Wellenhof et al.* [2001]. In glaciology, GPS has been applied to study the motion and velocity of ice streams, postglacial rebound, dynamics of ice shelves, and surface-elevation of ice sheets as well as thickness changes [among others *Tregoning et al.*, 1999; *Capra et al.*, 2000; *Hamilton et al.*, 1998]. Linking GPR and GPS provides accurate information of the position of GPR tracks and along-track surface elevation [*Urbini et al.*, 2001].

GPS data were processed at the Institut für Planetare Geodäsie, Technische Universität Dresden, using GPSurvey software with default parameters. The movement of the respective reference stations employed on a flowing glacier was taken into account. Processing yields GPS time, longitude, latitude, and elevation along the radar profiles where elevation data are given in heights of World Geodetic System 1984 ellipsoid (WGS84). Accuracy is within some millimeters to centimeters for longitude and latitude and within some centimeters for the elevation.

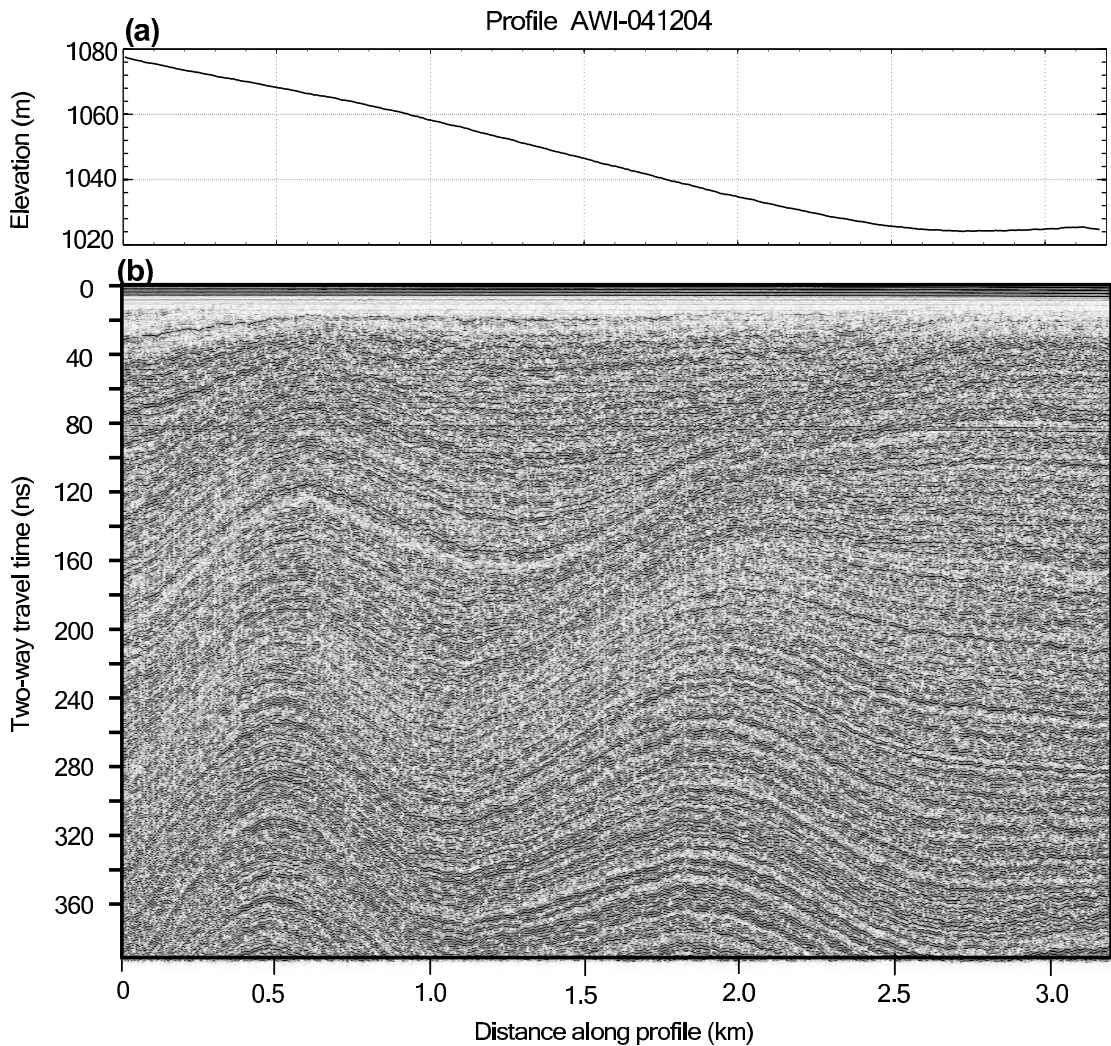


Figure 3.1: (a) Elevation (WGS84) along profile AWI-041204 (unpublished data from Potsdam Glacier, 2004). (b) Processed radargram of profile AWI-041204. Grey scale refers to amplitude of the signal. The total record length of 400 ns is shown.

3.1.4 Combining GPR and GPS data

GPR and GPS data have to be combined such that each radar trace is assigned values of longitude, latitude, and elevation. The start and end points of the radar surveys coincide with GPS signals the positions of which were exactly determined from GPS measurements. Furthermore the start and stop time of GPR data acquisition was noted in the field protocol for each GPR profile. In order to exactly determine the time interval during which radar-data acquisition took place, several files were extracted from the processed GPS data, including time–longitude–latitude, time–elevation, time–velocity (i.e., speed of the snow vehicle), distance–elevation, and distance–velocity. By comparing time–velocity and distance–velocity, intervals of radar-data acquisition could easily be recognized, assuming a speed of the snow vehicle between

2–8 km h⁻¹ (\sim 0.6–2.2 m s⁻¹). Thus, the respective time periods were extracted from the processed GPS data files, together with the corresponding values of latitude, longitude, elevation, and distance along-profile, using adapted scripts established at the Institut für Planetare Geodäsie, TU Dresden (S. Roemer, personal communication, 2005). The start and stop positions of these files were checked by comparison with the positions of the GPS signals. From the total distance along-profile obtained from the GPS data, a corrected trace interval $\Delta x'$ was calculated for the radar data, assuming equidistant traces:

$$\Delta x' = \frac{x_{GPS}}{nt} \quad (3.1.7)$$

where x_{GPS} is the total distance from GPS data and nt the number of traces of the GPR profile. The equidistant spacing may not be true throughout all profiles, however, this introduces only minor errors that can be neglected when compared to other error sources (discussed in Paper II and briefly summarized in section 3.3.3). Using Equation (3.1.7), each trace was assigned a modified position, fitting the profile length to the GPS distance. Generally, the values of $\Delta x'$ agreed within 0.01–0.03 m with the original trace interval $\Delta x = 0.5$ m with the largest deviation found to be 0.05 m. Such deviations most likely result from sliding of the odometer on the surface, thus leading to erroneous length intervals along-profile when calculated from Δx .

After correction using Equation (3.1.7), the GPR horizons as well as the GPS data were resampled at 5 m spacing of subsequent traces and waypoints, respectively. This value was chosen in order to account for the 10-fold stacking of the GPR data during processing, originally spaced by \sim 0.5 m. Moreover, deviations from non-equidistant spacing of individual traces are assumed to be averaged out by this technique. Furthermore GPS positions are not available for each (unstacked) trace, as can be concluded from the sampling interval of GPS tracking and the speed of the snow vehicle. Hence, for each profile a GPR file was obtained, giving values of distance and TWT, and a corresponding GPS file, giving likewise distance (equal to the values of the GPR file), longitude, latitude, and elevation. For the combination of these files the offset of 5 m between GPS and GPR antenna was taken into account. Finally, each radar trace at 5 m spacing was assigned longitude, latitude, and elevation from the corresponding GPS record.

3.2 Firn cores and snow pits

To facilitate the interpretation of the radar data and to date the tracked internal layers, shallow firn cores were drilled along the radar profiles, their depth varying between 12–13 m. At several drilling sites furthermore snow pits were dug, being 2 m deep and probed with 40 samples per pit.

The firn cores and snow samples were transported in frozen condition to AWI Bremerhaven and analyzed in the cold laboratory. Analysis of the snow samples consisted of determination

of the electrolytic conductivity of the melted samples. Prior to this method, measurement of the stable oxygen isotope ^{18}O was carried out by mass spectrometry, yielding $\delta^{18}\text{O}$ profiles for the snow pits, where $\delta^{18}\text{O}$ denotes content of ^{18}O relative to ^{16}O of standard mean ocean water. The density of the snow samples was determined in situ by weighing the samples and calculating ρ_{sample} from the known volume of the probing cylinders. Snow-sample data were used to link firn-core data to the surface due to minor core quality in the upper 1–2 m of drilling.

Analyses of firn cores covered determination of dielectric parameters by dielectric profiling (DEP) and measurement of density using gamma-attenuation profiling (GAP).

The DEP technique is applied by moving two curved electrodes along the firn core, measuring the real dielectric permittivity ϵ' and the electrical conductivity σ . The curved-electrode setup follows the design of a parallel-plated capacitor, but is more complicated to treat. Details and discussion are given by *Wilhelms* [1996]; *Wilhelms et al.* [1998]. The frequency used to measure the dielectric parameters is 250 kHz, thus being representative for radar frequencies up to the GHz range [*Wilhelms*, 1996].

GAP is performed using a gamma densimeter [*Wilhelms*, 1996]. A radioactive source (e.g. ^{137}Cs) emits monochromatic gamma radiation, which is collimated to a beam of 2 mm and radiated through the firn or ice core, along its diameter. The beam is collimated again after passing through the ice, and its intensity is measured using a scintillation detector. The electrons in the ice column scatter the photons of the radiation beam, thus weakening it according to Beer's Law:

$$I_d = I_0 e^{-\alpha d \rho} \quad (3.2.1)$$

with α the mass absorption coefficient of the material (firn/ice), d the diameter of the core, ρ the density, I_d the measured intensity after the beam passed the ice core, and I_0 the intensity of the emitted beam. Simultaneously the core's diameter is measured with a laser beam. Diameters have been controlled manually every 100 mm using a sliding caliper. Thus, from Equation (3.2.1) ρ can be calculated. Along the firn cores DEP was performed every 5 mm and GAP every 2 mm, yielding high-resolution profiles of dielectric parameters and density. Errors for these methods are given by *Wilhelms* [1996] and are briefly summarized in Paper II. Furthermore $\delta^{18}\text{O}$ was determined at samples of 30 mm size, similar to the snow-sample analysis. An example of firn-core parameters is depicted in Figure 3.2, the firn core was drilled in the Antarctic season 2003/2004 in the accumulation zone on Potsdam Glacier at an elevation of 1008 m.

The $\delta^{18}\text{O}$ -profiles of the firn cores were used to establish depth–age scales by counting the peaks which indicate summers [e.g. *McMorrow et al.*, 2004]. Not all firn cores exhibited a $\delta^{18}\text{O}$ -profile with pronounced maxima and minima, these were neglected due to the ambiguities introduced by their dating. From the depth–age scales and the density profiles annual accumulation rates were determined for all dated firn cores.

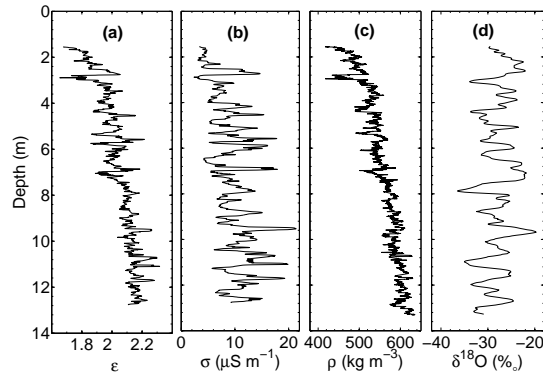


Figure 3.2: Measured parameters of FB0404: (a) Real part of dielectric permittivity, (b) electrical conductivity, (c) density (GAP), (d) $\delta^{18}\text{O}$. Unpublished data from Potsdam Glacier.

3.3 Combination of GPR and firn-core data

The combination of GPR data and firn-core data provides valuable information about several aspects of glaciological research. Using appropriate models derived from dielectric parameters and the density distribution, the tracked IRHs can be converted from two-way travel time to depth and from depth to cumulative snow mass. Moreover, the combined analysis of GPR horizons and firn-core parameters allows to highlight the origin and nature of specific IRHs in the radargrams at drilling locations. A variety of modeling studies has been carried out by several authors in order to study the origin of reflections seen in the radargrams, based on synthetic radargrams derived from firn-core properties [among others *Eisen et al.*, 2004, 2006; *Miners et al.*, 2002]. As this work focuses on the application of GPR for the purpose of accumulation studies, the most important result of the combination of GPR and firn cores yields the determination of accumulation rates from IHRs that are dated by reference firn cores. An outline of these procedures is given below.

3.3.1 Conversion of radar layers to depth and cumulative mass

The tracked IRHs are available in the time-domain, i.e., giving information about the two-way travel time of the signal to the IRH along the profiles. In order to derive their distribution with depth, information about the propagation velocity of the radar waves in the subsurface is mandatory, as already explained in section 3.1.2. Equation (3.1.4) shows that the velocity can be calculated from the DEP-derived values of dielectric permittivity ϵ' . As ϵ' is given in steps of 5 mm, the interval velocity for each depth-interval measured along the firn cores can be calculated from Equation (3.1.4). Integration of the obtained velocity-depth distribution yields a

model for TWT–depth, following the procedures of *Eisen et al.* [2002]. By applying this model to the tracked IHRs they can be converted from TWT to depth.

For the determination of accumulation rates the cumulative mass of the firn column up to the depth of the IRH at each point along-profile needs to be known. To this end, the firn-core derived profiles of density are integrated over depth, establishing a model for cumulative mass–depth. This model is likewise applied to the tracked IRHs, hence, from their depth values along-profile the distribution of cumulative mass is derived. Figure 3.3 depicts the models used in this study obtained from the respective firn cores in the two investigation areas.

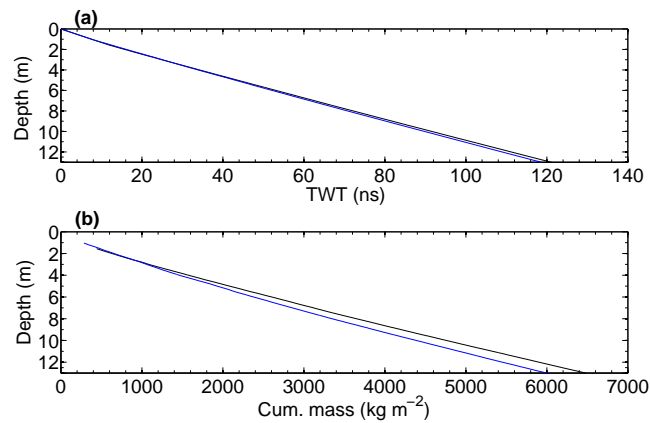


Figure 3.3: (a) Models for TWT–depth obtained from firn-core studies on Potsdam Glacier (black) and near Kottasberge (blue); (b) Models for cumulative mass–depth from firn-core studies on Potsdam Glacier (black) and Kottasberge (blue)

The model calculation is based on the mean profiles of density and dielectric permittivity of all firn cores of the respective area of investigation, since there is no further information about lateral variation of these variables between the drilling sites. In Paper II the deviation of density profiles from two firn cores (the one with the highest mean density and the one with the lowest mean density) from the average profile of ρ is discussed, finding only small differences. Thus, the errors introduced by actual differences from the mean values are negligible compared to other error sources (discussed in the papers and briefly summarized below). In order to obtain a TWT–depth and cumulative mass–depth distribution for those parts of the IRHs that exceed the depth range of the firn cores, the models are extrapolated. Extrapolation was carried out up to 25 m below the surface, thus covering the deepest tracable IRH that could be dated by a reference firn core on Potsdam Glacier. More information about extrapolation is given in Paper II. Figure 3.5b shows several tracked IRHs together with their cumulative mass and depth distribution along the radargram of profile AWI-041204 depicted in Figure 3.1.

3.3.2 Origin of reflecting layers in radargrams

Once the radar data are converted to depth, a comparison between the depth of prominent reflections in the radargrams and firn-core parameters becomes possible, yielding information about the origin of layers seen by GPR. As explained before, the IRHs seen in GPR records are due to reflections at interfaces in the firn or ice where contrasts of density or conductivity occur. Figure 3.4 shows a comparison between the upper ~ 140 ns (13.5 m) of the processed radargram AWI-041204 (see Figure 3.1) and the profiles of density and conductivity of the firn core drilled at the start point of the GPR profile. From the depicted comparison it is obvious that some of the IRHs coincide with peaks in the density and some with peaks in conductivity. Yet for most of the IRHs density as well as conductivity show peaks, thus, it cannot be clearly stated whether these IRHs are due to density or conductivity changes. However, for peaks spaced less than ~ 0.2 m (i.e., the approximate vertical resolution of GPR profiling at 500 MHz) interferences between closely spaced peaks, whether in conductivity or in density or both, lead to the observed reflection, as is the case for the first two marked peaks from above, resulting in the same reflection band in the radargram.

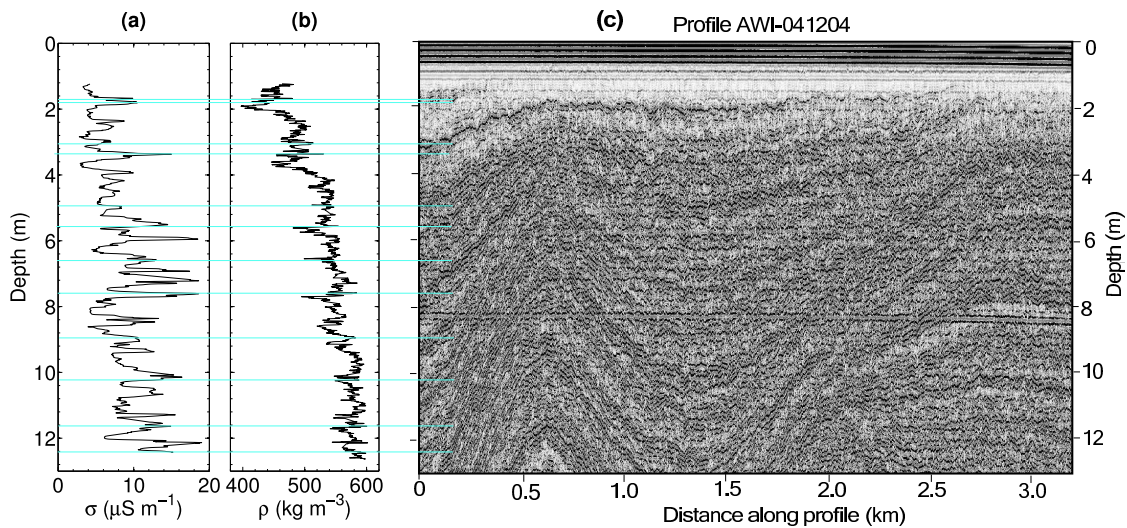


Figure 3.4: Comparison between GPR profile and firn-core parameters of the adjacent firn core (FB0402, data partly published in Paper II). (a) Conductivity, (b) density (from GAP), (c) radargram AWI-041204, the upper 13.5 m (~ 140 ns) of Figure 3.1 are shown here (unpublished data from Potsdam Glacier, 2004). Density/conductivity peaks are marked with a blue line and linked to prominent reflections in the radargram. Note that the horizon at ~ 8.5 m is an artifact stemming from a software failure.

Ice lenses with a higher density are observed in several snow pits and firn cores of this study, yet they are a very local phenomenon in the area of investigation. Thus, it can be concluded that the observed IRHs do not arise from ice lenses but from density fluctuations between different

depositional layers and from firn compaction. Apart from the eruptions of Pinatubo and Cerro Hudson, which are not easily seen in Antarctic firn cores from near-coastal sites (U. Ruth, personal communication, 2005), there are no significant volcanic eruption reported within the time period covered by the firn cores of this study. Thus, conductivity changes are possibly due to other acidic impurities, most likely stemming from marine sources [Kaczmarska *et al.*, 2004]. In total, both density and conductivity changes seem to be responsible for the observed layering on Potsdam Glacier, at least in the upper 12 m. This observation is in accordance with previous studies focusing likewise on shallow investigation depths [e.g. Nishio and Ohmae, 1985]. Yet the exact determination of the contributions of density and conductivity changes to the observed reflections requires usage of a density-and-conductivity mixed permittivity (DECOMP) [Wilhelms, 2005] obtained from DEP. The mathematical description thereof has to be inverted for density and conductivity [Wilhelms, 2005]. This is beyond the scope of this study, but detailed information can be found in Wilhelms [2005]; Eisen *et al.* [2006]. Generally, in the upper hundreds of meters density changes are more prominent than conductivity changes, since the transformation of snow to firn and to ice takes place within these depths. Therefore density is believed to have a dominating influence on reflections in this depth interval, as discussed by several studies [e.g. Fujita *et al.*, 1999; Eisen *et al.*, 2004]. Here, density peaks significantly contribute to the origin of radar layers, although influence of conductivity cannot be ruled out completely: application of a 2 cm running mean on the conductivity profile as suggested by Eisen *et al.* [2006] in order to reduce statistical noise removes only some of the conductivity peaks in Figure 3.4a.

Yet for the determination of accumulation rates from internal layers it is most important that the reflections have been shown to be of isochronal origin [Eisen *et al.*, 2004; Vaughan *et al.*, 2004] and can usually be tracked over several tens to hundreds of kilometers across the ice sheet. Thus, by assigning each IRH an age from a reference depth-age scale, area-wide accumulation rates can be determined.

3.3.3 Accumulation rates along GPR profiles

From section 3.2 it follows that the dated firn cores can be used to derive annual accumulation rates and interannual variability. Hence, at the drilling sites the *temporal* variability of accumulation rates is available at high resolution. In order to obtain GPR-derived accumulation rates and to address the *spatial* variability, the depth-age scale of a reference firn core has to be transferred to the tracked and converted IRHs.

As demonstrated in Figure 3.5 this is achieved by comparing the depth values of the IRHs at the drilling site to the depth-age scale of the adjacent firn core, assigning each IRH an age. This age can be compared to the dating as derived from other dated firn cores along the GPR profile where possible, following the test of isochronal accuracy given by Spikes *et al.* [2004]. From the

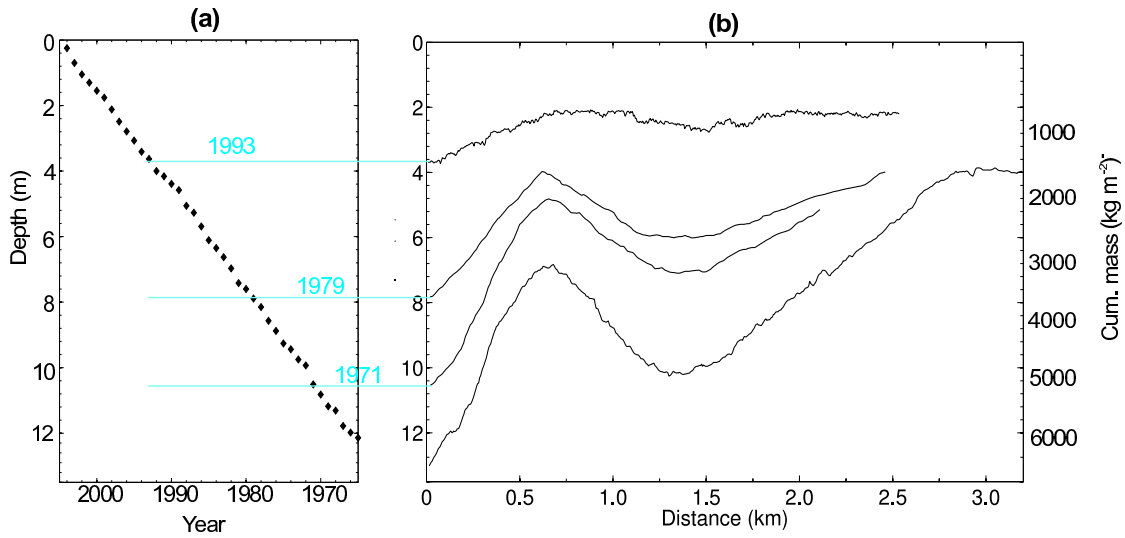


Figure 3.5: (a) Left: Depth-age scale of FB0402. (b) Tracked IRHs along profile AWI-041204 (see Figure 3.1). The distribution of cumulative mass and depth is shown. Comparing the depth of the IRHs at $x = 0$ km with the depth-age scale depicted in (a) yields ages of the IRHs.

ages and the distribution of cumulative mass of selected IRHs accumulation rates along-profile can be determined by dividing the difference in cumulative mass by the age difference:

$$a_{12} = \frac{\Delta m}{\Delta t} = \frac{m(\text{IRH2}) - m(\text{IRH1})}{t(\text{IRH1}) - t(\text{IRH2})} \quad (3.3.1)$$

where IRH2 is older (deeper) than IRH1, and a_{12} denotes the accumulation rate over the time period Δt (t in years AD). The same procedure yields accumulation rates in relation to the age of the surface at the time of data collection.

Hence, from dated IRHs a *spatial* distribution of accumulation between firn-core drilling sites is obtained, giving information about the spatial variability along the GPR profile. Equation (3.3.1) implies that from dated IRHs *mean* accumulation rates for the respective time periods Δt between the IHRs are derived - in this study some ten years. Using statistical analysis, the spatial representativity of firn-core derived accumulation rates for the area of investigation can be assessed from the GPR data. Moreover, the calculation of correlation length of spatial accumulation series yields valuable information concerning the validation of satellite-based ice-mass changes which are averaged over several hundreds of kilometers. In summary, the combination of firn-core studies and GPR profiles provides a useful method for the determination of *temporal* as well as *spatial* variability of accumulation rates. The accumulation rates in the area of investigation of this study are analyzed and discussed in detail in the accompanying papers.

A general discussion of errors is given in Paper II and Paper III, comprising errors from tracking the IRHs, from conversion of TWT to depth and cumulative mass, errors in DEP and GAP measurements, and dating uncertainty. The latter makes up for the largest error source, thus, the mean accuracy of the accumulation data discussed in this study results as 10–15 %.

Chapter 4

Scope of papers

Paper I: Anschütz, H., O. Eisen, W. Rack, and M. Scheinert, 2006. Periodic surface features in coastal East Antarctica

Geophys. Res. Lett., 33, L22501, doi:10.1029/2006GL027871

This paper discusses the periodicity of the accumulation pattern on the main flow line of Potsdam Glacier, central DML, derived from GPR profiling and firn-core analysis. Surface elevation and topography are obtained from GPS data. Undulations of surface slope and accumulation pattern show a strong correlation which is further analyzed by means of auto- and cross-covariance functions. The statistical analysis emphasizes the highly periodic oscillations of both slope and accumulation. The observed features are therefore interpreted similarly to the megadunes known from the polar plateau, yet showing much smaller lateral extension and generally higher accumulation than the megadunes. Thus it is suggested that the observed undulations are likely caused by a special feedback system between atmosphere and cryosphere.

Paper II: Anschütz, H., O. Eisen, D. Steinhage, H. Oerter, and M. Scheinert, 2006. Investigating small-scale variations of the recent accumulation rate in coastal Dronning Maud Land, East Antarctica, accepted to *Annals of Glaciology*, 46

In this paper the spatial and temporal distribution of the recent accumulation rate on Potsdam Glacier in central DML is presented. Spatial variability for the time periods 1970-1980, 1980-2004, and 1970-2004 is very high, as expressed by one-fold standard deviations of nearly 50 % of the respective mean values. Temporal variations obtained from the area-wide mean values between 1970-1980 and 1980-2004 are much less than spatial variations. The high spatial variability is likely explicable by windborne redistribution of blowing snow, following the findings given in Paper I. Accumulation rates are decreasing in the direction of glacier flow, in accordance with former observations showing a large blue-ice area farther downstream. The vicinity of the blue-ice area explains why the results presented here are less than findings from large-

scale compilations. Interannual and decadal-scale variability of accumulation is furthermore obtained from two dated firn cores. Implications of the results for interpretation of satellite data are discussed.

Paper III: Anschütz, H., D. Steinhage, O. Eisen, H. Oerter, and L. Eberlein, 2006. Temporal variation of accumulation patterns in western and central Dronning Maud Land, Antarctica

submitted to *Journal of Glaciology*

The spatial and temporal variations of accumulation rates near Kottasberge in western DML are presented and discussed. A comparison with previous studies in this region is given as well as a comparison with the spatio-temporal behaviour of accumulation rates on Potsdam Glacier which has been discussed in detail in Paper II. Accumulation rates are far smoother near Kottasberge than on Potsdam Glacier. Yet interannual variability at Kottasberge obtained from four dated firn cores is likewise very high. Pointwise analysis of temporal variations along the GPR profiles reveals that the values are not constant, but vary according mainly to variations in spatial variability and in surface slope. Therefore it is concluded that temporal and spatial variations are linked on small spatial scales of some ten kilometers, suggesting influences from local-scale near-surface wind pattern and glacier flow.

Chapter 5

PAPER I

Anschütz, H., O. Eisen, W. Rack, and M. Scheinert, 2006. Periodic surface features in coastal East Antarctica

Geophys. Res. Lett., 33, L22501, doi:10.1029/2006GL027871.

Copyright 2006 American Geophysical Union

Reprinted by permission of the American Geophysical Union



Periodic surface features in coastal East Antarctica

Helgard Anshütz,¹ Olaf Eisen,^{1,2} Wolfgang Rack,¹ and Mirko Scheinert³

Received 21 August 2006; revised 25 September 2006; accepted 3 October 2006; published 25 November 2006.

[1] We found evidence for highly periodic dunes in a near-coastal area of Dronning Maud Land, East Antarctica. Analysis of accumulation patterns, derived from ground-penetrating radar (GPR) internal layering, and GPS-based characteristics of surface topography, by means of auto- and cross-covariance, indicate quasi-harmonic oscillations of surface undulations, surface slope, and accumulation. The dunes occur at an elevation range of 1000–1350 m with the dominant wavelength of 5 km and undulations of ~ 10 m. Accumulation and slope are anticorrelated at zero lag, with a mean annual accumulation of some $140 \text{ kg m}^{-2} \text{ yr}^{-1}$ and variations on the order of $\pm 100 \text{ kg m}^{-2} \text{ yr}^{-1}$. Our findings have implications for studies aiming at the mass balance of coastal areas in Antarctica. **Citation:** Anshütz, H., O. Eisen, W. Rack, and M. Scheinert (2006), Periodic surface features in coastal East Antarctica, *Geophys. Res. Lett.*, *33*, L22501, doi:10.1029/2006GL027871.

1. Introduction

[2] Undulating features of surface topography and snow accumulation are a well-known phenomenon throughout Antarctica. Covarying undulations in topography, surface slope, and accumulation pattern have been reported since the earlier days of Antarctic research. *Black and Budd* [1964] report oscillations in the accumulation pattern derived from stake readings in Wilkes Land. Their profiles range from 180–380 km inland at an elevation range of 1000 to 3000 m. Surface slope along their stake line also shows oscillations, related to those in accumulation. *Pettré et al.* [1986] observed undulating patterns in accumulation in Terre Adélie, with a wavelength of 40 km. In order to explain those features they suggested a gravity-inertia wave at the break of slope. However, their stakes are spaced at intervals of 10 km so they are not able to derive any small-scale variations on the order of only a few kilometers. *Goodwin* [1990] discusses the influence of katabatic winds and the dependence of accumulation rates on surface aspect. He associates locally higher accumulation rates with the occurrence of longitudinal dunes, with lateral dimensions of 10–100 m, at elevations between 1870–2230 m. Referring to *Black and Budd* [1964], he furthermore explains that circulations forced by meso-scale topography modify wind flow induced by broad-scale orography, offsetting the accumulation minima to the West with respect to the

elevation maxima. Although these earlier observations indicate dune-like patterns in more coastal areas, one has to be aware that they are based on stake readings with stake spacing of some 100 m or even more, thus lacking small-scale continuity as well as high-precision elevation data due to the lack of GPS equipment. All these observations are expressions of the generally accepted process that blowing snow tends to accumulate in local depressions, whereas local rises experience less accumulation or even ablation (see *King et al.* [2004] for a recent summary). Surface slope in the prevailing wind direction is a key parameter in the description of this process [*Frezzotti et al.*, 2002a].

[3] The probably most stunning phenomenon of interaction between accumulation distribution and surface topography are the megadune fields on the East Antarctic plateau, covering areas of roughly 500 000 km². Detailed descriptions were derived from satellite imagery showing the ripple-like patterns extending over hundreds of kilometers [*Fahnestock et al.*, 2000]. Megadunes are characterized as gentle but highly regular undulations on the surface, whose genesis is ruled by an unusual feedback mechanism between cryosphere and atmosphere [*Frezzotti et al.*, 2002a]. Wavelengths are on the order of a few kilometers and amplitudes of a few meters, their subparallel crests extending over several hundred kilometers. Increased accumulation occurs on the windward side and less accumulation on the leeward side, thus producing a dune-like nearly-periodic accumulation pattern related to the surface topography [*Frezzotti et al.*, 2002a]. Windward slopes are often covered with severe sastrugi, whereas on the leeward faces and in the interdune troughs glazed surfaces dominate surface characteristics in snow-megadune areas [*Frezzotti et al.*, 2002b]. A recent map of megadune distribution, based on ICESat's GLAS altimetry data, locates megadune fields only in the interior of the East Antarctic ice sheet, several hundreds of kilometers away from the coast [*Shuman et al.*, 2006]. Moreover, *Scambos and Bauer* [2006] observed that megadunes occur in areas of moderate regional slope and low accumulation on the flanks of the ice sheet at an elevation range between 2500–3800 m.

[4] Here, we provide evidence that highly periodic surface undulations are also present near coastal sites. We present ground-based data from Potsdam Glacier in Neuschwabenland, the coastal area of Dronning Maud Land, East Antarctica. Ground-penetrating radar (GPR) data complemented by firm-core studies indicate a strongly oscillating accumulation distribution that varies with surface slope. Statistical analysis by means of auto- and cross-covariance functions of accumulation series as well as of surface slope emphasizes the periodicity. In order to avoid confusion we will address these features as periodic dunes, especially since they lack the lateral extent and extreme morphology of the megadunes. As explained above, the latter experience extremely low accumulation on the leeward sides, where

¹Alfred-Wegener-Institut für Polar- und Meeresforschung, Bremerhaven, Germany.

²Also at Versuchsanstalt für Wasserbau, Hydrologie und Glaziologie, ETH Zürich, Switzerland.

³Institut für Planetare Geodäsie, Technischen Universität Dresden, Dresden, Germany.

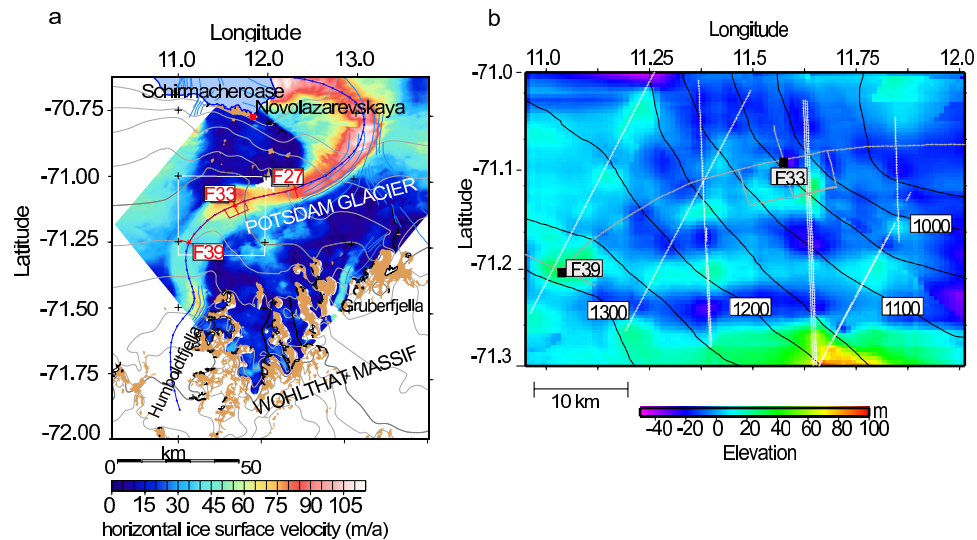


Figure 1. (a) Overview of the area of investigation. Dark line with dots: main glacier flow line; points marked Fxx: start/end points of the radar profiles along the main flow line; light (red) lines: additional GPR profiles. Distances from F39 to F33 and from F33 to F27 amount to 25 km each. Color scale indicates glacier-flow velocity [Bäffler *et al.*, 2002]. Flow direction is from F39 to F27. Light grey lines: elevation contour lines at 200 m spacing; dark grey line: 1000 m elevation contour line. The white rectangle corresponds to the area depicted in (b). (b) Undulations of elevation; color scale refers to differences between original and smoothed DEM. The DEM has been obtained from GPS (grey lines) and ICESat (white lines) data. Black lines indicate elevation contour lines at 50 m spacing (obtained from the smoothed DEM).

snow sampling reveals large grains and extensive depth hoar [Albert *et al.*, 2004; Frezzotti *et al.*, 2002b]. Comparable observations are not as pronounced or even missing in our study area near the Antarctic coast.

2. Area of Investigation and Data Set

[5] The study area is situated on Potsdam Glacier south of the Schirmacheroase and north of Wohlthat Massif (Figure 1a), about 120 km away from the ice-shelf edge. Wide areas of Potsdam Glacier are above 1000 m a.s.l. and have a mean annual temperature below -20°C . Ice thickness >1200 m in most parts of the glacier. Bedrock topography is generally smooth with some subglacial peaks [Damm and Eisenburger, 2005]. Generally the higher-elevation parts experience accumulation with the exception of small ablation areas around several nunataks. However, in the northeastern part of this glacier, near and east of the Schirmacheroase, a large ablation area is found [Bormann and Fritzsche, 1995, and references therein] that reaches up to the eastern Wohlthat Massif. Previous work in this area [e.g., Korth and Dietrich, 1996] consisted of geodetic-glaciological traverses to Humboldtjella and Gruberfjella (Figure 1a). From the InSAR analysis of ERS-1/2 satellite data, Dietrich *et al.* [1999] established a horizontal velocity vector field. In the area of investigation glacier flow is about $20\text{--}30$ m yr^{-1} at higher elevations and up to $70\text{--}80$ m yr^{-1} in the lower parts. Laterally convergent flow occurs at the lower elevations, whereas at the higher parts lateral divergence is observed [Bäffler *et al.*, 2002; Bäffler *et al.*, 2003].

[6] During the Antarctic summer season 2003/2004 radar surveys at a frequency of 500 MHz were carried out along a profile of 50 km length on the main glacier-flow line (Figure 1). Traces were recorded every 0.5 m. Simultaneously, kinematic GPS data were collected at 1 s intervals,

with the GPS equipment mounted to a snow mobile. An airborne radio-echo sounding survey near the main flow line was carried out as well. Snow pits and firn cores (12 m deep) complemented the field data, aiming for the determination of the recent accumulation rate. Along the firn cores measurements of density and dielectric profiling (DEP [Wilhelms, 2005]) were carried out in intervals of 5 mm as well as determination of $\delta^{18}\text{O}$ in 3 cm intervals, which was used for dating. (A detailed description of data acquisition and processing is given by H. Anschütz *et al.* (Investigating small-scale variations of the recent accumulation rate in coastal Dronning Maud Land, East Antarctica, submitted to *Annals of Glaciology*, 2006, hereinafter referred to as Anschütz *et al.*, submitted manuscript, 2006).) From the processed GPR data two internal reflection horizons (IRHs) are tracked throughout the GPR profiles and dated by the $\delta^{18}\text{O}$ profile of one reference firn core. The respective dating uncertainty of each IRH amounts to ± 2 a. Combining the age and the respective cumulative mass of the IRHs yields accumulation rates. Surface topography is derived from the processed GPS data.

3. Accumulation Characteristics and Surface Features

[7] The time-integrated effect of ice flow interacting with a variable accumulation pattern is memorized in the internal-layer architecture [e.g., Arcone *et al.*, 2005]. Our processed radargrams clearly show undulations of several meters over few kilometers of the internal layer depths, larger than expected for this area (Figure 2). Firn-core data (Anschütz *et al.*, submitted manuscript, 2006) were input to convert GPR data from two-way traveltime (TWT) to depth [Eisen *et al.*, 2002]. Linking two continuous layers to the reference firn core provides estimates of along-profile

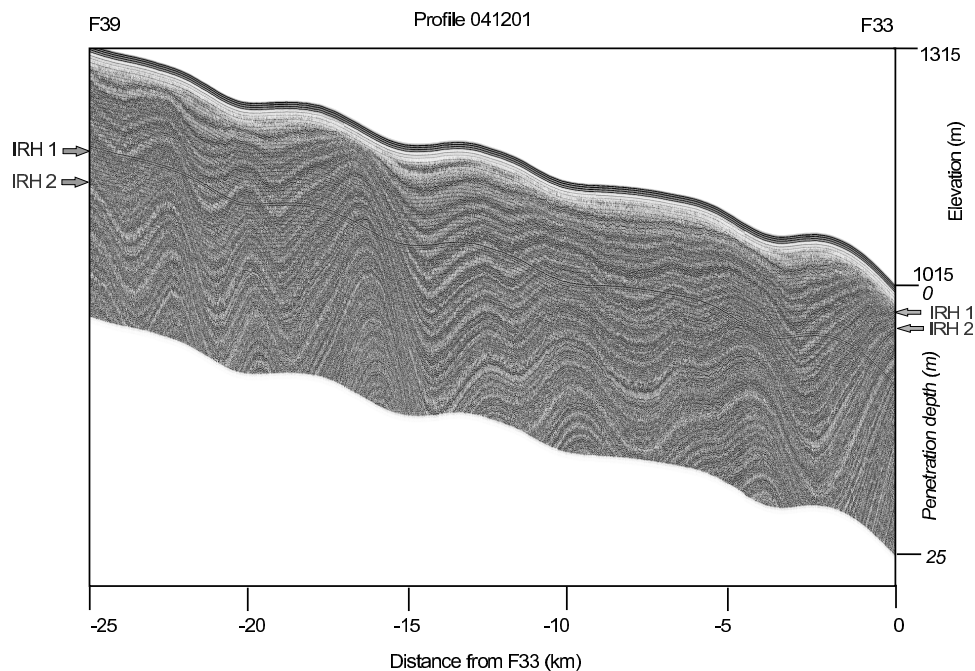


Figure 2. Processed radargram of profile 041201, going from F39 to F33 along the main flow line (see Figure 1). Arrows indicate the two tracked and dated IRHs. Note the vertically enlarged scale of the radar section in relation to the elevation scale.

accumulation (Anschütz et al., submitted manuscript, 2006) for the periods 1970–1980, 1970–2004, and 1980–2004, with a mean accumulation error of 12% (Figure 3c). Errors are mainly introduced by the dating uncertainty. However, this spatially systematic uncertainty only affects the temporal variability and the absolute accumulation values but not the spatial variability nor the undulations of the accumulation pattern and conclusions drawn in this study.

[8] The surface elevation declines from almost 1350 m a.s.l. in South-West to about 850 m a.s.l. in the North-East. On this decreasing trend a regularly undulating pattern is overlain, clearly visible in the linearly detrended surface elevation (Figure 3a) and in surface slope (Figure 3b). Topography undulations are around 10 m, and elevation maxima occur almost equidistantly at a 5 km interval. Beyond 7 km downstream of the central firn core (at F33, see Figure 1), towards a known blue-ice area, the undulations cease and surface slope is nearly constant.

[9] Undulations in GPR-layer depth coincide with the undulations in surface topography, but their peaks are displaced further downstream with increasing depth in relation to the local maxima in surface elevation. The accumulation pattern derived from the two dated IRHs (Figure 3c) shows a high spatial variability overlain on a generally decreasing trend in the direction of glacier flow down to 7 km beyond the central firn-core location. Although the accumulation oscillates less periodically than slope or surface elevation, it still seems regular.

4. Highly Periodic Dunes

[10] Other studies already reported anticorrelation of surface slope and accumulation [e.g., Black and Budd, 1964; Frezzotti et al., 2005]. In order to further examine

the periodicity described above, we calculated the auto-covariance (ACV) functions of the accumulation and the surface slope as well as the cross-covariance (CCV) between those variables (Figure 4). The pronounced regular side maxima in the ACV functions emphasize the presence of oscillations. The largest magnitude of the CCV function of slope and accumulation occurs at zero lag with a value of -0.62 , emphasizing that slope and accumulation are anticorrelated. Power spectral analyses of the accumulation and slope series reveal the wavelength of the features. The respective CCV function indicates a dominant wavelength at around 5.05 km. In all three spectra (auxiliary material) other wavelengths have much lower powers, and the respective main peaks are significant at the 99.7%-confidence level.¹ We therefore conclude that the observed surface undulations and accumulation variations are quasi harmonic and strongly linked to each other. These characteristics, being more detailed than reported in former analyses, remind of megadunes [Frezzotti et al., 2002a], although they lack the spatial extension of the megadune fields. Moreover, observation of surface structure and its variability is basically in accordance with the description of Frezzotti et al. [2002a], who report large longitudinal sastrugi on the uphill sides of the megadunes and glazed surfaces on downhill sides. Generally, the mean accumulation in this coastal area is higher than on the polar plateau and the differences between the leeward and windward surface features are not as pronounced as in the megadune areas. We likewise observed large sastrugi fields, associated with locally increasing surface elevation, whereas smoother surfaces tended to be located in troughs.

¹Auxiliary materials are available in the HTML. doi:10.1029/2006GL027871.

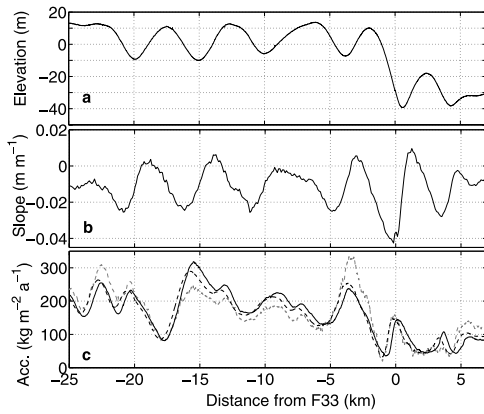


Figure 3. (a) Linearly detrended surface elevation, (b) surface slope, and (c) GPR-based accumulation pattern on the main flow line. The solid line in Figure 3c corresponds to the time period 1980–2004, the dashed to 1970–2004, and the dashed grey line to 1970–1980. Glacier flow is from left to right. Note that only features within the first 7 km downstream of the central firm core are shown.

[11] From the radargram along the uppermost 25 km of the main flow line (Figure 2) it is obvious that relative motion between the accumulation pattern and firm column takes place, as observed on the polar plateau [Frezzotti *et al.*, 2002a]. Buried crests of former dunes are slightly displaced to the crests of current surface dunes.

[12] By comparing the maxima in depth of the deepest continuous IRH (1970 ± 2 years) with those from the shallower continuous IRH (1980 ± 2 years) we can determine the relative migration velocities. From those phase lags between maxima in layer depth only half the velocity is derived due to interferences as demonstrated by Arcone *et al.* [2005] using trigonometric argumentation. Taking this into account, we calculated migration velocities which are basically in the range of glacier-flow velocities. However, uncertainties of this estimation, introduced by the horizontal placement of the troughs in depth distribution and especially by the dating uncertainty of the IRHs, prevent a clear prediction about possible dune migration from groundborne data. Analysis of SAR data from ERS-1/2 (April 1996) allows us to derive detrended elevation values along the main flow line which can be compared with the detrended surface elevation from the GPS data recorded during the expedition in January 2004 (Figure 3a). The detrended surface-elevation curve from the GPS data is displaced upstream in relation to the one derived from the SAR data (auxiliary material). From the displacements (peak-to-peak and trough-to-trough, respectively) we obtain mean migration velocities for the time period of 8 years (1996–2004). The mean relative migration velocity of the surface undulations results as 60 m yr^{-1} with a 1σ standard deviation of 20% in opposite direction to the glacier flow. The uncertainty of this estimation is about 8%. From Figure 1b it is obvious that the dunes are oriented mainly in East-West direction, thus introducing an angle of 25–45 degree between their orientation and the direction of the GPR profiles. Taking this into account, the obtained migration velocities reduce to values ranging from about 35–58 m yr^{-1} with an average velocity of 45 m yr^{-1} and a standard

deviation of 22%. However, the DEM indicating the orientation of the dunes (discussed below) should be considered with caution because of the sparse data base.

5. Dune Extension and Genesis

[13] Unlike the megadune fields, our dune-like patterns are not clearly visible in satellite imagery, e.g. MODIS. This can be explained by the generally higher accumulation, about one order of magnitude higher compared to the polar plateau, and the less pronounced differences in reflection characteristics in our case. Analysis of ICESat altimetry data (Release-12, -24, and -26, <http://nsidc.org/data/icesat>) combined with groundborne GPS data allows us to derive a preliminary digital elevation model (DEM) of the investigation area. After smoothing this DEM using a median filter and calculating the differences between the original and the smoothed DEM we conclude that the periodic dune patterns laterally extend several tens of kilometers parallel to the mean surface slope (Figure 1b). Between about 11.2 E and 12.0 E they are almost parallel to the mountain range of the Wohlthat Massif, but further west they bend towards the North/North-East. Assuming katabatic winds from the mountains of Wohlthat Massif, the dunes would be transverse to the main wind direction. Beyond the western edge of Wohlthat Massif the wind pattern follows the main surface slope and changes direction, resulting in a bent dune orientation. No meteorological data are available so far to prove these assumptions. Up to now there are no AWS installed nearby and model data from atmospheric models are not able to resolve small-scale near-surface wind patterns in this orographically complicated region (M. v. d. Broeke, personal communication, 2006). The analysis of wind pattern in this area in future field campaigns would be helpful to further explain the existence of the dunes.

[14] In principle, bedrock topography could also cause an undulating surface, which then changes the accumulation pattern. Yet bedrock topography from a nearby airborne radio-echo sounding does not indicate any regular features that could be responsible for the observed small-scale surface undulations [Damm and Eisenburger, 2005; D. Steinhage, personal communication, 2006]. We thus suggest that the periodic dunes are generated by a feedback system between

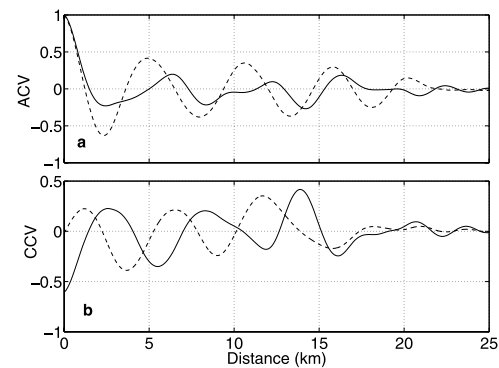


Figure 4. Auto-covariance functions (a) for surface slope (dashed line) and accumulation (solid line) and cross-covariance (b) between accumulation–slope (solid) and accumulation–detrended surface elevation (dashed).

atmosphere and cryosphere similar to the description by Frezzotti et al. [2002a] and Pettré et al. [1986], and not by dynamic influence of the bedrock topography on the surface.

[15] In summary, we conclude that undulations of surface slope interact with the wind pattern to generate highly regular dunes in this near-coastal area. This finding has implications for other coastal areas where similar periodic dunes exist. The regional representativity of firn-core interpretations in those areas is likely very limited, since orographic variations on the order of a few meters per kilometers significantly influence snow accumulation. Moreover, change detection for coastal areas is the focus of several remote sensing missions, like ICESat, GRACE, or Cryosat-2, aiming at Antarctica's continental mass balance. Although coastal accumulation patterns were expected to be complex due to wind action, as evident from blue ice areas, the occurrence of highly periodic dunes on small spatial scales further complicates the picture. Future studies in coastal areas should keep an eye on surface features and closely examine snow structure and surface topography in order to assess the distribution and magnitude of other dune patterns at coastal sites.

[16] **Acknowledgments.** Preparation of this work was supported by the Deutsche Forschungsgemeinschaft (DFG) through the VISA project, funded under grants Di 473/17 and Jo 191/8. O.E. was supported by the DFG "Emmy Noether"-scholarship EI 672/1. Comments from M. Frezzotti, T. Scambos, and C. Shuman significantly improved the manuscript.

References

- Albert, M., C. Shuman, Z. Courville, R. Bauer, M. Fahnestock, and T. Scambos (2004), Extreme firn metamorphism: Impact of decades of vapor transport on near-surface firn at a low-accumulation glazed site on the East Antarctic plateau, *Ann. Glaciol.*, *39*, 73–78.
- Arcone, S. A., V. B. Spikes, and G. S. Hamilton (2005), Stratigraphic variation within polar firn caused by differential accumulation and ice flow: Interpretation of a 400 MHz short-pulse radar profile from West Antarctica, *J. Glaciol.*, *51*(174), 407–422.
- Bäbfler, M., R. Dietrich, and C. Shum (2002), Investigation of ice dynamics at the grounding zone of an Antarctic ice shelf utilizing SAR interferometry, in *Proceedings of the Weikko A. Heiskanen Symposium in Geodesy 1–4 Oct 2002, Columbus, Ohio, USA*, edited by C. Jekeli and C. K. Shum, Ohio State Univ., Columbus.
- Bäbfler, M., R. Dietrich, and C. Shum (2003), Horizontal velocity field, strain analysis and grounding zone location for the area of Nivlisen ice shelf, Dronning Maud Land, poster presentation at FRINGE Workshop, Eur. Space Agency, Frascati, Italy, 1–5 Dec.
- Black, H., and W. Budd (1964), Accumulation in the region of Wilkes, Wilkes Land, Antarctica, *J. Glaciol.*, *5*, 3–15.
- Bormann, P., and D. Fritzsche (Eds.) (1995), *The Schirmacher Oasis, Queen Maud Land, East Antarctica, and Its Surroundings*, Justus Perthes, Gotha, Germany.
- Damm, V., and D. Eisenburger (2005), Ice thickness and sub-ice topography in Central Dronning Maud Land deduced by radio echo sounding, *Geol. Jahrb., Reihe B*, *97*, 109–127.
- Dietrich, R., R. Metzger, W. Korth, J. Polzin, and M. Scheinert (1999), Combined use of field observations and SAR interferometry to study ice dynamics and mass balance in Dronning Maud Land, Antarctica, *Polar Res.*, *18*, 291–298.
- Eisen, O., U. Nixdorf, F. Wilhelms, and H. Miller (2002), Electromagnetic wave speed in polar ice: Validation of the CMP technique with high-resolution dielectric profiling and gamma-density measurements, *Ann. Glaciol.*, *34*, 150–156.
- Fahnestock, M. A., T. A. Scambos, C. A. Shuman, R. J. Arthern, D. P. Winebrenner, and R. Kwok (2000), Snow megadune fields on the East Antarctic Plateau: Extreme atmosphere-ice interaction, *Geophys. Res. Lett.*, *27*(22), 3719–3722.
- Frezzotti, M., S. Gandolfi, and S. Urbini (2002a), Snow megadunes in Antarctica: Sedimentary structure and genesis, *J. Geophys. Res.*, *107*(D18), 4344, doi:10.1029/2001JD000673.
- Frezzotti, M., S. Gandolfi, F. L. Marca, and S. Urbini (2002b), Snow dunes and glazed surfaces in Antarctica: New field and remote-sensing data, *Ann. Glaciol.*, *34*, 81–88.
- Frezzotti, M., et al. (2005), Spatial and temporal variability of snow accumulation in East Antarctica from traverse data, *J. Glaciol.*, *51*(172), 113–124.
- Goodwin, I. (1990), Snow accumulation and surface topography in the katabatic zone of Eastern Wilkes Land, Antarctica, *Antarct. Sci.*, *2*, 235–242.
- King, J. C., P. S. Anderson, D. G. Vaughan, G. W. Mann, S. D. Mobbs, and S. B. Vosper (2004), Wind-borne redistribution of snow across an Antarctic ice rise, *J. Geophys. Res.*, *109*, D11104, doi:10.1029/2003JD004361.
- Korth, W., and R. Dietrich (1996), *Ergebnisse geodätischer Arbeiten im Gebiet der Schirmacheroase/Antarctica 1988–1993, Dtsch. Geod. Komm., Reihe B*, vol. 301, Bayer. Akad. der Wiss., Munich, Germany.
- Pettré, P., J. Pinglot, M. Pourchet, and L. Reynaud (1986), Accumulation in Terre Adélie, Antarctica: Effect of meteorological parameters, *J. Glaciol.*, *32*, 486–500.
- Scambos, T., and R. Bauer (2006), GPR and GPS data: Characteristics of snow megadunes and their potential effect on ice core interpretation, digital media, Natl. Snow and Ice Data Center, Boulder, Colo.
- Shuman, C., M. Fahnestock, T. Scambos, M. Albert, R. Bauer, and V. Suchdeo (2006), Antarctic megadunes characteristics from ICESat elevation data, *Geophys. Res. Abstr.*, *8*, 08686.
- Wilhelms, F. (2005), Explaining the dielectric properties of firn as a density- and conductivity mixed permittivity (DECOMP), *Geophys. Res. Lett.*, *32*, L16501, doi:10.1029/2005GL022808.

H. Anschütz, O. Eisen, and W. Rack, Alfred-Wegener-Institut für Polar- und Meeresforschung, Am alten Hafen 26, D-27568 Bremerhaven, Germany. (hanschuetz@awi-bremerhaven.de; oeisen@awi-bremerhaven.de; wrack@awi-bremerhaven.de)

M. Scheinert, Institut für Planetare Geodäsie, Technischen Universität Dresden, D-01062 Dresden, Germany. (mikro@ipg.geo.tu-dresden.de)

Periodic surface features in coastal East Antarctica: auxiliary material

Helgard Anschütz¹, Olaf Eisen^{1,2}, Wolfgang Rack¹, Mirko Scheinert³

Short title: AUXILIARY MATERIAL

¹Alfred-Wegener-Institut für Polar- und Meeresforschung Bremerhaven, Germany

²Versuchsanstalt für Wasserbau, Hydrologie und Glaziologie (VAW), ETH Zürich,
Switzerland

³Institut für Planetare Geodäsie, Technische Universität Dresden, Germany

Abstract. These pages comprise the auxiliary material to the publication *Periodic surface features in coastal East Antarctica*. We include a comparison between linearly detrended surface-elevation data obtained from GPS and from SAR, respectively. Furthermore we provide spectra of accumulation series as well as of surface-slope series and of the CCV function between those parameters.

Figure Captions

Figure 1. Detrended surface elevation on the main flow line obtained from GPS data (solid, 2004) and from ERS-1/2-SAR data (dashed, 1996). Note that the respective peaks and troughs of the GPS data are displaced upstream in relation to those of the SAR data. (Glacier flow is from left to right.)

Figure 2. Spectra of surface slope (a), accumulation (b), and of the cross-covariance function (c) between accumulation and slope. The solid lines denote the respective spectra, the dashed lines show the 3-fold standard deviations.

Figures

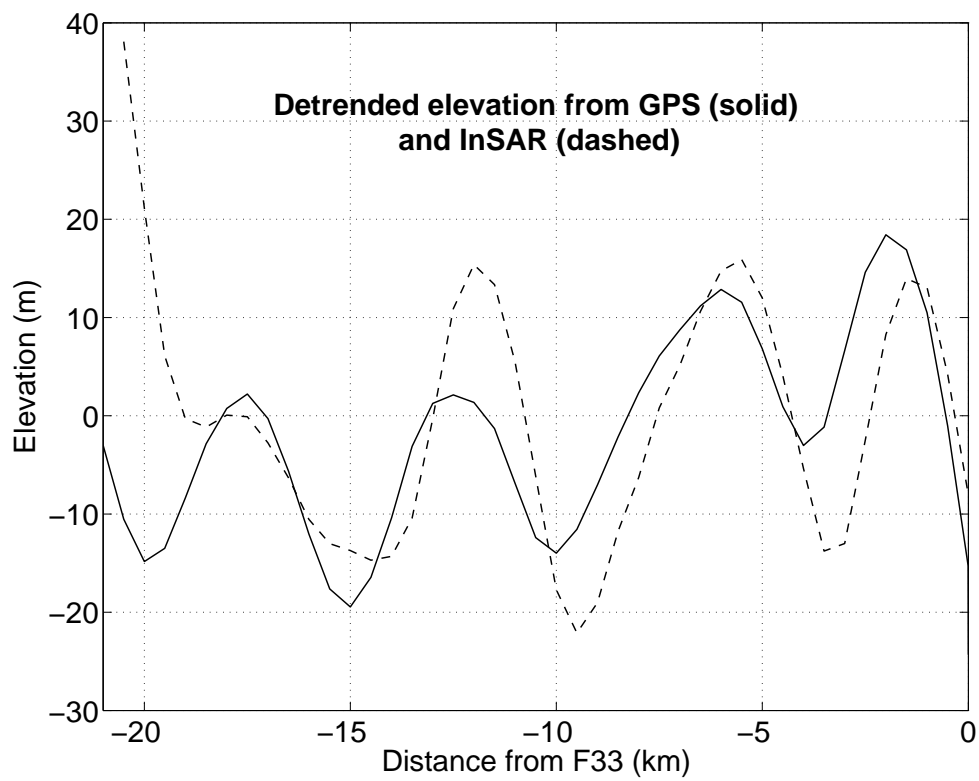


Figure 1. Detrended surface elevation on the main flow line obtained from GPS data (solid, 2004) and from ERS-1/2-SAR data (dashed, 1996). Note that the respective peaks and troughs of the GPS data are displaced upstream in relation to those of the SAR data. (Glacier flow is from left to right.)

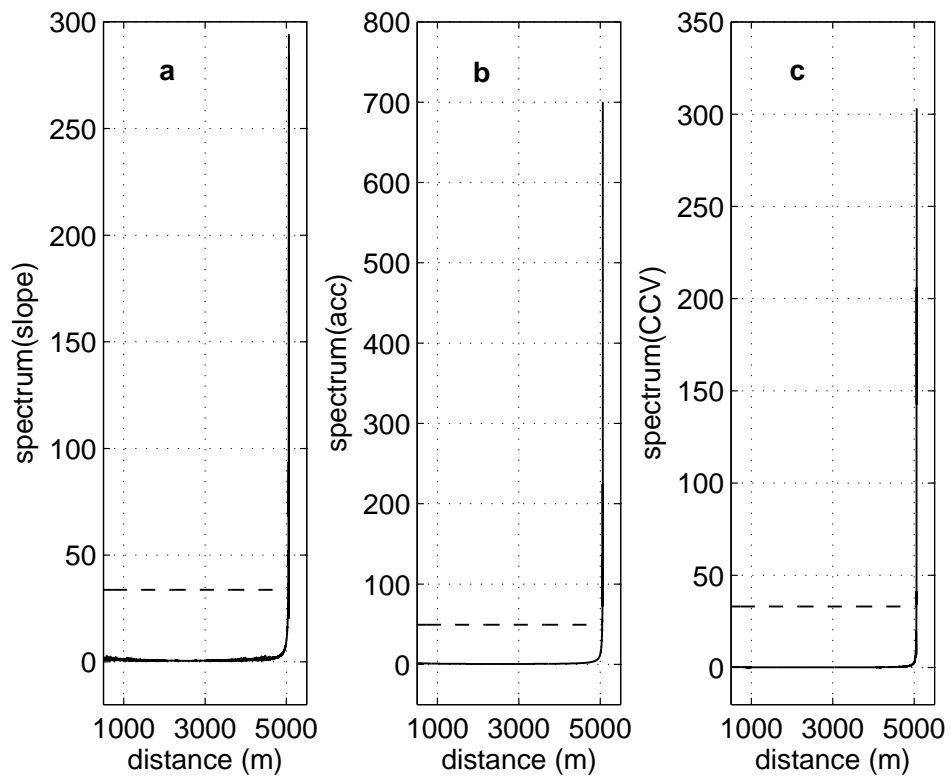


Figure 2. Spectra of surface slope (a), accumulation (b), and of the cross-covariance function (c) between accumulation and slope. The solid lines denote the respective spectra, the dashed lines show the 3-fold standard deviations.

Chapter 6

PAPER II

Anschütz, H., O. Eisen, D. Steinhage, H. Oerter, and M. Scheinert, 2006. Investigating small-scale variations of the recent accumulation rate in coastal Dronning Maud Land, East Antarctica,

accepted to *Annals of Glaciology*, 46

Reprinted by permission of the International Glaciological Society

Investigating Small-Scale Variations of the Recent Accumulation Rate in Coastal Dronning Maud Land, East Antarctica

Helgard ANSCHÜTZ,¹ Olaf EISEN,^{1,2} Hans OERTER,¹ Daniel STEINHAGE,¹ Mirko SCHEINERT³

¹*Alfred-Wegener-Institut für Polar- und Meeresforschung Bremerhaven, Germany*

E-mail: hanschuetz@awi-bremerhaven.de

²*Versuchsanstalt für Wasserbau, Hydrologie und Glaziologie (VAW), ETH Zürich, Switzerland*

³*Institut für Planetare Geodäsie, TU Dresden, Germany*

ABSTRACT. The accumulation rate on Potsdam Glacier, East Antarctica, and its spatial and temporal variations are examined using ground-penetrating radar, snow samples, and firn-core studies. Physical properties in snow samples and along firn cores provide distributions of density with depth, showing only small spatial variation. Counting of peaks in $\delta^{18}\text{O}$ along the firn cores yields an age–depth distribution that is transferred to the stratigraphy of isochronal internal layers observed with radar. From two radar horizons we determine the spatial accumulation pattern, averaged over the time periods 1970–1980 and 1980–2004. The shape of internal layers indicates an ablation area at the eastern margin of the investigation area. Accumulation rates show a very high spatial variability with a mean value of $141 \text{ kg m}^{-2} \text{ a}^{-1}$ for the time period 1970–2004 and a standard deviation of almost 50%. Mean temporal variation of only a few per cent throughout the investigated area for the observed time interval is much less than the spatial variations. The mean accumulation values are somewhat less than values reported before from this region. Accumulation pattern and surface topography are linked in a way indicating that windborne redistribution of snow significantly contributes to the observed spatial variations of accumulation rates. The accumulation data and their variability complement and validate present and future satellite studies of Antarctica's mass balance.

INTRODUCTION

Surface mass-balance studies of the Antarctic ice sheet are of vital importance for an enhanced understanding of the Earth's climate and its changes (Rignot and Thomas, 2002; van der Veen, 2002) as the polar regions are able to contribute significantly to global sea-level change (Wingham and others, 1998). It is therefore crucial to determine the mass fluxes of the Antarctic ice sheet, for example by using remote sensing techniques and satellite-based methods. Variations of accumulation and density on temporal and spatial scales also influence the relation between elevation changes and changes in gravity and mass. The knowledge of spatial and temporal patterns of ice-mass changes provides key information especially for the validation of the time-varying gravity field as sensed by GRACE (Scheinert and others, 2005). (For a general overview of the GRACE mission see Tapley and others (2004)). For this reason small-scale variations of the accumulation rate play a significant role and need to be investigated closely by groundborne operations.

Usually accumulation data are derived from firn cores, snow pits or stake readings (*e.g.*, Oerter and others, 2000; Kreutz and others, 2000; Isaksson and Karlen, 1994; Melvold and others, 1998). But they yield only information about the local accumulation rate at the probing location. In recent years, ground-penetrating radar (GPR) measurements have proved a useful tool to map relative variations in surface-mass balance over larger areas and connect snow pits and firn-core drilling sites (*e.g.*, Richardson and others, 1997; Pinglot and others, 2001; Rotschky and others, 2004; Sinisalo and others, 2003; Spikes and others, 2004). Internal reflection horizons (IRHs) detected by GPR can be used to match signals found in different firn cores along the GPR profiles and assist proper correlations between the firn cores. The

observed IRHs arise from contrasts of dielectric permittivity in the subsurface. In the upper hundreds of meters density has the most significant influence, affecting the real part of the dielectric permittivity (Fujita and others, 1999). IRHs are shown to be of isochronal origin (Eisen and others, 2004; Vaughan and others, 2004) and from their estimated age and a density-depth distribution the mean accumulation rate for a certain period can be calculated.

In this study, we present GPR and firn-core data from a relatively small area in East Antarctica where no reliable accumulation data of high resolution have been available so far. High frequency GPR measurements were carried out on Potsdam Glacier in Neuschwabenland, the coastal part of Dronning Maud Land (DML), during the Antarctic summer season 2003/2004. Shallow firn cores were drilled at selected locations along the radar profiles. Two internal reflection horizons are traced throughout several GPR profiles and dated by a reference firn core. The firn-core analyses give relations between traveltime–depth and density–depth that can be used to derive the regional accumulation pattern from these tracked IRHs.

STUDY AREA

The study area is located south of the Schirmacheroase and north of Wohlthat Massif (Figure 1a). Most parts of Potsdam Glacier are above 1000 m a.s.l. and have a mean annual air temperature below -20°C (Bormann and Fritzsche, 1995). The average ice thickness is more than 1200 m and subglacial topography is characterized by deep valleys with some subglacial highs (Damm and Eisenburger, 2005; Meyer and others, 2005). The surface elevation declines from almost 1350 m a.s.l. in the southwestern

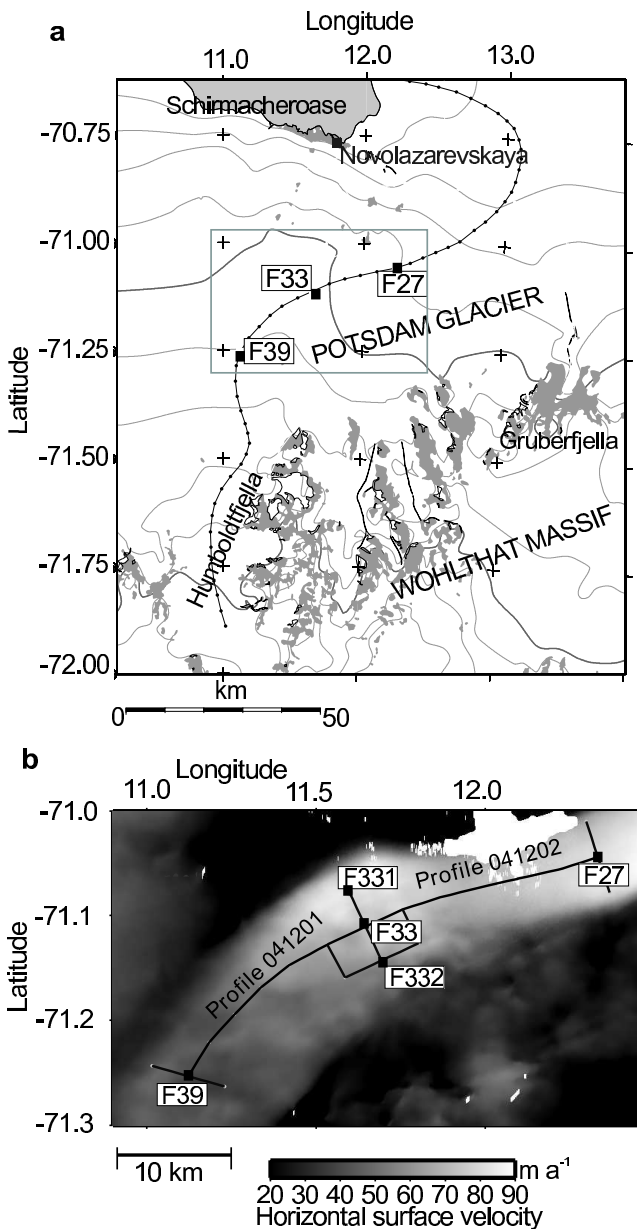


Fig. 1. a) Overview of the area of investigation. Black line: main flow line of Potsdam Glacier (Bäbler and others, 2002); black squares: start/end points of GPR profiles along the flow line. (Map source: Antarctic digital database 4.0.) Grey lines: contour lines of elevation at 200 m intervals; thick grey line: 1000 m contour line; large grey rectangle: area depicted in b. b) Sketch of GPR profiles (black lines) and firn-core locations (black squares) with point names (Fxxx). Profiles 041201/041202 correspond to the main flow line; glacier flow is from left to right. Distances F39–F33 and F33–27 amount to 25 km each. Grey scale indicates magnitude of glacier-flow velocity.

part of the area of investigation to about 850 m a.s.l. in the north-eastern part. Accumulation dominates in this region with the exception of small ablation areas around several nunataks. Only in the very northeastern part of this glacier, near and east of the Schirmacheroase, a large ablation area is found that reaches up to the eastern Wohlthat Massif (Bormann and Fritzsche, 1995). Analysis of a firn core drilled at 70°58'S, 11°22'E, some 15 km away from our radar profiles, showed snow and firn with some ice layers up to a depth of 27 m. From 27–51 m stratified ice

layers were found, and below 50 m unstratified ice with small bubbles occurred (Bormann and Fritzsche (1995) and references therein).

Studies of ice flow in this region have been undertaken among others by Korth and Dietrich (1996). They carried out differential GPS measurements and stake readings along the GPS signals on traverse lines going from Novolazarevskaya station to Humboldtjella and Gruberfjella, respectively (Figure 1a). The flow pattern of Potsdam Glacier has also been deduced by interferometric SAR analysis (Dietrich and others, 1999), as well as the line of highest flow velocity, hereinafter referred to as the main flow line. The velocities in the direction of glacier flow in the area of investigation are increasing from about 20–30 m a⁻¹ in the higher elevation parts to 70–80 m a⁻¹ in the lower region. Vertical velocity is unknown. Glacier flow is mainly divergent in the higher elevation parts of the glacier whereas in the lower elevation parts laterally convergent flow is observed (Bäbler and others, 2002, 2003).

METHODS

GPR and GPS Data

During the expedition 2003/2004 a 50 km long radar survey line was collected along the main flow line of Potsdam Glacier. Three cross profiles were surveyed, each one being 8 km long (Figure 1b). We used a commercial RAMAC radar system (Malå Geoscience, Sweden) with a bistatic shielded 500 MHz antenna that was connected to the central unit via fibre optic cables. Data were stored on a Husky Px5 computer. The GPR antenna was mounted behind a Nansen sledge pulled by a snowmobile at an average speed of ~5 km h⁻¹. Traces were recorded every 0.5 m triggered by a distance wheel. Each trace consisted of 2048 samples in a 400 ns time window, thus mapping the upper ~35–38 m of the snowpack. Differential GPS data were collected simultaneously with GPR data. The roving station was mounted on the snowmobile, and two reference stations were situated at the field-camp, *i.e.*, about 1 km south of point F33 (see Figure 1), and at the Schirmacheroase, respectively. The GPS data were collected every second using a Trimble 4000SSI receiver and a choke-ring antenna. Processing of GPS data yields positions for the GPR profiles as well as surface elevation. The relative accuracy between the differential GPS points is generally in the range of several millimeters to a few centimeters for longitude and latitude and of some centimeters to about one decimeter for the elevation. However, due to the movement of the roving station over severe sastrugi fields, we assume that actual accuracy declines to some centimeters for longitude and latitude and reaches a few decimeters for the elevation. The radar data were processed using Paradigm Geophysical FOCUS version 5.0 software by applying gain control, filtering using a Bandpass butterworth filter with cut-off frequencies of 350 MHz and 850 MHz, and correction for the first arrival of the direct wave. From the processed radargrams IRHs were tracked semi-automatically using Landmark OpenWorks release 2003.0 software. Within the depth section covered by the firn cores (given below) two internal horizons could be tracked throughout more than one GPR profile.

Firn Cores and Snow Samples

At five locations (Figure 1b, Table 1) along the radar profiles shallow firn cores were drilled, being between 12.5–13.5 m deep. At the same sites 2 m deep snow pits were dug which were probed in intervals of 5 cm, giving 40 samples per pit. The den-

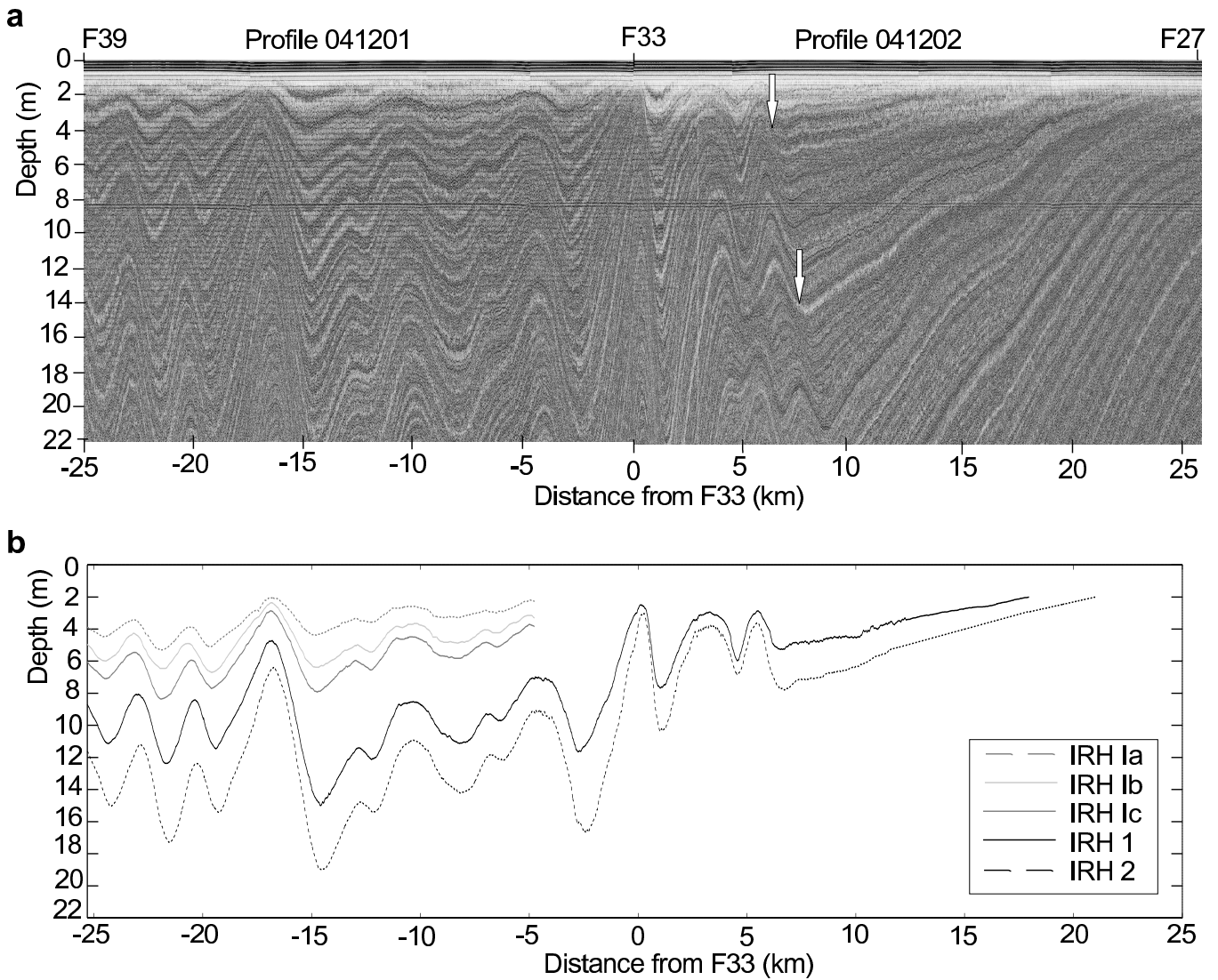


Fig. 2. a) Processed radargrams from profiles 041201 and 041202. The white arrows mark the IRHs chosen for the determination of the approximate beginning of the transition zone from accumulation to ablation. b) Depth distribution of tracked and dated IRHs. Black solid line: IRH 1 (1980), black dashed line: IRH 2 (1970), grey dashed line: IRH 1a (1995), light grey line: IRH 1b (1992), dark grey line: IRH 1c (1989).

sity of the snow samples was determined in situ from the weight and the known volume of the probing cylinder.

The firn cores and snow samples were transported to Germany and analyzed in the cold laboratory at AWI Bremerhaven for physical and chemical properties. Snow-sample data were used to link firn-core data to the surface due to poor core quality in the upper 1–2 m of drilling. The $\delta^{18}O$ ratio was determined by mass spectrometry for both the firn cores as well as the snow samples. Firn-core analysis covered measurements of density using gamma-attenuation profiling as well as dielectric profiling (GAP and DEP, respectively) that yield density, dielectric permittivity, and electrical conductivity of the firn (Wilhelms, 1996, 2005).

Determination of Accumulation Rates

We derive distributions of electromagnetic wave speed and cumulative mass with depth from the firn-core data. The mean values of density, dielectric permittivity, and conductivity of all five firn cores are used, since no further information about the lateral variations of those parameters between the firn-core drilling sites

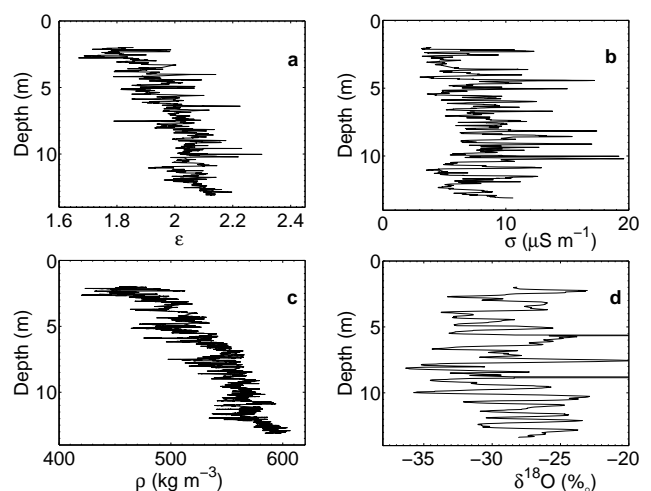


Fig. 3. Data from firn core F39: a) Dielectric permittivity, b) electrical conductivity, c) density (from GAP), and d) $\delta^{18}O$.

Table 1. Location of firn cores

Firn core	Point name*	Latitude	Longitude	Elevation (m)
FB0401	F33	71.110709 S	11.646268 E	1013
FB0402	F332	71.143130 S	11.693510 E	1076
FB0403	F39	71.253401 S	11.122667 E	1315
FB0404	F331	71.078270 S	11.599180 E	1008
FB0405	F27	71.044023 S	12.332327 E	848

*point names as in Figure 1b

is available. Cumulative snow mass is obtained by integration of the mean density profile derived from the GAP measurements. Calculation of electromagnetic wave speed from DEP-derived parameters follows the procedure described by Eisen and others (2002). Error estimates are given below. Since the firn cores reach only a depth of about 12 m below the surface, the data of the TWT–depth and cumulative mass–depth models were extrapolated up to a depth of 25 m. Extrapolation was done using Matlab’s polyfit routine by fitting a third order polynomial (Richardson and others, 1997; Frezzotti and others, 2005), yielding a correlation coefficient of $R = 0.90$. Age–depth profiles are determined by counting the $\delta^{18}O$ peaks which indicate summer maxima (McMorrow and others, 2004, and references therein).

Consistent dating of the different firn cores turned out to be difficult due to local variations in the $\delta^{18}O$ profiles which did not allow clear identification of maxima and minima for every firn core. However, firn core F39 shows a $\delta^{18}O$ profile with pronounced maxima and minima (Figure 3d) so it was used as a reference core for the interpretation of the radar data. F332 could likewise be dated sufficiently by its $\delta^{18}O$ profile. However, since the tracked IRHs do not reach up to this core, F332 could not be used for dating the GPR layers. The two tracked horizons (IRH 1 and IRH 2, see Figure 2b) are dated against F39 by comparing the depth of the respective IRH at the coring location with the depth–age scale of the firn core. The depth values for the IRHs at the drilling location are 8.65 m (IRH 1) and 11.55 m (IRH 2), and their estimated time of origin is 1970 and 1980, respectively, ± 2 years for each dating. Three more IRHs (IRH 1a, 1b, and 1c, see Figure 2b) that could only be tracked throughout the uppermost ~ 20 km along the main flow line are dated by the depth–age scale of F39 as well: their estimated times of origin are 1995, 1992, and 1989, ± 1 year for each dating.

The accumulation rate along the GPR profiles can be calculated by dividing the cumulative mass difference of two selected IRHs by their respective age difference.

Estimation of Errors

Errors in our density–depth distribution are assumed to be up to 14 % at a depth of 12 m determined from the difference between the mean values (*i.e.*, the model used) and F39 and F27, respectively (Figure 4c). This includes errors from the density measurements using GAP which are up to 10 kg m^{-3} (Wilhelms, 2005). Accuracy of DEP derived parameters is within 1 % (Wilhelms, 1996). Errors in TWT–depth conversion using DEP data are up to 1 % as shown by Eisen and others (2002). Errors in calculations of the cumulative mass from the density profiles are likewise up to 1 % due to error propagation. The dating uncertainty of the two IHRs used for determination of area-wide accumulation rates is ± 2 years. Errors in tracking of IHRs are up to ± 2 ns which yields depth variations of up to ± 0.2 m. However, for the

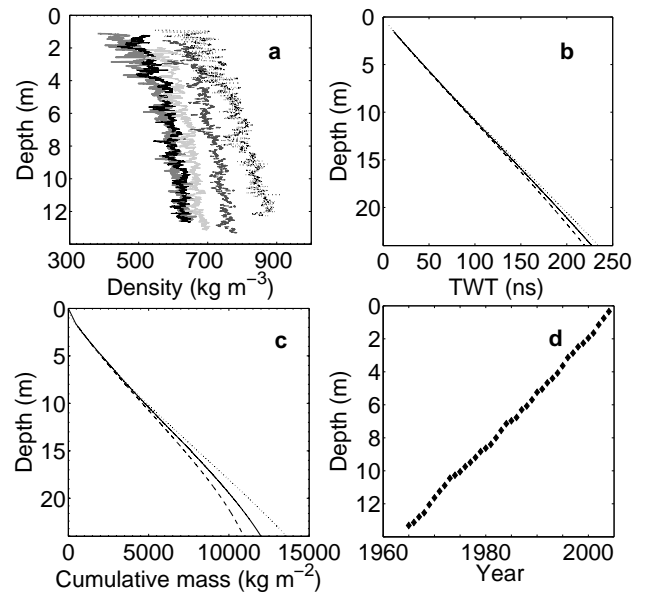


Fig. 4. a) Density distribution of all firn cores. Thick grey line: F33, solid black line: F332, light grey line: F39, dark grey line: F331, black dotted line: F27. Note that the density plots are offset by intervals of 50 kg m^{-3} in order to distinguish the individual cores. b) Model for TWT–depth and c) model for cumulative mass–depth. In either plot (b and c) the solid line corresponds to the model derived from the mean values, the dashed line to the one derived from firn core F39, and the dotted line to the one from F27. d) Depth–age scale as derived from the dating of firn core F39.

two dated IRHs (IRH 1 and 2) this latter uncertainty does not affect the estimated age since $8.65 \text{ m} \pm 0.2 \text{ m}$ and $11.55 \pm 0.2 \text{ m}$ still correspond to the years 1980 and 1970, respectively (Figure 4d). From analytic error propagation the overall root-mean square error in accumulation rates becomes 11.5 % for profile 041201. The largest error was found to be 20 %. We therefore assume that the accumulation values presented in this paper are accurate within about 12 % on average. Errors from ray-path geometry due to the separation of transmitting and receiving antenna are neglected, since transmitter and receiver are separated by only 0.18 m. For the same reason refraction within the snowpack can be neglected (Sinisalo and others, 2003).

RESULTS

GPR Profiles

In the processed radargrams the undulations of internal layers can clearly be seen (Figure 2a). Internal layers show large slopes along the profile 041201. At some locations the vertical distance between separate layers is very small (for example at -16 to -17 km) whereas a few kilometers away the same layers are spaced more widely (for example from about -10 to -15 km). Comparable undulating patterns have been reported before in DML, for example by Richardson-Näslund (2001). Closely spaced layers indicate areas with less accumulation whereas more widely spaced layers are associated with regions of higher accumulation. Along profile 041202 (Figure 2a) layers are ascending in the direction of glacier flow (with the exception of the local undulations in the first 6–7 km). Such patterns are characteristic for ablation areas and the transition from an accumulation area to an

ablation area, where internal horizons come to the surface due to surface erosion. However, it is not possible to resolve actual ablation from very low accumulation by GPR internal layering. A layer outcropping at the surface at a certain location along the GPR profile would only yield zero values for accumulation or ablation for this very point. Besides, the isochronal layers cannot be traced up to the surface since they are lost within the time window of the direct wave (here: the upper ~20 ns, equivalent to ~2 m, Figure 2a). Assuming zero advection, ascending layers with angles <90° relative to the surface would still provide accumulation, albeit low values (Figure 2a, near x=25 km). Without advection, therefore only layers emerging perpendicularly at 90° indicate ablation. Yet in our case we can conclude from the ascending IRHs that the transition zone from accumulation to ablation is present and visible in the radargram. Since we do have advection effects here, we cannot clearly define the beginning of the ablation area. Thus, we do not address the actual ablation area, but rather the transition zone where very low accumulation and also local ablation might occur. We define the beginning of this zone by the point where the first IRH would reach the surface. Using two different IRHs marked by the white arrows in Figure 2a and extrapolating from their respective slopes the points where they would reach the surface results in x=21.35 km and x=23.84 km, respectively. Since these IRHs could not be dated, we are unable to apply a sufficient correction for glacier-flow velocity. By choosing one very shallow and one rather deep IRH we can at least conclude that the transition zone from very low accumulation to ablation starts at this part of Potsdam Glacier between about 21–24 km downstream of F33. Thus, the actual ablation area is to be expected slightly farther downglacier which is in accordance with the description of Bormann and Fritzsche (1995) and Horwath and others (2006a).

Firn-Core Data and Density Distribution

The parameters derived from the firm-core analysis are depicted in Figure 3 for firm core F39. Dielectric permittivity as well as density increase with depth (Figure 3a and c) but the parameters do not reach values of solid ice ($\rho = 917 \text{ kg m}^{-3}$) within the depth section covered by the firm cores. Some of the peaks of the density coincide with observed ice lenses in the firm core.

Figure 4 shows the models for TWT–depth (b) and cumulative mass–depth (c) as derived from the mean values and from the "extreme" cores, i.e. the core with the lowest mean density (F39) and the core with the highest mean density (F27). Down to a depth of about 5–6 m the density values of the different firm cores are very similar (Figure 4a). Below this depth they start to differ slightly, up to ~100–150 kg m^{-3} at about 12 m depth. In the upper 6–7 m density variations within one specific firm core are usually larger than the variations between the different cores at the same depth. Generally, F27 shows the largest density values. This core was drilled on the lower elevation part of the glacier where the radar data indicate an ablation area nearby. Farther east a blue ice area is found (Bormann and Fritzsche, 1995; Korth and Dietrich, 1996; Horwath and others, 2006a) where the surface density should be higher than in the firm areas. Thus it can be assumed that density in the area of investigation will increase in the direction of glacier flow which is in accordance with our findings. However, density values of F27 are still in the range of firm density and do not reach the density of solid ice. Therefore we conclude that this part of the glacier is dominated by firm at least in the uppermost 12 m.

Table 2. Accumulation values in the area of investigation, given in $\text{kg m}^{-2} \text{ a}^{-1}$. Note that the first three lines (GPR-based accumulation rates) represent spatial means from the area of investigation whereas the last two lines (firm-core derived accumulation series) represent temporal accumulation means for the time period covered by the firm cores at the respective coring locations.

Method	Time period	Mean acc.	Std.*	Min.	Max.
GPR-IRHs	1970–1980	142	51	18	335
GPR-IRHs	1980–2004	140	48	27	318
GPR-IRHs	1970–2004	141	47	31	290
Firm core F332	1966–2003	161	39	60	327
Firm core F39	1968–2003	176	30	96	289

*one-fold standard deviation in % of the mean

Accumulation Rates

The mean accumulation rate in the area of investigation is derived for the time periods 1970–1980, 1970–2004, and 1980–2004, with 2004 corresponding to the surface at the time of data collection (Table 2). The depth distribution of the dated IRHs is depicted in Figure 2b. Taking into account a mean glacier-flow velocity of 45 m a^{-1} results in the accumulation distribution along the main flow line (Figure 6c). Furthermore, annual accumulation rates are obtained from the two dated firm cores (Table 2, Figure 5a).

DISCUSSION OF ACCUMULATION FEATURES
Temporal Characteristics

Comparing the mean values of the GPR-derived accumulation rates from Table 2 we conclude that the spatial variability exceeds the mean temporal variability for the time periods considered. This has been reported before at other places in East Antarctica, for example by Frezzotti and others (2005). The tem-

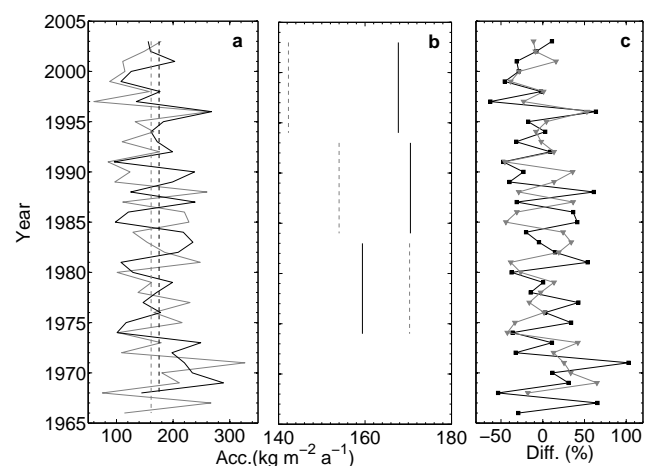


Fig. 5. a) Year-to-year accumulation values obtained from firm core F39 (black solid line) and F332 (grey solid line); the respective core means are depicted by the black dashed line (F39) and the grey dashed line (F332). b) Accumulation rates for a 10-year mean for F332 (grey, dashed) and F39 (black, solid). c) Variability expressed as per cent difference of the respective core mean. Grey line/grey triangles: F332, black line/black squares: F39.

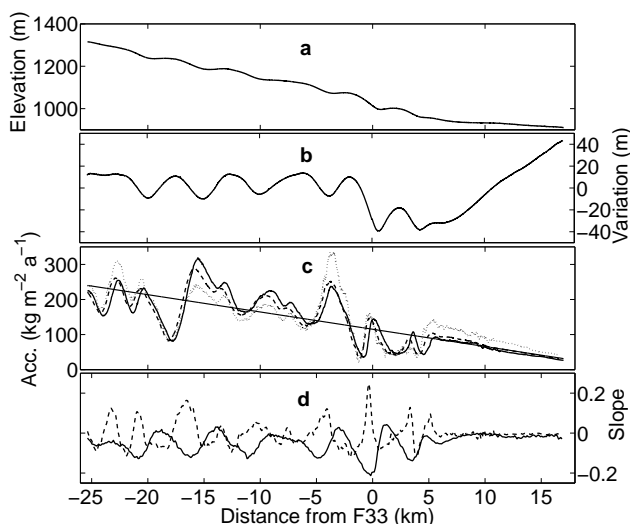


Fig. 6. a) Surface elevation, b) linearly detrended surface elevation, c) accumulation pattern, d) gradient of accumulation and surface slope on the main flow line. The solid curve in (c) corresponds to the time period 1980–2004, the dashed to 1970–2004, and the dotted curve to 1970–1980. The solid line shows the linear trend fitted to the accumulation pattern. The solid line in (d) corresponds to the slope of surface elevation (vertically exaggerated by a factor of 5) in m m^{-1} , and the dashed line represents the slope of accumulation (1980–2004) in $\text{kg m}^{-2} \text{a}^{-1} \text{m}^{-1}$.

poral variations in accumulation rates derived from GPR measurements for the time periods 1970–1980 and 1980–2004 are about 1.5 %, calculated from the mean values of the respective time periods. However, interannual variability obtained from the two dated firn cores (Figure 5a) is high, showing one-fold standard deviations of 30 and 39 %, respectively (Table 2). Differences in per cent of the firn-core mean values range from –63 % to +103 % for F332 and from –46 % to +65 % for F39 (Figure 5c). A mean over 10 years of the accumulation series obtained from the firn cores indicates a slight decrease at F332 and an even smaller increase at F39 for the time period 1984–1993 (Figure 5b). Although the time scales are rather short, this suggests that the accumulation pattern comprising the last 30 years is quite stable on decadal scales in relation to the annual variability.

Spatial Characteristics

Generally, our mean core-derived accumulation rates are about 12–23 % higher than the average GPR-based accumulation rates in the investigation area. We therefore conclude that the spatial representativity of the firn cores is limited as has been discussed before for West Antarctica (Spikes and others, 2004) and the western part of DML (Richardson-Näslund, 2001). The spatial variability of GPR-derived accumulation rates along the main flow line is very high (Figure 6c). Differences in per cent of the mean range from –81 % to +125 % for the time period 1980–2004, showing an undulating pattern. Accumulation rates show strong spatial gradients of up to $105 \text{ kg m}^{-2} \text{a}^{-1} \text{km}^{-1}$ with pronounced changes from increasing to decreasing accumulation in the direction of glacier flow, sometimes even within less than 1 km. For example, going from near F33 1 km upstream yields a 10-fold increase in accumulation (from about 30 to $330 \text{ kg m}^{-2} \text{a}^{-1}$) for the time interval 1970–1980. Average accumulation gradients are on the order of $23 \text{ kg m}^{-2} \text{a}^{-1} \text{km}^{-1}$. Generally, a decrease in accumulation in the direction of glacier flow is visible.

The linear trend along the profiles 041201/041202 amounts to $-4.9 \text{ kg m}^{-2} \text{a}^{-1} \text{km}^{-1}$. This is in accordance with the observation that IRHs tend to come to the surface at lower elevations on the main flow line (Figure 2a).

Surface slope and slope of accumulation (Figure 6d) show regular undulations similar to those in surface elevation (Figure 6a,b) and in accumulation (Figure 6c). Anschütz and others (2006) show that these undulations are likely caused by a feedback system between atmosphere and cryosphere similar to the features ruling the genesis of megadunes on the polar plateau (Frezzotti and others, 2002). Comparable association between surface slope and accumulation has been reported before in Antarctica (among others Black and Budd, 1964; Pettré and others, 1986; Goodwin, 1990; Vaughan and others, 2004; Eisen and others, 2005) and is attributed to wind influence (King and others, 2004) where accumulation maxima are located within surface-elevation troughs and on the windward slopes. Local deviations from this general pattern in our data are possibly due to different local-scale near-surface winds. Another reason probably arises from the correction for glacier flow where we used a measured mean flow speed of 45 m a^{-1} to correct the GPR layer depths and thus the accumulation pattern. Flow speed is not constant along the main flow line but increases with decreasing elevation. Measurements of spatial variations of ice flow are too inaccurate to allow a more detailed correction of the isochronal layers. Thus, accumulation maxima can be slightly misplaced due to locally incorrect consideration of glacier-flow speed. However, the spatial variability of the accumulation rate is not affected by these errors.

Comparison with Other Studies

Other groundborne data in this region are sparse, but there are a few accumulation values available from pit studies and stake readings.

Bormann and Fritzsche (1995) report a mean accumulation value derived from pit studies in the vicinity of a drill hole at $70^{\circ}58' \text{ S}$, $11^{\circ}22' \text{ E}$, about 15 km north of our radar profiles 041201/041202, that is about $130 \text{ kg m}^{-2} \text{a}^{-1}$ (1950–1984) which is in accordance with our mean values.

The mean annual accumulation from the stake readings presented by Korth and Dietrich (1996) on Insel traverse route (going from Novolazarevskaya station to Humboldtjella, see Figure 1a) is $131 \text{ kg m}^{-2} \text{a}^{-1}$ with a standard deviation of 140 % because some of the stakes are located in an ablation area. This comparison should be viewed with caution, since the stake readings cover the period 1988–1993 so the time interval of the different accumulation values is not the same. Furthermore, Korth and Dietrich (1996) do not state actual values for the densities used to calculate the accumulation. However, their mean value is in the range of our mean values, indicating that the overall distribution of accumulation is quite stable for the different time periods, although there are obvious small-scale differences. Their values obtained at stakes in the vicinity of our profiles, about 1 km away from the main flow line, are about $250 \text{ kg m}^{-2} \text{a}^{-1}$ which is much larger than our nearby values of some $50 \text{ kg m}^{-2} \text{a}^{-1}$. Yet accumulation rates for the time intervals 1980–1989, 1980–1992, and 1980–1995 along profile 041201 (calculated from IRH Ia, Ib, and Ic, see Figure 2b) are between 18% and 35% higher than the other values in our study. Taking into account the report from Korth and Dietrich (1996) this might indicate a higher accumulation at this part of the glacier during the 1980s and early 1990s of about 25 % compared with the previous period (1970–1980). Due to the dating uncertainty of F39 caution has to be used

with these findings. However, dating uncertainty does not affect the accumulation pattern itself or the spatial variability which is clearly demonstrated by our study.

The accumulation values in the area of investigation we presented here are less than those reported by Giovinetto and Zwally (2000) who derive values of some $200\text{--}250\text{ kg m}^{-2}\text{ a}^{-1}$ for this region of Antarctica. Vaughan and others (1999) report the same as Giovinetto and Zwally (2000). Both studies are concerned with larger areas and neglect small-scale features. Our mean value of $141\text{ kg m}^{-2}\text{ a}^{-1}$ (1970–2004) is less than these findings because an ablation area is in the vicinity of our study area which influences our results. Van de Berg and others (2006) derive specific surface mass balance (SSMB) from a regional atmospheric climate model, estimating precipitation, sublimation and melt. Snowdrift processes are not considered. The horizontal resolution is about 55 km. They derive values of some $200\text{ kg m}^{-2}\text{ a}^{-1}$ for the vicinity of our study area which is likewise larger than our mean accumulation values. Our study reveals a significant influence of blowing snow on the accumulation values in the area of investigation. So neglecting this process likely results in an overestimated SSMB for this area as given by Van de Berg and others (2006). Large-scale compilations like those cited above are usually based on a limited number of scattered observations. They do not take into account the spatial representativity of the respective point measurements which may be obscured by local-scale variability. Our study demonstrates a very high spatial variability in this area of coastal DML and indicates a limited representativity of firn-core derived accumulation data which are on average higher than the GPR-derived accumulation values. This might explain the higher accumulation rates in large-scale compilations of this area.

Implications for Satellite-Data Interpretation

Satellite observations of surface elevation, for instance by ERS-1/2 and ICESat, and gravity from the GRACE mission (Tapley and others, 2004) can provide mass-distribution changes according to the mission-specific spatial and temporal resolutions. Combining GRACE data and altimetry data helps to discriminate ice-mass changes (Zwally and others, 2005) from height changes induced by glacial isostatic adjustment or by changes in snow and firn density (Wahr and others, 2000). However, the effective spatial resolution of GRACE monthly solutions is only some hundred kilometers. To account for the GRACE error behaviour and to separate mass signals from different geographic origins adapted filter techniques have to be utilized (Swenson and Wahr, 2002; Horwath and Dietrich, 2006b). Hence, GRACE provides only integrated mass-balance estimates over large areas.

Trends in ice-mass changes over a few years derived from satellite observations may be either due to interannual fluctuations in net ice surface-mass balance or due to long-term ice dynamics. In order to distinguish between the two effects, information on the temporal and spatial covariance of the interannual surface mass balance fluctuation is needed.

With regard to spatial covariance, Anschütz and others (2006) report spatial autocorrelation lengths of only about 1 km for surface-mass balance fluctuations. For values averaged over some hundred kilometers the small-scale variations (deposition noise) are averaged out, hence, the standard deviation of temporal fluctuations will be smaller than the values of 30–39 % obtained from the firn-core time series (Table 2). Therefore, such small-scale fluctuations will not be resolved by GRACE. Concerning temporal covariance, there is, again, a large portion of small-scale deposition noise in the firn core data: the autocorrelation length

of the firn core time series is only 0.6 a (Figure 5a). However, the accumulation pattern seems fairly stable on decadal scales (Figure 5b).

The GRACE mission, launched in 2002, is planned to cover 8 years in total. Considering the discussion above, long-term surface mass balance changes showing a considerably large spatial pattern would be sensed by GRACE. Hence, regional studies of mass fluctuations are very important to qualify the spatiotemporal behaviour of the ice surface mass balance in larger areas and to discriminate surface mass balance fluctuations from long-term ice dynamics. In this context, the results presented by this study combined with further estimates yielded by other authors for adjacent regions (e.g. Richardson-Näslund, 2001; Rotschky and others, 2004; Frezzotti and others, 2005) provide valuable ground-based information to validate and interpret GRACE observations.

CONCLUSIONS

We have combined GPR data and firn-core data to investigate the accumulation pattern on Potsdam Glacier in Neuschwabenland, East Antarctica. Accumulation rates show a very high spatial variability in the area of investigation with a standard deviation of almost 50 %. The generally decreasing trend of accumulation in the direction of glacier flow is overlain by local features. In accordance with other authors (Richardson-Näslund, 2001; Rotschky and others, 2004; Frezzotti and others, 2005; Arcone and others, 2005; Spikes and others, 2004) we conclude that it is important to take into account the spatial representativity of point measurements such as firn cores, snow pits or stake readings when examining accumulation rates.

Comparing the results from our study with previous work based on stake readings nearby we found locally lower accumulation values, however, the previous study comprises a shorter time period. We found indications that during the late 1980s and early 1990s accumulation has been slightly higher (about 25 % compared to the period 1970–1980). Large-scale studies on Antarctic accumulation show values between $200\text{--}250\text{ kg m}^{-2}\text{ a}^{-1}$ for our investigation area. The lower values found in our study are presumably owed to an ablation area that influences our results and has not been accounted for in the large-scale compilations, as well as significant influence of blowing snow on the local accumulation rates.

Our results provide useful insight in small-scale features affecting the accumulation in this area and can be helpful in further studies, especially for validating satellite-based mass-balance estimates. Monitoring of local-scale accumulation changes in coastal areas provides valuable information to increase our knowledge about ice-mass fluxes from ice streams and outlet glaciers like Potsdam Glacier (Hamilton and others, 2005).

This study also complements published data sets and enhances the evaluation and interpretation of ice-mass changes in this area of East Antarctica.

ACKNOWLEDGEMENTS

This work was supported by the Deutsche Forschungsgemeinschaft (DFG) through the VISA project, funded under grants Di 473/17 and Jo 191/8. O.E. was supported by the DFG “Emmy Noether”-scholarship EI 672/1. Comments from G. Hamilton, R. Pettersson, and an anonymous reviewer greatly improved the manuscript. The contribution of the field team and help in the laboratory is gratefully acknowledged.

References

- Anschütz, H., O. Eisen, W. Rack and M. Scheinert, 2006. Periodic surface features in coastal East Antarctica, *Geophys. Res. Lett.*, **33**, L22501, doi:2006GL027871.
- Arcone, Steven A., Vandy B. Spikes and Gordon S. Hamilton, 2005. Stratigraphic variation within polar firn caused by differential accumulation and ice flow: interpretation of a 400 MHz short-pulse radar profile from West Antarctica, *J. Glaciol.*, **51**(174), 407–422.
- Bäbler, M., R. Dietrich and C. Shum, 2002. Investigations of Ice Dynamics at the Grounding Zone of an Antarctic Ice Shelf Utilizing SAR-Interferometry, Jekeli, Ch., ed., Proceedings of the Weikko A. Heiskanen Symposium in Geodesy 1-4 Oct 2002, Columbus, Ohio, USA.
- Bäbler, M., R. Dietrich and C. Shum, 2003. Horizontal velocity field, strain analysis and grounding zone location for the area of Nivlisen ice shelf, Dronning Maud Land, Poster presentation at FRINGE Workshop, Frascati, Italy, December 1-5 2003.
- Black, H. and W. Budd, 1964. Accumulation in the region of Wilkes, Wilkes Land, Antarctica, *J. Glaciol.*, **5**(37), 3–15.
- Bormann, P. and D. Fritzsche, eds., 1995. The Schirmacher Oasis, Queen Maud Land, East Antarctica, and its surroundings, Justus Perthes Verlag, Gotha, Germany.
- Damm, V. and D. Eisenburger, 2005. Ice thickness and sub-ice topography in Central Dronning Maud Land deduced by Radio Echo Sounding, *Geol. Jb.*, **B97**, 109–127.
- Dietrich, R., R. Metzger, W. Korth, J. Polzin and M. Scheinert, 1999. Combined use of field observations and SAR interferometry to study ice dynamics and mass balance in Dronning Maud Land, Antarctica, *Polar Research*, **18**(2), 291–298.
- Eisen, O., U. Nixdorf, F. Wilhelms and H. Miller, 2002. Electromagnetic wave speed in polar ice: Validation of the CMP technique with high-resolution dielectric profiling and gamma-density measurements, *Ann. Glaciol.*, **34**, 150–156.
- Eisen, O., U. Nixdorf, F. Wilhelms and H. Miller, 2004. Age estimates of isochronous reflection horizons by combining ice core, survey, and synthetic radar data, *J. Geophys. Res.*, **109**(B1), B01406, doi:10.1029/2003JB02858.
- Eisen, O., W. Rack, U. Nixdorf and F. Wilhelms, 2005. Characteristics of accumulation rate in the vicinity of the EPICA deep-drilling site in Dronning Maud Land, Antarctica, *Ann. Glaciol.*, **41**, 41–46.
- Frezzotti, M., S. Gandolfini and S. Urbini, 2002. Snow megadunes in Antarctica: Sedimentary structure and genesis, *J. Geophys. Res.*, **107**(D18), 4344, doi:10.1029/2001JD000673.
- Frezzotti, M., M. Pouchet, O. Flora, S. Gandolfini, M. Gay, S. Urbini, C. Vincent, S. Becagli, R. Gragnanind M. Proposito, M. Severi, R. Traversi, R. Udisti and M. Fily, 2005. Spatial and temporal variability of snow accumulation in East Antarctica from traverse data, *J. Glaciol.*, **51**(172), 113–124.
- Fujita, S., H. Maeno, S. Uratsuka, T. Furukawa, S. Mae, Y. Fujii and O. Watanabe, 1999. Nature of radio echo layering in the Antarctic ice sheet detected by a two-frequency experiment, *J. Geophys. Res.*, **104**(B6), 13049–13060, doi:10.1029/1998JB900034.
- Giovinetto, M.B. and H.J. Zwally, 2000. Spatial distribution of net surface mass accumulation on the Antarctic ice sheet, *Ann. Glaciol.*, **31**, 171–178.
- Goodwin, I., 1990. Snow accumulation and surface topography in the katabatic zone of Eastern Wilkes Land, Antarctica, *Ant. Sci.*, **2**(3), 235–242.
- Hamilton, G., V. Spikes and L. Stearns, 2005. Spatial patterns in mass balance of the Siple Coast and Amundsen Sea sectors, West Antarctica, *Ann. Glaciol.*, **41**, 105–110.
- Horwath, M., R. Dietrich, M. Bäbler, U. Nixdorf, D. Steinhage, D. Fritzsche, V. Damm and D. Reitmayr, 2006a. Nivlisen, an Antarctic Ice Shelf in Dronning Maud Land: Geodetic-Glaciological Results from a Combined Analysis of Ice Thickness, Ice Surface Height and Ice Flow Observations, *J. Glaciol.*, **52**(176), 17–30.
- Horwath, M. and R. Dietrich, 2006b. Errors of regional mass variations inferred from GRACE monthly solutions, *Geophys. Res. Lett.*, **33**, L07502, doi:10.1029/2005GL025550.
- Isaksson, E. and W. Karlen, 1994. Spatial and temporal patterns in snow accumulation, western Dronning Maud Land, Antarctica, *J. Glaciol.*, **40**(135), 399–409.
- King, J., P. Anderson, D. Vaughan, G. Mann, S. Mobbs and S. Vosper, 2004. Wind-borne redistribution of snow across an Antarctic ice rise, *J. Geophys. Res.*, **109**(D11), D1104, doi:10.1029/2000JD004361.
- Korth, W. and R. Dietrich, 1996. Ergebnisse geodätischer Arbeiten im Gebiet der Schirmacheroase/Antarctica 1988-1993, vol. 301 of *Angewandte Geodäsie*, Deutsche Geodätische Kommission, Verlag der Bayerischen Akademie der Wissenschaften, München, Germany.
- Kreutz, K., P. Mayewski, L. Meeker, M. Twickler and S. Whitlow, 2000. The effect of spatial and temporal accumulation rate variability in West Antarctica on soluble ion deposition, *Geophys. Res. Letters*, **27**(16), 2517–2520.
- McMorrow, A., T. van Ommen, V. Morgan and M. Curran, 2004. Ultra-high-resolution seasonality of trace-ion species and oxygen isotope ratios in antarctic firn over four annual cycles, *Ann. Glaciol.*, **39**, 34–40.
- Melvold, K., J.O. Hagen, J.F. Pinglot and N. Gundestrup, 1998. Large spatial variations in accumulation rate in Jutulstraumen ice stream, Dronning Maud Land, Antarctica, *Ann. Glaciol.*, **27**, 231–238.
- Meyer, U., D. Steinhage, U. Nixdorf and H. Miller, 2005. Airborne Radio Echo Sounding in Central Dronning Maud Land, *Geol. Jb.*, **B97**, 129–140.
- Oerter, H., F. Wilhelms, F. Jung-Rothenhäusler, F. Göktas, H. Miller and W. Graf, 2000. Accumulation rates in Dronning Maud Land, Antarctica, as revealed by dielectric-profiling measurements of shallow firn cores, *Ann. Glaciol.*, **30**, 27–34.
- Pettré, P., J.F. Pinglot, M. Pourchet and L. Reynaud, 1986. Accumulation in Terre Adélie, Antarctica: Effect of meteorological parameters, *J. Glaciol.*, **32**(112), 486–500.
- Pinglot, J.F., J.O. Hagen, K. Melvold, T. Eiken and C. Vincent, 2001. A mean net accumulation pattern derived from radioactive layers and radar soundings on Austfonna, Nordaustlandet, Svalbard, *J. Glaciol.*, **47**(159), 555–566.
- Richardson, C., E. Aarholt, S. Hamran, P. Holmlund and E. Isaksson, 1997. Spatial distribution of snow in western Dronning Maud Land, East Antarctica, mapped by a ground-based snow radar, *J. Geophys. Res.*, **102**(B9), 20343–20353.
- Richardson-Näslund, C., 2001. Spatial distribution of snow in Antarctica and other glacier studies using ground-penetrating radar, (Ph.D. thesis, Stockholm University, Sweden).
- Rignot, E. and R.H. Thomas, 2002. Mass Balance of Polar Ice Sheets, *Science*, **297**, 1502–1506.
- Rotschky, G., O. Eisen, U. Nixdorf and H. Oerter, 2004. Spatial distribution of surface mass balance on Amundsenisen plateau, Antarctica, derived from ice-penetrating radar studies, *Ann.*

- Glaciol.*, **39**, 265–270.
- Scheinert, M., L. Eberlein, W. Rack, H. Anschütz, B. Bayer, M. Horwath, J. Müller, S. Roemer, S. Riedel, D. Steinhage, R. Dietrich, W. Jokatz and H. Müller, 2005. Validation and Interpretation of Satellite Data in Dronning Maud Land, East Antarctica, with the Help of Geodetic, Geophysical and Glaciological Methods - Observation Campaigns 2003-2005 and First Results, Poster presentation at the 22nd International Polar Meeting. Jena, Germany, September 18-24.
- Sinisalo, A., A. Grinsted, J. Moore, E. Kärkäs and R. Pettersson, 2003. Snow-accumulation studies in Antarctica with ground-penetrating radar using 50, 100 and 800 MHz antenna frequencies, *Ann. Glaciol.*, **37**, 194–198.
- Spikes, V., G. Hamilton, S. Arcone, S. Kaspari and P. Mayewski, 2004. Variability in accumulation rates from GPR profiling on the west Antarctic plateau, *Ann. Glaciol.*, **39**, 238–244.
- Swenson, S. and J. Wahr, 2002. Methods for inferring regional surface-mass anomalies from Gravity Recovery and Climate Experiment (GRACE) measurements of time-variable gravity, *J. Geophys. Res.*, **107**(B9), 2193, doi:10.1029/2001JB000576.
- Tapley, B., S. Bettadpur, M. Watkins and C. Reigber, 2004. The gravity recovery and climate experiment: Mission overview and early results, *Geophys. Res. Lett.*, **31**, L09607, doi:10.1029/2004GL019920.
- Vaughan, D., P. Anderson, J. King, G. Mann, S. Mobbs and R. Ladkin, 2004. Imaging of firn isochrones across an Antarctic ice rise and implications for patterns of snow accumulation rate, *J. Glaciol.*, **50**(170), 413–418.
- Vaughan, D.G., J.L. Bamber, M. Giovinetto, J. Russell and A.P.R. Cooper, 1999. Reassessment of Net Surface Mass Balance in Antarctica, *J. Climate*, **45**(150), 933–946.
- van der Veen, C. J., 2002. Polar ice sheet and global sea level: how well can we predict the future?, *Global and Planetary Change*, **32**, 165–194.
- van de Berg, W., M. van den Broeke, C. Reijmer and E. van Meijgaard, 2006. Reassessment of the Antarctic surface mass balance using calibrated output of a regional atmospheric climate model, *J. Geophys. Res.*, **111**, D11104, doi:10.1029/2005JD006495.
- Wahr, J., D. Wingham, and C. Bentley, 2000. A method of combining ICESat and GRACE satellite data to constrain Antarctic mass balance, *J. Geophys. Res.*, **105**(B7), 16,279–16,294.
- Wilhelms, F., 1996. Leitfähigkeits- und Dichtemessung an Eisbohrkernen / Measuring the Conductivity and Density of Ice Cores (in German), vol. 191 of *Berichte zur Polarforschung*, Alfred-Wegener-Institut, Bremerhaven, Germany.
- Wilhelms, F., 2005. Explaining the dielectric properties of firn as a density-and-conductivity mixed permittivity (DECOMP), *Geophys. Res. Letters*, **32**, L16501, doi:10.1029/2005GL022808.
- Wingham, D., A. Ridout, R. Scharroo, R. Arthern and C. Shum, 1998. Antarctic elevation change from 1992 to 1996, *Science*, **282**, 456–458.
- Zwally, J., M. Giovinetto, J. Li, H. Cornejo, M. Beckley, A. Brenner, J. Saba and D. Yi, 2005. Mass changes of the Greenland and Antarctic ice sheets and shelves and contribution to sea-level rise:1992–2002, *J. Glaciol.*, **51**(175), 509–527.

Chapter 7

PAPER III

Temporal variation of accumulation patterns in western and central Dronning Maud Land, Antarctica

Helgard Anschütz¹, Daniel Steinhage¹, Olaf Eisen¹, Hans Oerter¹, Lutz Eberlein²

Abstract. Spatial and temporal variations of the recent accumulation rate are investigated utilizing ground-penetrating radar (GPR) measurements and firn-core studies. The study area is located on Ritscherflya in western Dronning Maud Land, Antarctica, at an elevation range between 1400–1560 m a.s.l. GPR-derived layer depths show little undulation along a 22 km profile on an ice-flow line. Accumulation rates are derived from tracked internal reflection horizons (IRHs) and the dating of a reference firn core. Average accumulation rates are about $190 \text{ kg m}^{-2} \text{ a}^{-1}$ (1980–2005) with a one-fold standard deviation of 5 % along the GPR profile. The interannual variability obtained from four dated firn cores is one order of magnitude higher, showing standard deviations around 30 %. Mean temporal variations of GPR-derived accumulation rates are of the same magnitude or even higher than spatial variations. Temporal differences between 1980–1990 and 1990–2005 obtained from two dated IRHs are not constant along the GPR profile. Comparison with similarly obtained accumulation data from another coastal area in central Dronning Maud Land confirms this observation. The spatial and temporal variations of the accumulation rate are useful for the validation of satellite data, e.g. from the GRACE mission, in further studies.

Introduction

The last years have seen increasing efforts in analyzing future sea-level change [e.g. *Wingham et al.*, 1998; *van der Veen*, 2002; *Thomas et al.*, 2004; *Alley et al.*, 2005; *Church and White*, 2006; *Monaghan et al.*, 2006]. However, uncertainties are still high, the largest introduced by the uncertain contribution of the Antarctic ice sheet [e.g. *Davis et al.*, 2005; *Rignot and Thomas*, 2002; *Rignot et al.*, 2004; *Vaughan*, 2005]. New satellite missions like GRACE [*Tapley et al.*, 2004], ICESat [*Zwally et al.*, 2002], and the upcoming CryoSat-2 are expected to give new insights in Antarctica's mass balance, especially in coastal and mountainous areas, where the steep slopes prevented a sufficient determination of surface-elevation changes from ERS data [*Vaughan*, 2005]. Several recent studies report mass rates for the West and East Antarctic ice shield (WAIS and EAIS) from Grace, yielding different results: *Velicogna and Wahr* [2006] derive values of $-148 \pm 21 \text{ km}^3 \text{ a}^{-1}$ (WAIS) and $0 \pm 56 \text{ km}^3 \text{ a}^{-1}$ (EAIS), *Chen et al.* [2006] report $-77 \pm 14 \text{ km}^3 \text{ a}^{-1}$ for WAIS and $+80 \pm 16 \text{ km}^3 \text{ a}^{-1}$ for EAIS, and *Ramillien et al.* [2006] give values of $-107 \pm 23 \text{ km}^3 \text{ a}^{-1}$ for West Antarctica and $+67 \pm 28 \text{ km}^3 \text{ a}^{-1}$ for East Antarctica. The uncertainties and the differences highlight the necessity of ground-truthing for the satellite-based estimates.

Moreover, these ice-mass changes from GRACE are averaged over several hundred kilometers, thus neglecting small-scale effects. *King et al.* [2006] propose an optimal average radius for temporal GRACE solutions of $\sim 500 \text{ km}$ over continental areas. Small-scale variations of parameters affecting changes of the ice sheet are of major importance in order to validate those satellite data. Spatial and temporal variations of accumulation rates and density influence the changes of ice-sheet elevation. It is therefore crucial to investigate these parameters and their spatio-temporal changes on small scales by groundborne observations.

Often accumulation data have been derived from point measurements such as firn cores, snow pits, or stake readings [e.g. *Oerter et al.*, 1999; *Kreutz et al.*, 2000; *Isaksson and Karlen*, 1994; *Melvold et al.*, 1998]. However, they yield only accumulation data at the probing location, leaving open the question of spatial representativity, as discussed by *Richardson et al.* [1997]. They recommend ground-penetrating radar (GPR) studies in order to investigate the spatial variability of accumulation rates around a drilling site. GPR has widely been applied in recent years [e.g. *Richardson and Holmlund*, 1999; *Rotschky et al.*, 2004; *Sinisalo et al.*, 2003; *Spikes et al.*, 2004; *Eisen et al.*, 2005]. Internal reflection horizons (IRHs) detected by GPR can be used to match signals found in different firn cores along the GPR profiles. The observed IRHs are due to contrasts of dielectric permittivity in the subsurface where in the upper hundreds of meters density has the most significant in-

¹Alfred-Wegener-Institut für Polar- und Meeresforschung
Bremerhaven, Germany

²Institut für Planetare Geodäsie, TU Dresden, Germany

fluence, affecting the real part of the dielectric permittivity [e.g. Fujita et al., 1999]. IRHs are shown to be isochronous [Eisen et al., 2004; Vaughan et al., 2004], thus from their estimated age and a density-depth distribution the mean accumulation rate for a certain period can be calculated.

In this paper we present groundborne data comprising GPR profiles and shallow firn cores on a small grid on Ritscherflya in western Dronning Maud Land (DML), Antarctica. Accumulation rates are obtained along selected tracked IRHs which are dated by firn-core parameters. We discuss the spatial variability of accumulation rates on the scale of a few kilometers and the temporal variability on decadal scale. Moreover, interannual variability of accumulation rates obtained from dated firn cores is presented. We compare our results with other nearby studies from western DML as well as with similarly obtained data from a coastal site in central DML.

Study Area

The area of investigation is located in the grounded coastal part of DML, some 10 km north of Kottasberge, which are part of the Heimefrontfjella mountain range (Figure 1). This area is characterized by gentle surface undulations at elevations between 1400 and 1560 m a.s.l. and a glacier-flow velocity of some 50 m a^{-1} . Distance to the Weddell Sea coast is about 300 km. Ice thickness in the area of investigation reaches some 2000 m with a rather smooth bedrock topography [Steinhage et al., 2001].

The Heimefrontfjella mountain range marks the boundary between the inland-ice plateau (Amundsenisen) and Ritscherflya with the mountains damming the ice flow coming down from the plateau. The mountain chains are directed from South-West to North-East. Altitudes range from $> 2500 \text{ m a.s.l.}$ on Amundsenisen plateau to $1200\text{--}1500 \text{ m a.s.l.}$ at the foot of the mountains [van den Broeke and Bintanja, 1995].

Previous accumulation studies north of Kottasberge and nearby have been carried out by Oerter et al. [1999], Richardson-Näslund [2004], and Rotschky et al. [submitted to J. Glaciol., 2006]. Näslund [1998] describes interactions of landscape, ice sheet, and climate in this area of Dronning Maud Land. Along the traverse route from Neumayer station on the Ekströmisen ice shelf to Kottasberge (Figure 1a) and further on to the EPICA¹ deep-drilling station Kohlen on Amundsenisen plateau firn cores have been drilled and analyzed [Oerter et al., 1999]. The accumulation along the traverse up to Kottasberge is monitored by a stake line of 500 m spacing between the individual stakes [Rotschky et al., 2006].

Methods

GPR and GPS

In the Antarctic summer season 2004/2005 GPR measurements were carried out on an ice-flow line and on cross

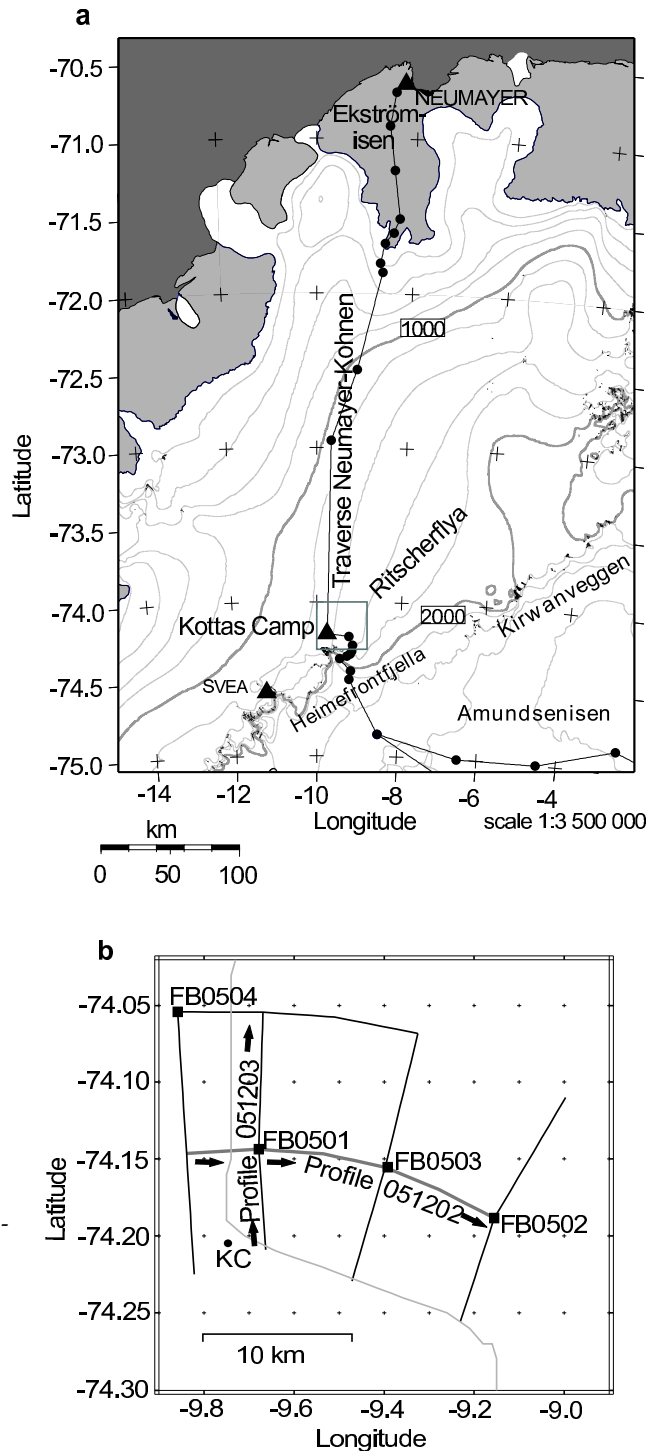


Figure 1. a) Overview of the area of investigation. Thin grey lines: elevation contour lines at 200 m spacing; thick grey lines: 1000 m and 2000 m contour lines. The black line indicates the traverse route from Neumayer station to Kohlen station (not shown); the black filled circles are waypoints for navigation. The dark grey rectangle corresponds to the area depicted in b. Map source: Antarctic digital data base 4.0. b) Sketch of GPR profiles and firn-core locations (black squares). Thick grey line: profile on the ice-flow line (against the flow direction); thin grey line: stake line along traverse Neumayer–Kottasberge. Arrows indicate direction of GPR profiles. Glacier flow is from right to left. KC: Kottas Camp.

¹European Project for Ice Coring in Antarctica

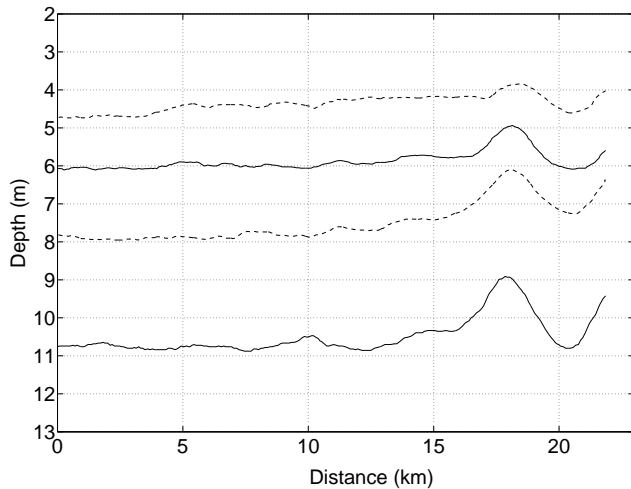


Figure 2. Depth distribution of the tracked IRHs of profile 051202. The solid horizons are used for calculation of the accumulation rate.

profiles (Figure 1b) using a bistatic shielded 500 MHz antenna (RAMAC, Malå Geoscience, Sweden) which was pulled by a snow vehicle at an average speed of about 5 km h^{-1} . Traces were recorded every 0.5 m in a time window of 400 ns, triggered by an odometer. GPR data were later on processed by applying gain control, filtering using a band-pass Butterworth filter with cut-off frequencies of 350 and 850 MHz, and correction for the first arrival of the direct wave. From the processed radar data IRHs were tracked throughout the GPR profiles where possible. We restrict ourselves here to the upper 12 m, i.e., the depth range covered by the firn cores (see below) since only isochronous layers up to this depth are datable against the firn cores. On the profile 051202, going against the flow direction on an ice-flow line (Figure 1b), four IRHs are tracked within this depth range. Their distribution of depth is rather smooth (Figure 2).

Simultaneously with GPR data acquisition kinematic GPS data were collected at a sampling interval of one second, using a Trimble 4000SSi receiver and a choke-ring antenna. The roving station was mounted on the snow vehicle, and the reference station was located on Weigel Nunatak, 10 km south of Kottas Camp (Figure 1). Processing of GPS data yields information about the surface elevation along the GPR profiles as well as GPR tracks.

Firn Cores

At four selected points (Figure 1b, Table 1) of the GPR profiles shallow firn cores were drilled, between 12.0–12.7 m deep. Firn-core analyses included density measurements using γ -attenuation profiling (GAP) in intervals of 2 mm and dielectric profiling (DEP) in 5 mm intervals [Wilhelms, 1996, 2005]. The latter yields information about the dielectric permittivity and the electrical conductivity of the firn. Moreover, mass spectrometry was used to derive a $\delta^{18}\text{O}$ profile for each core. Sample size was 25–30 mm for this

Table 1. Locations of firn cores

Firn core	Longitude	Latitude	Elevation ^a
FB0501	-9.6786	-74.1438	1447 m
FB0502	-9.1556	-74.1885	1569 m
FB0503	-9.3977	-74.1555	1488 m
FB0504	-9.8585	-74.0541	1420 m

^aWGS84

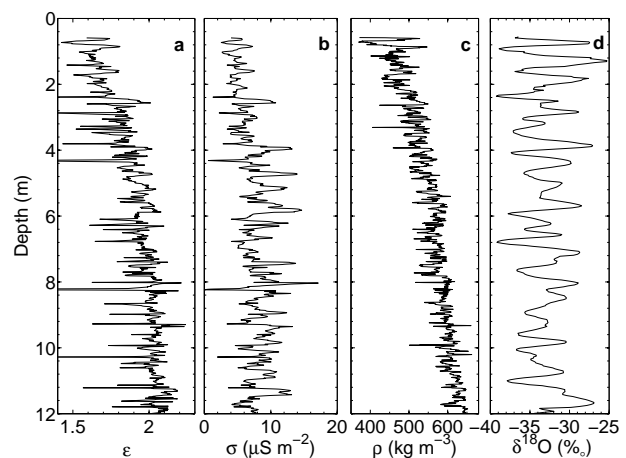


Figure 3. Measured parameters for FB0501: a) dielectric permittivity, b) electrical conductivity, c) density (from GAP), d) $\delta^{18}\text{O}$ profile.

method. Firn-core parameters are depicted exemplarily for firn core FB0501 in Figure 3.

Cumulative snow mass was obtained by integrating density profiles from GAP. Radar wave speed was calculated from the profiles of dielectric permittivity to convert two-way travel time (TWT) of tracked horizons to depth and to cumulative mass, respectively, following Eisen *et al.* [2002] and Anschütz *et al.* [accepted to Ann. Glaciol., 2006]. For establishing such models for TWT–depth and cumulative mass–depth the mean profiles of density and dielectric permittivity of all four firn cores were used, since there is no further information about lateral variations of those variables between the drilling sites. However, profiles of density and dielectric permittivity of the four firn cores show only small deviations, where fluctuations within one specific core are mostly higher than differences between the firn cores at the same depth (not shown).

Determination of Accumulation Rates

The $\delta^{18}\text{O}$ profile of FB0501 (Figure 3d) has been used to establish a depth-age scale as a dating reference for the tracked IRHs on profile 051202 and on profile 051203 (cross profile, see Figure 1b). Dating was done by annual layer counting, where the $\delta^{18}\text{O}$ peaks indicate summer maxima

[e.g. *McMorrow et al.*, 2004]. Using this scale, the respective IRHs were dated by comparing their depth values at the coring location with the age given by the depth-age scale. Accumulation rates along GPR profiles are calculated by dividing their cumulative mass difference by their age difference. Furthermore the density profiles of the firn cores were used to calculate annual accumulation rates from the snow mass of the yearly layers. Hence, annually resolved accumulation rates were obtained from the depth-age scales of the four dated firn cores.

In addition to the accumulation rates from the firn cores, we focus in the following discussion on the accumulation distribution obtained from two IRHs on profile 051202 (Figure 2, the solid lines); due to ambiguities in tracing the several IRHs throughout the GPR profiles and dating uncertainties other IRHs are left out. For comparison we also present accumulation data from the cross profile 051203 (see Figure 1b). The two profiles intersect at the drilling location of FB0501. The estimated time of origin of the two IRHs represented by the solid lines in Figure 2 is 1980 ± 1 year and 1990 ± 1 year, respectively. The isochronous property of the IRHs on profile 051202 was tested by comparing the age of the two IRHs at the positions of FB0501, FB0502, and FB0503, giving differences of up to ± 1 year, which is in the range of the dating uncertainties. We thus regard the IRHs as isochrones.

Calculation of errors follows the discussion of *Anschütz et al.* [accepted to *Ann. Glaciol.*, 2006]. Deviation of the density profiles from the different firn cores are up to 7 %, including measurement errors from GAP (up to 10 kg m^{-3} [*Wilhelms*, 2005]). This value represents the errors introduced by local density fluctuations with respect to the mean density profile used for the calculation of cumulative mass-depth. Errors from DEP measurements are up to 1 % [*Wilhelms*, 1996] and conversion from TWT to depth yields likewise errors of 1 % [*Eisen et al.*, 2002]. Conversion of the tracked IRHs to cumulative mass results in errors of ~ 1 % [*Anschütz et al.*, accepted to *Ann. Glaciol.*, 2006]. The dating uncertainty for the IRHs used here is ± 1 year and the uncertainty in tracking the IRHs is up to ± 2 ns, equivalent to about ± 0.2 m depth uncertainty. The latter introduces an additional uncertainty of another ± 1 year with respect to the depth-age scale of FB0501. Using the values given above, measurement and model errors result in a mean error of 10–15 % for the accumulation data presented here, similar to those reported by *Anschütz et al.* [accepted to *Ann. Glaciol.*, 2006] for a different area.

Results and Discussion

Accumulation Rates and Variability

GPR-based accumulation rates are given in Table 2 for the profiles 051202 and 051203. A mean glacier-flow velocity of 50 m a^{-1} was taken into account for the calculation of the GPR-derived accumulation rates on the profile 051202. The accumulation rates presented here are spatially averaged

Table 2. Accumulation values obtained from GPR

Profile	Time period	Mean acc. ^a	Std. ^b	Min. ^a	Max. ^a
051202	1980–1990	209	7	171	226
051202	1990–2005	176	5	145	185
051202	1980–2005	191	5	159	199
051203	1980–1990	192	11	135	232
051203	1990–2005	170	12	139	234
051203	1980–2005	170	9	149	220

^a in $\text{kg m}^{-2} \text{ a}^{-1}$

^b one-fold standard deviation in % of the mean

over 5 m.

The accumulation pattern seems quite homogeneous in this area as can be seen from Figure 4d. The spatial variability of the accumulation values can be expressed by the one-fold standard deviation, which amounts to 5–7 % of the respective mean value for profile 051202 (Table 2). Along this profile spatial differences in per cent of the respective mean value for the time periods 1980–1990 and 1990–2005 vary from -18 % to +8 % (Figure 4d). The cross profile 051203 reveals accumulation values that are of the same range compared with those on profile 051202, but with a slightly higher spatial variability, as expressed by a standard deviation of some 10 % (Table 2). Here, the spatial differences for the time periods 1980–1990 and 1990–2005 show values between -30 to +38 % of the respective mean (Figure 5d).

The accumulation pattern on the ice-flow line at Kottasberge is quite smooth (Figure 4b), except for the undulations between about 17–22 km. These features can be explained by the surface-elevation profile (Figure 4a) which shows a steeper increase along this section of the profile. Since the discussed IRHs are very shallow (Figure 2) in relation to the ice thickness we propose that the undulations in accumulation observed here arise mainly from the surface undulations and the interaction of surface topography and wind influence [*King et al.*, 2004]. Moreover, the bedrock topography is too smooth to generate the small-scale accumulation distribution observed in this study [*Steinhage et al.*, 2001].

Suggesting wind influence as the main reason for the accumulation pattern implies that accumulation maxima should be located within local surface-elevation troughs and on the windward sides of surface undulations, whereas accumulation minima are to be expected on hills and on the leeward sides [among others *Black and Budd*, 1964; *Pettré et al.*, 1986; *Frezzotti et al.*, 2005; *Vaughan et al.*, 2004; *Eisen et al.*, 2005]. Interestingly, accumulation pattern and surface topography show more such coincidence for profile 051203, going from South to North (Figure 5), than for profile 051202, going from West to East (Figure 4). Yet local-scale wind field is unknown, and the nearby Kottasberge

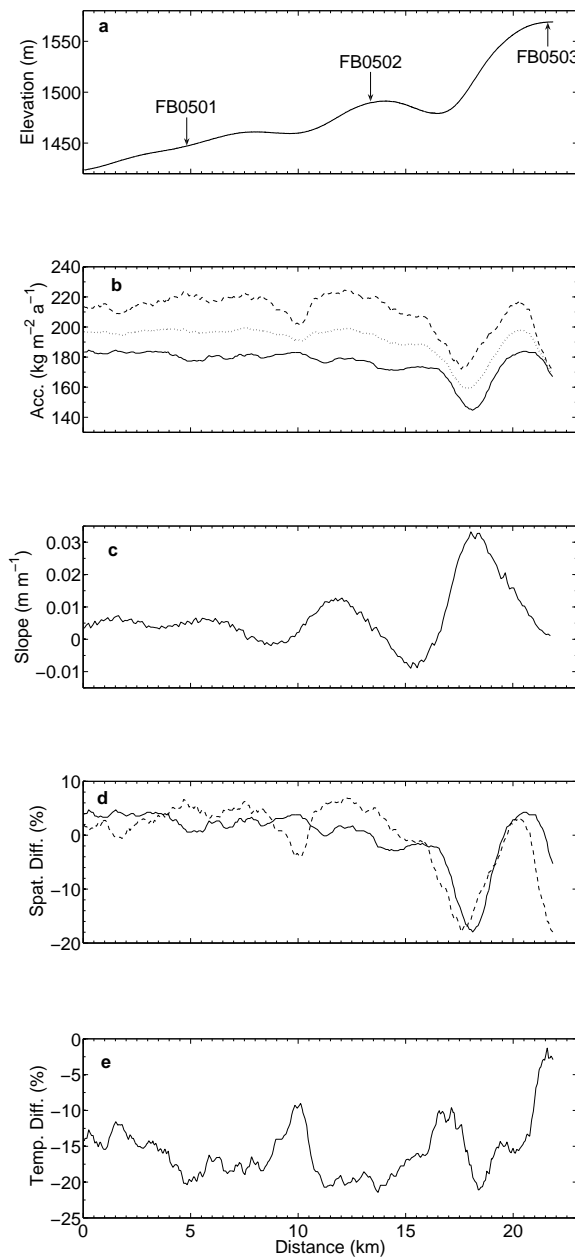


Figure 4. a) Surface elevation (WGS84) of profile 051202 at Kottasberge, going from West to East, b) accumulation: 1980–1990 (dashed line), 1980–2005 (dotted line), and 1990–2005 (solid line), c) surface slope, d) spatial differences in per cent of the respective mean for the time periods 1990–2005 (solid line) and 1980–1990 (dashed line), e) temporal differences between 1980–1990 and 1990–2005, calculated from equation (1). The locations of firn cores FB0501, FB0502, and FB0503 are given in a). FB0501 marks the intersection with profile 051203 (Figure 5).

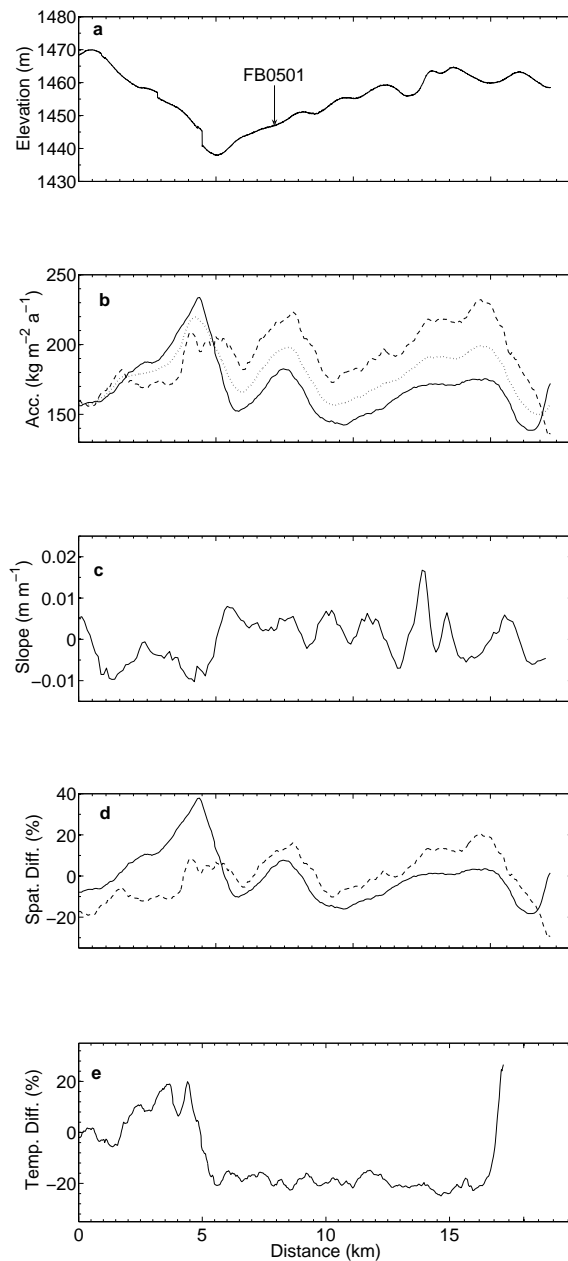


Figure 5. a) Surface elevation (WGS84) on profile 051203 at Kottasberge, going from South to North and crossing profile 051202 perpendicularly, b) accumulation: 1980–1990 (dashed line), 1980–2005 (dotted line), and 1990–2005 (solid line), c) surface slope, d) spatial differences in per cent of the respective mean for the time periods 1990–2005 (solid line) and 1980–1990 (dashed line), e) temporal differences between 1980–1990 and 1990–2005, calculated from equation (1). The location of firn core FB0501 is given in a).

Table 3. Accumulation values obtained from firn cores

Firn core	Time period	Mean acc. ^a	Std. ^b	Min. ^a	Max. ^a
FB0501	1976–2003	221	28	108	328
FB0502	1970–1999	227	32	98	370
FB0503	1970–2002	199	28	96	359
FB0504	1984–1999	195	33	112	305

^a in $\text{kg m}^{-2} \text{a}^{-1}$

^b one-fold standard deviation in % of the mean

are capable to modify the regional wind direction. *Van den Broeke and van Lipzig* [2004] report predominantly easterly winds in this area of Antarctica, but the horizontal resolution of their model is about 55 km, which does not capture small-scale effects. Dominance of easterly winds agrees only partly with the distribution of accumulation and surface features along profile 051202. Yet assuming katabatic wind flow down from the nearby plateau region south of Kottasberge, the accumulation pattern of profile 051203 becomes explicable by wind influence. Another reason for the deviation from the general pattern on profile 051202 probably arises from consideration of glacier-flow velocity: we used a mean surface-flow speed of 50 m a^{-1} to correct our GPR layer depths and derive accumulation rates on profile 051202. However, this value is only determined by GPS observations of one reference point on the ice-flow line during the expedition and might vary locally. We therefore suppose that interaction of local wind pattern, glacier flow, and surface topography significantly influences the local-scale accumulation pattern.

Mean accumulation values of the four firn cores as well as minima and maxima are given in Table 3. Note that the firn cores do not reach up to the year 2005 (the age of the surface at the time of data collection) due to minor core quality in the upper 1–2 m. Therefore a mean accumulation rate was used to estimate the age of the first datable layer, obtained from two nearby snow pits. The interannual variability derived from the dated firn cores (Figure 6a,b) is one order of magnitude higher than the spatial variability along the connecting GPR profile (Table 3), emphasizing that accumulation rates exhibit large fluctuations on annual scales.

In order to derive information about temporal variability on scales relevant to the duration of current satellite missions, we apply a 5-year mean and a 10-year mean on the accumulation series obtained from the firn cores. Note that the time scales are too short to sufficiently apply a *running* mean of 5 or 10 years to our firn-core derived accumulation series. When considering 5-year or 10-year means (Figure 6d-f), a fairly stable accumulation pattern is revealed, except for FB0503, which shows a slight decrease over the last two decades.

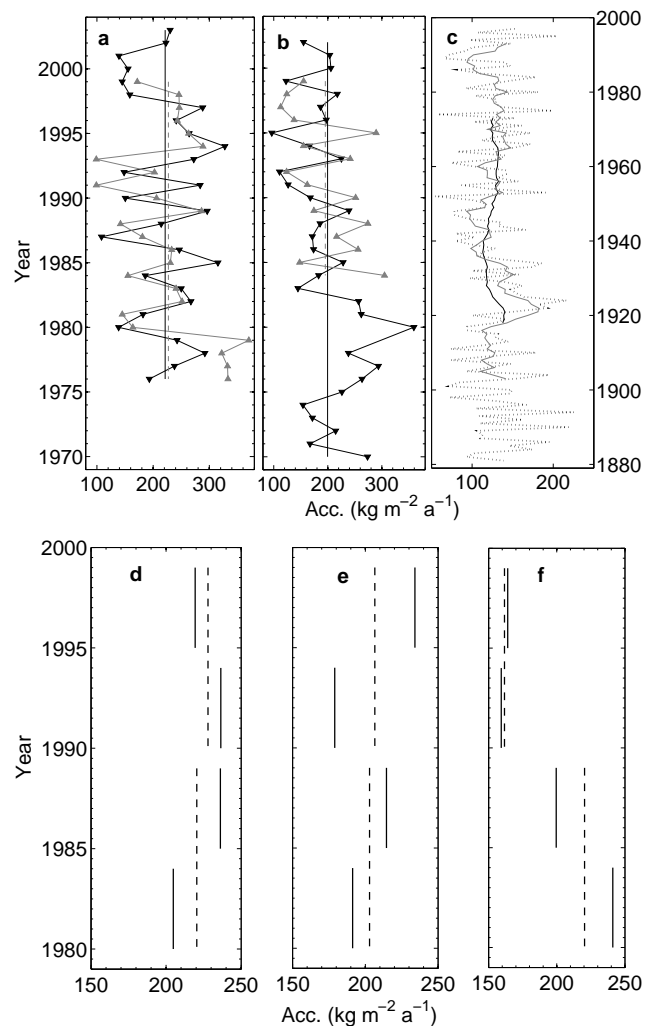


Figure 6. Year-to-year accumulation of the firn cores from this study (a,b) and of FB9802 [*Oerter et al.*, 1999]. a) Solid black curve/black triangles: FB0501, solid grey curve/grey triangles: FB0502, solid black line: mean of FB0501, dashed grey line: mean of FB0502 b) Solid black curve/black triangles: FB0503, solid grey curve/grey triangles: FB0504, solid black line: mean of FB0503, dashed grey line: mean of FB0504. c) FB9802: annual accumulation rates (dotted curve), 5-year running mean (dark grey), 25-year running mean (black). d)–f) 5-year (solid lines) and 10-year means (dashed lines) of d) FB0501, e) FB0502, f) FB0503. Note that FB0504 has been left out of calculating means over several years due to its short time scale in comparison to the three other cores.

Comparison with Other Studies Nearby

Oerter et al. [1999] report accumulation values at Kottas Camp of $129 \text{ kg m}^{-2} \text{ a}^{-1}$ with a one-fold standard deviation of 29 % obtained from a firn core (FB9802) drilled in December 1997, covering the time period 1881–1997. We apply a 5-year running mean on the accumulation series of FB9802, in order to gather information about temporal variations averaged over the projected mission duration of GRACE. Moreover, to account for the time scales covered by our radar data, we also apply a 25-year running mean to enable a better comparison of temporal variations between radar and firn-core data. The 5-year running mean and 25-year running mean of FB9802 show standard deviations of 14 % and 6 % of the core mean, respectively. Hence, firn core FB9802 reveals likewise a rather smooth accumulation pattern on longer time scales and a high annual variability (Figure 6c). Together with our firn cores (discussed above) this indicates that the temporal accumulation pattern on scales of 5–25 years is fairly stable, most probably because post-deposition noise and interannual fluctuations are averaged out. Moreover, we compare the standard deviation for the 25-year running mean of FB9802 with the spatial variability of our GPR derived accumulation rates, and find that temporal variability on the scale of some decades and spatial variability on the scale of some 20 km are very similar (6 % and 5 %, respectively). Contrarily, studies from the polar plateau show that spatial variability on the kilometer-scale is one order of magnitude higher than temporal variability on multidecadal scales there [Frezza et al., 2005].

Considering the area-wide mean values (Table 2), our study reveals somewhat higher accumulation rates than those reported by *Oerter et al.* [1999]. The same holds for comparison of FB9802 with our firn-core data (Table 3). In order to take into account the different time periods covered by FB9802 and our firn cores, we calculate the mean accumulation of FB9802 from 1970–1997, i.e., the time period that overlaps with our firn cores, and derive $126 \text{ kg m}^{-2} \text{ a}^{-1}$. Hence, the time periods covered do not seem to be responsible for the different accumulation rates of FB9802 and our study. Yet the spatial representativity of firn cores is generally rather small [e.g. *Richardson-Näslund*, 2004; *Spikes et al.*, 2004; *Rotschky et al.*, 2004] and FB9802 is separated by some 7–18 km from our respective firn-core locations and by about 3 km from the start of profile 051203. When comparing only accumulation rates from our investigation area that are in the immediate proximity of Kottas Camp, i.e., the start of profile 051203 (Figure 1b), we derive accumulation rates around $150 \text{ kg m}^{-2} \text{ a}^{-1}$ (Figure 5b), which are more in accordance with the value of $129 \text{ kg m}^{-2} \text{ a}^{-1}$ reported by *Oerter et al.* [1999].

Rotschky et al. [2006] present accumulation data obtained from stake readings along the transect from Neumayer station ($70^\circ 39' \text{ S}$, $08^\circ 15' \text{ W}$) to Kottas Camp and farther on to the mountain range of Kottasberge. Data obtained at stakes within 20–30 km of our radar profiles range from 150 – $250 \text{ kg m}^{-2} \text{ a}^{-1}$ (Figure 7a), however, with a high spatial vari-

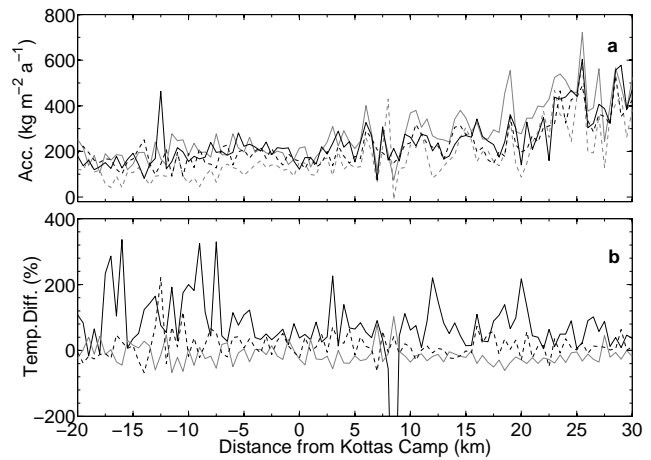


Figure 7. a) Accumulation values from stake-line readings in the vicinity of Kottas Camp: black solid line: 1998, black dashed line: 1999, grey solid line: 2000, grey dashed line: 2001. b) Temporal differences calculated as in equation (1). Black solid line: 1998–1999, grey solid line: 1999–2000, black dashed line: 2000–2001. Negative values on the abscissa correspond to stakes located north of Kottas Camp, positive values are stakes to the south.

ability. The transect up to Kottas Camp and the spatial variability of the accumulation data, complemented by GPR profiling, is further discussed by *Richardson-Näslund* [2004] with similar results. The stake-line data confirm the observation that in the immediate vicinity of Kottas Camp accumulation values are slightly lower which is in accordance with our findings, as discussed above. Moreover, *Rotschky et al.* [submitted to *J. Glaciol.*, 2006] obtain an accumulation map of western DML by interpolation of all available firn-core data, reporting values of about $180 \text{ kg m}^{-2} \text{ a}^{-1}$ for our investigation area. Hence, our study provides values in the range of former observations, but contributes small-scale variability of accumulation rates on spatial and temporal scales to the data published so far.

Temporal Variation of Spatial Characteristics

Accumulation series from firn cores, as those discussed above, yield only information about temporal behaviour at the drilling location. Dated IRHs enable the determination of temporal variation of spatial characteristics along GPR profiles. Considering the temporal difference (td) of GPR-based accumulation rates on profile 051202 between the time intervals 1990–2005 and 1980–1990 results in a mean value of -16 % as calculated from

$$td = \frac{a(t_1) - a(t_2)}{a(t_2)} \cdot 100\% \quad (1)$$

where a denotes accumulation and the t_i the respective time periods, in this case $t_1 = 1990$ – 2005 and $t_2 = 1980$ – 1990 . Yet, this value is not constant along the profile 051202. In fact, considering td pointwise along 051202 reveals that

temporal variations range from -1.3% up to -23% (Figure 4d). Comparing spatial and temporal differences along this profile, the variations seem to be linked, i.e., the largest temporal differences tend to occur at the places with largest relative spatial differences. Analysis of td on the cross-flow profile 051203 results in similar findings: the temporal differences are likewise varying locally. Spatio-temporal characteristics of the stake-line data within 20–30 km around Kottas Camp (Figure 7) confirm this observation, as there is, again, a quite similar behaviour of spatial and temporal accumulation pattern visible, for instance between -15 and -10 km and around 20 km. In total, it seems that the spatial characteristics of accumulation are not constant in the considered region and time scales. This observation leads us to the conclusion that it is important to consider the temporal differences pointwise along profiles and not only from the mean values. Small-scale features seem to affect the temporal pattern as well as the spatial distribution.

Accumulation rates have been obtained likewise by combined analysis of GPR and firm-core studies on Potsdam Glacier, a near-coastal site in central Dronning Maud Land in 2003/2004. The spatial variability is discussed in detail by Anschütz et al. [accepted to Ann. Glaciol., 2006], reporting standard deviations of some 50 % which is one order of magnitude higher than the standard deviations along the GPR profiles at Kottasberge. On Potsdam Glacier, spatial differences from the respective mean value vary from -87 to +128 % for the time period 1970–1980 and from -79 to +130 % for the time period 1980–2004 (Figure 8b). The temporal variations of a few per cent as reported by Anschütz et al. [accepted to Ann. Glaciol., 2006], are obtained from the area-wide mean values of the time periods 1970–1980 and 1980–2004, yet analysis of temporal variations along the profile on the main glacier-flow line yields a varying pattern (Figure 8c) as at Kottasberge. The mean temporal difference of accumulation rates on Potsdam Glacier for the observed time periods t_1 and t_2 amounts to -3 % with values varying from -53 % up to as much as 145 %, as calculated from Equation (1) with $t_1 = 1980–2004$ and $t_2 = 1970–1980$. Again, the largest temporal variations occur near maxima of spatial variability, indicating that temporal and spatial variations are not independent on these scales.

Anschütz et al. [2006] discuss the influence of the surface topography on the spatial accumulation pattern on Potsdam Glacier and find dune-like features of high periodicity, comparable to the megadunes observed on the polar plateau [Frezzotti et al., 2002]. Upstream migration of these dunes at a rate of some 50 m a^{-1} [Anschütz et al., 2006] as well as locally varying glacier-flow speed might also influence the temporal accumulation variations observed on Potsdam Glacier.

Comparing the spatial and the temporal variations on Potsdam Glacier (Figure 8b,c) and at Kottasberge (Figures 4d,e and 5d,e) with the respective surface slopes (Figures 8a, 4c, 5c), we suggest that in areas of strong interaction between surface elevation, slope, and accumulation, temporally varying

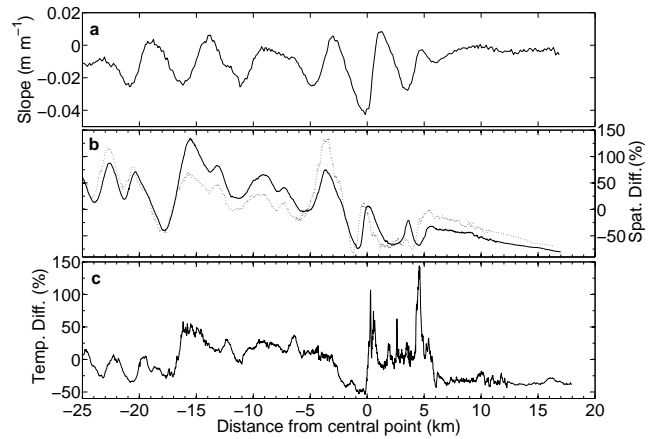


Figure 8. a) Slope on the main glacier-flow line of Potsdam Glacier. b) Spatial variation of accumulation on Potsdam Glacier, expressed as differences to the respective mean value, given in per cent of the mean: 1980-2004 (solid line) and 1970-1980 (dashed line). c) Temporal variations between the time periods 1970-1980 and 1980-2004 as calculated from equation (1).

mean accumulation rates lead to changing spatial accumulation patterns. The absolute value of the temporal differences between the mean accumulation rates from 1980–1990 and from 1990–2005 at Kottasberge is somewhat higher than on Potsdam Glacier between 1970–1980 and 1980–2004 (16 % compared to 3 %). However, as the two studies do not cover exactly the same time period caution has to be used with this comparison. The point-to-point variations of the temporal accumulation pattern at Kottasberge (Figures 4e and 5e) exhibit less pronounced differences compared to those on Potsdam Glacier (Figure 8c).

In order to analyze a possible correlation between spatial and temporal variations, we calculate the correlation coefficients R for spatial differences in per cent of the respective mean and temporal differences td along the GPR profiles at Kottasberge and on Potsdam Glacier. We obtain values of 0.24 ($t_1 = 1990–2005$) and 0.69 ($t_2 = 1980–1990$) for profile 051202 and correlation coefficients of 0.66 ($t_1 = 1990–2005$) and 0.55 ($t_2 = 1980–1990$) for profile 051203 at Kottasberge. The profile on the glacier-flow line of Potsdam Glacier reveals $R = 0.48$ for $t_1 = 1980–2004$ and $R = 0.28$ for $t_2 = 1970–1980$. This indicates that spatial and temporal variations are at least weakly correlated in our investigation areas. However, inaccuracies of glacier-flow velocity as well as dating uncertainties prevent a more detailed investigation. We thus suggest that influences of surface-topography, wind field, and glacier flow are responsible for the relation between spatial and temporal accumulation pattern. Near-surface winds tend to be complicated in nunatak-dominated areas [Jonsson, 1995] as would be seen on Potsdam Glacier. Since mostly rather the spatial variability is discussed when considering accumulation rates obtained from GPR [e.g. Richardson-Näslund, 2004; Rotschky et al., 2004;

Spikes et al., 2004] further research is necessary to reveal the correlations between spatial and temporal variability.

Conclusions

Small-scale spatial variations of the recent accumulation rate as well as decadal-scale and interannual temporal variations on Ritscherflya in western Dronning Maud Land have been discussed, obtained from combined analysis of GPR and firn-core data. Our radar data indicate that spatial variability in this investigation area is rather low compared with other coastal sites, yet the year-to-year accumulation values obtained from firn cores reveal a large temporal variability on annual scales. Mean accumulation rates at Kottasberge for the time period 1980–2005 amount to $170\text{--}190\text{ kg m}^{-2}\text{ a}^{-1}$ with standard deviations between 5–12 %. We find that spatial and temporal variations are linked, indicating that complex wind regimes, glacier flow, and surface topography may be responsible for the discussed features. However, further analysis using accurate knowledge of glacier-flow velocity is necessary. In principle, the depth distribution of GPR derived internal layers of isochronic origin allows to derive estimates of relative accumulation variations along the profiles, since closely spaced layers are associated with less accumulation in relation to more widely spaced layers [Richardson et al., 1997; Anschütz et al., accepted to *Ann. Glaciol.*, 2006]. Hence, linking temporal and spatial variations implies that in future studies relative temporal differences can likewise be estimated from spatial variability of the depth of isochronal layers, even if a depth-age scale is not available.

Other studies report values between about $130\text{--}200\text{ kg m}^{-2}\text{ a}^{-1}$ in the vicinity of our investigation area at Kottasberge. Our results confirm the values from previous studies and provide additional detailed information about small-scale spatial and temporal variability.

Temporal variations are important for validating satellite data like the time-variable gravity obtained from the GRACE mission. Ice-mass changes derived from satellite data assume a temporally constant accumulation rate [Velicogna and Wahr, 2002]. The decadal-scale accumulation variability obtained from four dated firn cores and one older firn core [Oerter et al., 1999] indicates a fairly stable accumulation distribution which would justify the assumption of a temporally constant accumulation rate. Yet our study revealed temporal fluctuations of GPR-based accumulation which coincide widely with spatial variations. Considering only the mean accumulation values of the respective time periods does not reveal the local temporal differences which are especially pronounced on Potsdam Glacier. Since gravity changes obtained from satellite missions are averaged over large areas, temporal differences on spatial scales might lead to biases in the derived ice-mass changes. As discussed by Eisen et al. [2005], knowledge of the spatio-temporal behaviour of accumulation rates is also important for the correct interpretation of ice-core data, especially in areas with

significant flow speed, since ice cores drilled there contain upstream effects. Thus, our study provides valuable insight in local-scale characteristics of temporal and spatial accumulation pattern, serving as ground-truthing for satellite data and as a base for interpretation of ice-core records from this and comparable areas.

Acknowledgments. This work was supported by the Deutsche Forschungsgemeinschaft (DFG) through the VISA project, funded under grants Di 473/17 and Jo 191/8. O.E. was supported by the DFG “Emmy Noether”-scholarship Ei 672/1. M. Scheinert (TU Dresden) provided the processed GPS data. The help of the field team and in the ice laboratory is gratefully acknowledged.

References

- Alley, R., P. U. Clark, P. Huybrechts, and I. Joughin, Ice-sheet and sea-level changes, *Science*, *310*, 456–460, 2005.
- Anschütz, H., O. Eisen, W. Rack, and M. Scheinert., Periodic surface features in coastal East Antarctica *Geophys. Res. Lett.*, *33*, L22501, 2006.
- Anschütz, H., O. Eisen, H. Oerter, D. Steinhage, and M. Scheinert, Investigating small-scale variations of the recent accumulation rate in coastal Dronning Maud Land, East Antarctica, accepted to *Ann. Glaciol.*, 2006.
- Black, H., and W. Budd, Accumulation in the region of Wilkes, Wilkes Land, Antarctica, *J. Glaciol.*, *5*(37), 3–15, 1964.
- Chen, J., C. Wilson, D. Blankenship, and B. Tapley, Antarctic mass rates from GRACE, *Geophys. Res. Lett.*, *33*, L11502, 2006.
- Church, J., and N. White, A 20th century acceleration in global sea-level rise, *Geophys. Res. Lett.*, *33*, L01602, 2006.
- Davis, C., Y. Li, J. McConnell, M. Frey, and E. Hanna, Snowfall-driven growth in East Antarctic ice sheet mitigates recent sea-level rise, *Science*, *308*, 1898–1901, 2005.
- Eisen, O., U. Nixdorf, F. Wilhelms, and H. Miller, Electromagnetic wave speed in polar ice: Validation of the CMP technique with high-resolution dielectric profiling and gamma-density measurements, *Ann. Glaciol.*, *34*, 150–156, 2002.
- Eisen, O., U. Nixdorf, F. Wilhelms, and H. Miller, Age estimates of isochronous reflection horizons by combining ice core, survey, and synthetic radar data, *J. Geophys. Res.*, *109*(B1), B04106, 2004.
- Eisen, O., W. Rack, U. Nixdorf and F. Wilhelms, Characteristics of accumulation rate in the vicinity of the EPICA deep-drilling site in Dronning Maud Land, Antarctica, *Ann. Glaciol.*, *41*, 41–46, 2005.
- Frezzotti, M., S. Gandolfi, and S. Urbini, Snow megadunes in Antarctica: Sedimentary structure and genesis, *J. Geophys. Res.*, *107*(D18), 4344, 2002.
- Frezzotti, M., et al., Spatial and temporal variability of snow accumulation in East Antarctica from traverse data, *J. Glaciol.*, *51*(172), 113–124, 2005.
- Fujita, S., H. Maeno, S. Uratsuka, T. Furukawa, S. Mae, Y. Fujii, and O. Watanabe, Nature of radio echo layering in the Antarctic ice sheet detected by a two-frequency experiment, *J. Geophys. Res.*, *104*(B6), 13,049–13,060, 1999.
- Isaksson, E., and W. Karlen, Spatial and temporal patterns in snow accumulation, western Dronning Maud Land, Antarctica, *J. Glaciol.*, *40*(135), 399–409, 1994.
- Jonsson, S., Synoptic forcing of wind and temperature in a large cirque 300 km from the coast of East Antarctica, *Antarctic Science*, *7*(4), 409–420, 1995.

- King, J., P. Anderson, D. Vaughan, G. Mann, S. Mobbs, and S. Vosper, Wind-borne redistribution of snow across an Antarctic ice rise, *J. Geophys. Res.*, *109*, D11104, 2004.
- King, M., P. Moore, P. Clarke, and D. Lavallée, Choice of optimal averaging radii for temporal grace gravity solutions, a comparison with GPS and satellite altimetry, *Geophys. J. Int.*, *166*, 1–11, 2006.
- Kreutz, K., P. Mayewski, L. Meeker, M. Twickler, and S. Whitlow, The effect of spatial and temporal accumulation rate variability in West Antarctica on soluble ion deposition, *Geophys. Res. Lett.*, *27*(16), 2517–2520, 2000.
- McMorrow, A., T. van Ommen, V. Morgan, and M. Curran, Ultra-high-resolution seasonality of trace-ion species and oxygen isotope ratios in Antarctic firn over four annual cycles, *Ann. Glaciol.*, *39*, 34–40, 2004.
- Melvold, K., J. Hagen, J. Pinglot, and N. Gundestrup, Large spatial variations in accumulation rate in Jutulstraumen ice stream, Dronning Maud Land, Antarctica, *Ann. Glaciol.*, *27*, 231–238, 1998.
- Monaghan, A., D. Bromwich, R. Fogt, S. Wang, P. Mayewski, D. Dixon, A. Ekaykin, M. Frezzotti, I. Goodwin, E. Isaksson, S. Kaspari, V. Morgan, H. Oerter, T. van Ommen, C. van der Veen, and J. Wen, Insignificant Change in Antarctic Snowfall Since the International Geophysical Year, *Science*, *313*, 827–831, 2006a.
- Näslund, J., Ice sheet, climate, and landscape interactions in Dronning Maud Land, Antarctica, Ph.D. thesis, Stockholm University, Sweden, 1998.
- Oerter, H., W. Graf, F. Wilhelms, A. Minikin, and H. Miller, Accumulation studies on Amundsenisen, Dronning Maud Land, Antarctica, by means of dielectric profiling and stable-isotope measurements: first results from the 1995-96 and 1996-97 field seasons, *Ann. Glaciol.*, *29*, 1–9, 1999.
- Pettré, P., J. Pinglot, M. Pourchet, and L. Reynaud, Accumulation in Terre Adélié, Antarctica: Effect of meteorological parameters, *J. Glaciol.*, *32*(112), 486–500, 1986.
- Ramillien, G., A. Lombard, A. Cazenave, E. Ivins, M. Llues, F. Remy, and R. Biancale, Interannual variations of the mass balance of the Antarctica and Greenland ice sheets from GRACE, *Global and Planetary Change*, *53*, 198–208, 2006.
- Richardson, C., and P. Holmlund, Spatial variability at shallow snow-layer depths in central Dronning Maud Land, East Antarctica, *Ann. Glaciol.*, *29*, 10–16, 1999.
- Richardson, C., E. Aarholt, S. Hamran, P. Holmlund, and E. Isaksson, Spatial distribution of snow in western Dronning Maud Land, East Antarctica, mapped by a ground-based snow radar, *J. Geophys. Res.*, *102*(B9), 20,343–20,353, 1997.
- Richardson-Näslund, C., Spatial characteristics of snow accumulation in western Dronning Maud Land, Antarctica, *Global and Planetary Change*, *42*, 31–43, 2004.
- Rignot, E., and R. Thomas, Mass balance of polar ice sheets, *Science*, *297*, 1502–1506, 2002.
- Rignot, E., G. Casassa, P. Gogineni, W. Krabill, A. Rivera, and R. Thomas, Accelerated ice discharge from the Antarctic peninsula following the collapse of Larsen B ice shelf, *Geophys. Res. Lett.*, *31*, L18401, 2004.
- Rotschky, G., O. Eisen, U. Nixdorf, and H. Oerter, Spatial distribution of surface mass balance on Amundsenisen plateau, Antarctica, derived from ice-penetrating radar studies, *Ann. Glaciol.*, *39*, 265–270, 2004.
- Rotschky, G., W. Rack, W. Dierking, and H. Oerter, Retrieving snowpack properties and accumulation estimates from a combination of SAR and scatterometer measurements, *IEEE Trans. Geosci. Remote Sens.*, *44*(4), 943–956, 2006.
- Rotschky, G., P. Holmlund, E. Isaksson, R. Mulvaney, H. Oerter, M. van den Broeke, and J. Winther, A new surface accumulation map for western Dronning Maud Land, Antarctica, from interpolation of point measurements, *submitted to J. Glaciol.*, 2006.
- Sinialo, A., A. Grinsted, J. Moore, E. Kärkäs, and R. Pettersson, Snow-accumulation studies in Antarctica with ground-penetrating radar using 50, 100 and 800 MHz antenna frequencies, *Ann. Glaciol.*, *37*, 194–198, 2003.
- Spikes, V. B., G. Hamilton, S. Arcone, S. Kaspari, and P. Mayewski, Variability in accumulation rates from GPR profiling on the west Antarctic plateau, *Ann. Glaciol.*, *39*, 238–244, 2004.
- Steinhage, D., U. Nixdorf, U. Meyer, and H. Miller, Subglacial topography and internal structure of central and western Dronning Maud Land, Antarctica, determined from airborne radio echo sounding, *J. Applied Geophys.*, *47*, 183–189, 2001.
- Tapley, B., S. Bettadpur, M. Watkins, and C. Reigber, The gravity recovery and climate experiment: Mission overview and early results, *Geophys. Res. Lett.*, *31*, L09607, 2004.
- Thomas, R., et al., Accelerated sea-level rise from West Antarctica, *Science*, *306*, 255–258, 2004.
- van den Broeke, M. and R. Bintanja, Summertime atmospheric circulation in the vicinity of a blue-ice area in Dronning Maud Land, Antarctica, *Boundary Layer Meteorology*, *72*, 411–438, 1995.
- van den Broeke, M. and N. van Lipzig, Changes in Antarctic temperature, wind and precipitation in response to the Antarctic Oscillation, *Ann. Glaciol.*, *39*, 119–126, 2004.
- van der Veen, C. J., Polar ice sheet and global sea level: how well can we predict the future?, *Global and Planetary Change*, *32*, 165–194, 2002.
- Vaughan, D., How does the Antarctic ice sheet affect sea level rise?, *Science*, *308*, 1877–1878, 2005.
- Vaughan, D., P. Anderson, J. King, G. Mann, S. Mobbs, and R. Larkin, Imaging of firn isochrones across an Antarctic ice rise and implications for patterns of snow accumulation rate, *J. Glaciol.*, *50*(170), 2004.
- Velicogna, I., and J. Wahr, A method for separating Antarctic post-glacial rebound and ice-mass balance using future ICESat Geoscience Laser Altimeter System, Gravity Recovery and Climate Experiment, and GPS satellite data, *J. Geophys. Res.*, *107*(B10), 2263, 2002.
- Velicogna, I., and J. Wahr, Measurements of time-variable gravity show mass loss in Antarctica, *Science*, *311*, 1754–1756, 2006.
- Wilhelms, F., *Leitfähigkeits- und Dichtemessung an Eisbohrkernen / Measuring the Conductivity and Density of Ice Cores (in German)*, vol. 191 of *Berichte zur Polarforschung*, Alfred-Wegener-Institut, Bremerhaven, Germany, 1996.
- Wilhelms, F., Explaining the dielectric properties of firn as a density-and-conductivity mixed permittivity (decomp), *Geophys. Res. Lett.*, *32*, L16501, 2005.
- Wingham, D., A. Ridout, R. Scharroo, R. Arthern, and C. Shum, Antarctic elevation change from 1992 to 1996, *Science*, *282*, 456–458, 1998.
- Zwally, H., et al., Icesat's laser measurements of polar ice, atmosphere, ocean, and land, *Journal of Geodynamics*, *34*, 405–445, 2002.

Helgard Anschütz, Alfred-Wegener-Institut für Polar- und Meeresforschung, Am alten Hafen 26, D-27568 Bremerhaven, Germany (e-mail: Helgard.Anschuetz@awi.de)

This preprint was prepared with AGU's L^AT_EX macros v5.01, with the extension package 'AGU⁺⁺' by P. W. Daly, version 1.6b from 1999/08/19.

Chapter 8

Summary and outlook

GPR profiling and shallow firn cores have been utilized to determine the recent accumulation rate in two investigation areas of Dronning Maud Land, East Antarctica. The method provides useful new insights in small-scale characteristics of accumulation features in the grounded coastal parts of DML which contribute significantly to Antarctica's mass balance but are not well captured by models so far.

The first investigation area, Potsdam Glacier in central DML, is characterized by a very high spatial variability of accumulation rates with a one-fold standard deviation of some 50 % around mean values of $140 \text{ kg m}^{-2} \text{ a}^{-1}$. Distribution of accumulation maxima and minima on an along-flow GPR profile likely results from windborne redistribution of blowing snow. Moreover, accumulation shows regular undulations that are related to those in surface slope. Analysis of these features by means of auto- and cross-covariance functions reveals a high periodicity, leading to the conclusion that the observed undulations are similar to the megadunes known from the polar plateau [Frezzotti *et al.*, 2002a], despite the lack of the lateral extent and the extreme morphology of the latter [Frezzotti *et al.*, 2002b] in this case. The presence of dunes at this coastal site not only provides a likely explanation for the undulations of the accumulation pattern, but it also complicates the picture of accumulation features with respect to the validation of satellite data. Spatial variations like those observed on Potsdam Glacier are likely sensed by GRACE, thus influencing the satellite-derived estimate of ice-mass changes.

Mean accumulation values in this area are less than those derived from large-scale compilations or regional atmospheric models, underlining the statement that those compilations tend to overestimate surface-mass balance in coastal regions [van de Berg *et al.*, 2006]. The presence of a blue-ice area nearby the study area influences the accumulation pattern. This blue-ice area is not accounted for in the large-scale compilations [Vaughan *et al.*, 1999; Giovinetto and Zwally, 2000], emphasizing the impacts of this study for accurate knowledge of local and regional accumulation pattern in this part of Antarctica. Temporal variations of accumulation rates on Potsdam Glacier are only a few per cent on decadal scales, when derived from mean

accumulation values obtained from dated GPR horizons. Yet interannual variability is high, as concluded from two dated firn cores.

The second study area, Kottasberge in western DML, exhibits much less spatial variability of accumulation rates with one-fold standard deviations of 5–10 % and mean values of some $190 \text{ kg m}^{-2} \text{ a}^{-1}$. The accumulation pattern is likewise explicable by wind influence and surface topography, although it implies a deviation from the prevalent wind direction for this area derived from models [*van den Broeke and van Lipzig, 2004*]. Temporal variations obtained from area-wide mean values are larger than on Potsdam Glacier. Pointwise determination of temporal differences on decadal scales along the GPR profiles reveals that temporal variations are not constant but vary from point to point. The same holds for the pointwise temporal variations obtained from GPR horizons on Potsdam Glacier. Comparison of temporal and spatial variations in both study areas shows a weak correlation, indicating that temporal variability on decadal scales and spatial variability on the scale of some hundreds of meters to tens of kilometers might be linked. This is likely attributed to complex interactions between locally varying wind pattern and precipitation regime with surface topography and glacier-flow. Yet wind pattern and glacier-flow velocity are too poorly resolved to derive more accurate conclusions here, and the dating uncertainty prevents a more detailed analysis, leaving the results presented in this study as a base for future work. Nevertheless, the possibility of linked temporal and spatial variability should be taken into account for the validation of satellite data. As discussed by *Velicogna and Wahr [2002]* and *Wahr et al. [2000]*, for the determination of ice-mass changes from combined GRACE and GLAS data a temporally constant accumulation rate is assumed. Therefore considerable spatial variability of temporal differences as revealed by this study might likely lead to biases in the derived ice-mass changes. Thus, the results presented here serve as valuable ground-truthing for satellite-based approaches to determine Antarctica's mass balance in coastal areas.

Future work should aim to further increase the amount of ground-based accumulation data, especially in regions adjacent to Potsdam Glacier, where only sparse data have been available prior to this study. The presence of dune-like features on Potsdam Glacier should be analyzed and evaluated in more detail, aiming for determination of their lateral extent and possible migration. Extending the along-flow GPR profiles farther downglacier would likewise be very interesting, since the shape of the internal layers indicates a nearby ablation zone which was not reached within the radar profiles of this study. The shape of layers in adjacent downglacier profiles will give further information about accumulation and ablation features and possibly also insight in interaction between ice-advection and accumulation/ablation pattern. In this context, glacier-flow velocity should be determined more accurately and taken into account for determination of pointwise temporal differences in accumulation rates. For the same reason the dating uncertainty needs to be improved. A closely spaced grid of GPR profiles would be useful for

deriving a three dimensional distribution of IRHs and thus accumulation features. Together with the airborne radio-echo sounding profile along the glacier-flow line (D. Steinhage, personal communication, 2005) such a data set would yield valuable information, including not only accumulation distribution but also insight in ice advection.

In the investigation area of Kottasberge glacier-flow velocity should be determined from satellite-based analyses like interferometric SAR technique, since the value used in this study relies only on GPS measurements of longitude and latitude of a reference point at the beginning and the end of the expedition (see Paper III). Generally, the vertical resolution even of the 500 MHz antenna in noisy environment is too low to resolve enough IRHs within the depth section covered by the firn cores, especially when depth and spacing of layers are strongly varying as on Potsdam Glacier. Therefore, either an antenna with a higher center frequency should be used (preferably 1 GHz) or deeper firn cores should be drilled, at least down to 30–40 m, but preferably about 100 m. Since a higher antenna frequency results in a shallower penetration depth and requires a smaller trace increment in order to obtain continuous reflections, the second option, i.e., deeper firn cores, would be favorable. Thus, more IRHs can be tracked and possibly dated, improving the analysis of spatial and temporal variability. In order to avoid ambiguities, only IRHs that are spaced more than the wavelength of the radar signal in firn or ice should be considered for accumulation calculations. For the validation of satellite data it is important to cover large areas on the surface of the Antarctic ice-sheet.

In summary, this study contributes accumulation data of high resolution in orographically complicated coastal regions of DML and provides valuable insight in the temporal and spatial pattern of recent accumulation rates, serving as validation of ice-mass changes obtained from satellite data.

Acknowledgements

I would like to express my thanks to Prof. Heinrich Miller for becoming my doctoral advisor. Prof. Heinrich Villinger (University Bremen) deserves thanks for taking over the additional report.

Special thanks is due to Olaf Eisen for valuable comments on this thesis and the publications, for explaining his scripts to me, and for general support. Thanks also to Daniel Steinhage for helpful comments and general support. Hans Oerter did the dating of the firm cores, as well as Urs Ruth. Andreas Frenzel and Frank Wilhelms helped to acquire data from DEP and GAP. Christine Wesche kindly offered help with the figure of DML and with ICESat data, and Wolfgang Rack supported the generation of a DEM of Potsdam Glacier. Max Voss patiently answered questions concerning GMT. Their help is gratefully acknowledged, as well as the help of all other people in the lab or in the field.

Prof. Reinhard Dietrich (TU Dresden) is thanked for the possibility to stay for two weeks at the Institut für Planetare Geodäsie at TU Dresden and process the GPS data of the season 2003/2004 there. Special thanks to Swen Roemer who introduced me to GPS processing and shared his scripts with me. Mirko Scheinert and Lutz Eberlein (TU Dresden) provided GPS data from 2004/2005 and information about glacier-flow velocity.

Mathias Hoffmann and Bettina Bayer deserve thanks for help with major and minor software problems, discussions, and coffee.

Everybody else who is not mentioned here explicitly and helped in one way or another during my work with this thesis is also gratefully thanked, especially my family and friends.

Bibliography

- Alley, R., P. Clark, P. Huybrechts, and I. Joughin, Ice-sheet and sea-level changes, *Science*, *310*, 456–460, 2005.
- Arthern, R., D. Winebrenner, and D. Vaughan, Antarctic snow accumulation mapped using polarization of 4.3-cm wavelength microwave emission, *J. Geophys. Res.*, *111*, D06107, 2006.
- Bamber, J., *Mass balance of the cryosphere*, Cambridge University Press, Cambridge, UK, 2004.
- Bentley, C., and J. Wahr, Satellite gravity and the mass balance of the Antarctic ice sheet, *J. Glaciol.*, *44*(147), 207–213, 1998.
- Bintanja, R., The contribution of snowdrift sublimation to the surface mass balance of Antarctica, *Ann. Glaciol.*, *27*, 251–259, 1998.
- Black, H., and W. Budd, Accumulation in the region of Wilkes, Wilkes Land, Antarctica, *J. Glaciol.*, *5*(37), 3–15, 1964.
- Bogorodsky, V., C. Bentley, and P. Gudmandsen., *Radioglaciology*, D. Reidel Publishing Company, Dordrecht, Holland, 1985.
- Capra, A., R. Cefalo, S. Gandolfi, G. Manzoni, I. Tabacco, and L. Vittuari, Surface topography of Dome Concordia (Antarctica) from kinematic interferential GPS and bedrock topography, *Ann. Glaciol.*, *30*, 42–46, 2000.
- Chen, J., C. Wilson, D. Blankenship, and B. Tapley, Antarctic mass rates from GRACE, *Geophys. Res. Lett.*, *33*, L11502, 2006.
- Church, J., and N. White, A 20th century acceleration in global sea-level rise, *Geophys. Res. Lett.*, *33*, L01602, 2006.
- Dahl-Jensen, D., N. Gundestrup, H. Miller, O. Watanabe, S. Johnsen, J. Steffensen, H. Clausen, A. Svensson, and L. Larsen, The NorthGRIP deep drilling programme, *Ann. Glaciol.*, *35*, 1–4, 2002.

- Davis, C., Y. Li, J. McConnell, M. Frey, and E. Hanna, Snowfall-driven growth in East Antarctic ice sheet mitigates recent sea-level rise, *Science*, 308, 1898–1901, 2005.
- Déry, S., and M. Yau, Large-scale mass balance effects of blowing snow and surface sublimation, *J. Geophys. Res.*, 107(D23), 4679, 2002.
- Dietrich, R., R. Metzig, W. Korth, J. Polzin, and M. Scheinert, Combined use of field observations and SAR interferometry to study ice dynamics and mass balance in Dronning Maud Land, Antarctica, *Polar Research*, 18, 291–298, 1999.
- Eisen, O., U. Nixdorf, F. Wilhelms, and H. Miller, Electromagnetic wave speed in polar ice: Validation of the CMP technique with high-resolution dielectric profiling and gamma-density measurements, *Ann. Glaciol.*, 34, 150–156, 2002.
- Eisen, O., U. Nixdorf, F. Wilhelms, and H. Miller, Age estimates of isochronous reflection horizons by combining ice core, survey, and synthetic radar data, *J. Geophys. Res.*, 109(B1), B04106, 2004.
- Eisen, O., F. Wilhelms, D. Steinhage, and J. Schwander, Improved method to determine radio-echo sounding reflector depths from ice-core profiles of permittivity and conductivity, *J. Glaciol.*, 52(177), 299–310, 2006.
- Eisen, O., W. Rack, U. Nixdorf, and F. Wilhelms, Characteristics of accumulation rate in the vicinity of the EPICA deep-drilling site in Dronning Maud Land, Antarctica, *Ann. Glaciol.*, 41, 41–46, 2005.
- EPICA community members, Eight glacial cycles from an Antarctic ice core, *Nature*, 429, 623–628, 2004.
- Fahnestock, M., T. Scambos, C. Shuman, R. Arthern, D. Winebrenner, and R. Kwok, Snow megadune fields on the East Antarctic plateau: Extreme atmosphere-ice interaction, *Geophys. Res. Lett.*, 27, 3719–3722, 2000.
- Frezzotti, M., S. Gandolfi, and S. Urbini, Snow megadunes in Antarctica: Sedimentary structure and genesis, *J. Geophys. Res.*, 107, 4344, 2002a.
- Frezzotti, M., S. Gandolfi, F. Marca, and S. Urbini, Snow dunes and glazed surfaces in Antarctica: New field and remote-sensing data, *Ann. Glaciol.*, 34, 81–88, 2002b.
- Frezzotti, M., M. Pourchet, O. Flora, S. Gandolfi, M. Gay, S. Urbini, C. Vincent, S. Becagli, R. Gragnan, M. Proposito, M. Severi, R. Traversi, R. Udisti, and M. Fily, Spatial and temporal variability of snow accumulation in East Antarctica from traverse data, *J. Glaciol.*, 51(172), 113–124, 2005.

- Fujita, S., H. Maeno, S. Uratsuka, T. Furukawa, S. Mae, Y. Fujii, and O. Watanabe, Nature of radio echo layering in the Antarctic ice sheet detected by a two-frequency experiment, *J. Geophys. Res.*, *104*(B6), 13,049–13,060, 1999.
- Fujita, S., T. Matsuoka, T. Ishida, K. Matsuoka, and S. Mae, A summary of the complex dielectric permittivity of ice in the megahertz range and its application for radar sounding of polar ice sheets, in *The Physics of Ice Core Records*, edited by T. Hondoh, pp. 185–212, Hokkaido University Press, Japan, 2000.
- Genthon, C., Space-time Antarctic surface mass-balance variability from climate models, *Ann. Glaciol.*, *39*, 271–275, 2004.
- Genthon, C., and G. Krinner, Antarctic surface mass balance and systematic biases in general circulation models, *J. Geophys. Res.*, *106*(D18), 20,653–20,664, 2001.
- Giovinetto, M., and C. Bentley, Surface balance in ice drainage systems of Antarctica, *Ant. J. U. S.*, *20*, 6–13, 1985.
- Giovinetto, M., and J. Zwally, Spatial distribution of net surface mass accumulation on the Antarctic ice sheet, *Ann. Glaciol.*, *31*, 171–178, 2000.
- Giovinetto, M., and J. Zwally, Accumulation in Antarctica and Greenland derived from passive-microwave data: a comparison with contoured compilations, *Ann. Glaciol.*, *21*, 123–130, 1995.
- Giovinetto, M., N. Waters, and C. Bentley, Dependence of Antarctic surface mass balance on temperature, elevation, and distance to open ocean, *J. Geophys. Res.*, *95*(D4), 3517–3531, 1990.
- Goodwin, I., Snow accumulation and surface topography in the katabatic zone of Eastern Wilkes Land, Antarctica, *Antarct. Sci.*, *2*, 235–242, 1990.
- Goosse, H., and T. Fichefet, Importance of ice-ocean interactions for the global ocean circulation: a model study, *J. Geophys. Res.*, *104*(C6), 23,337–23,355, 1999.
- Gudmandsen, P., Layer echoes in polar ice sheets, *J. Glaciol.*, *15*(73), 95–101, 1975.
- Hamilton, G., I. Whillans, and P. Morgan, First point measurements of ice-sheet thickness change in Antarctica, *Ann. Glaciol.*, *27*, 125–129, 1998.
- Hammer, C., Acidity of polar ice cores in relation to absolute dating, past volcanism, and radio-echoes, *J. Glaciol.*, *25*(93), 359–372, 1980.

- Hofmann-Wellenhof, H. Lichtenegger, and J. Collins, *GPS – Theory and Practice*, Springer Verlag, Wien, Austria, 2001.
- Hofstede, C., R. van de Wal, K. Kaspers, M. van den Broeke, L. Karlöf, J. Winther, E. Isaksson, G. Lappégard, R. Mulvaney, H. Oerter, and F. Wilhelms, Firm accumulation records for the past 1000 years on the basis of dielectric profiling of six cores from Dronning Maud Land, Antarctica, *J. Glaciol.*, 50(169), 279–291, 2004.
- Horwath, M., and R. Dietrich, Errors of regional mass variations inferred from GRACE monthly solutions, *Geophys. Res. Lett.*, 33, L07502, 2006.
- Huybrechts, P., and E. Le Meur, Predicted present-day evolution patterns of ice thickness and bedrock elevation over Greenland and Antarctica, *Antarct. Sci.*, 18, 299–306, 1999.
- Isaksson, E., and W. Karlén, Spatial and temporal patterns in snow accumulation, western Dronning Maud Land, Antarctica, *J. Glaciol.*, 40(135), 399–409, 1994.
- Isaksson, E., M. van den Broeke, J. Winther, L. Karlöf, J. Pinglot, and N. Gundestrup, Accumulation and proxy-temperature variability in Dronning Maud Land, Antarctica, determined from shallow firn cores, *Ann. Glaciol.*, 29, 17–22, 1999.
- Jackson, J., *Classical electrodynamics*, Wiley, New York, USA, 1975.
- Jonsson, S., Synoptic forcing of wind and temperature in a large cirque 300 km from the coast of East Antarctica, *Antarct. Sci.*, 7(4), 409–420, 1995.
- Joughin, I., and S. Tulaczyk, Positive Mass Balance of the Ross Ice Streams, West Antarctica, *Science*, 295, 2002.
- Kaczmarska, M., E. Isaksson, L. Karlöf, J. Winther, J. Kohler, F. Godtlielsen, L. Ringstad Olsen, C. Hofstede, M. van den Broeke, R. van de Wal, and N. Gundestrup, Accumulation variability from an ice core from coastal Dronning Maud Land, Antarctica, *Ann. Glaciol.*, 39, 339–345, 2004.
- Kanagaratnam, P., S. Gogineni, N. Gundestrup, and L. Larsen, High-resolution radar mapping of internal layers at the North Greenland Ice Core Project, *J. Geophys. Res.*, 106(D24), 33,799–33,812, 2001.
- Karlöf, L., E. Isaksson, J. Winther, N. Gundestrup, H. Meijer, R. Mulvaney, M. Pourchet, C. Hofstede, G. Lappégard, R. Pettersson, M. van den Broeke, and R. van de Wal, Accumulation variability over a small area in east Dronning Maud Land, Antarctica, as determined from shallow firn cores and snow pits: some implications for ice-core records, *J. Glaciol.*, 51(174), 343–352, 2005.

- King, J., The surface energy and mass balance at Halley, Antarctica, during winter, *J. Geophys. Res.*, *101*(D14), 19,119–19,128, 1996.
- King, J., P. Anderson, D. Vaughan, G. Mann, S. Mobbs, and S. Vosper, Wind-borne redistribution of snow across an Antarctic ice rise, *J. Geophys. Res.*, *109*, D11104, 2004.
- King, M., P. Moore, P. Clarke, and D. Lavallée, Choice of optimal averaging radii for temporal GRACE gravity solutions, a comparison with GPS and satellite altimetry, *Geophys. J. Int.*, *166*, 1–11, 2006.
- Korth, W., and R. Dietrich, *Ergebnisse geodätischer Arbeiten im Gebiet der Schirmacherose/Antarctica 1988-1993*, vol. 301 of *Angewandte Geodäsie (Reihe B)*, Deutsche Geodätische Kommission, Verlag der Bayerischen Akademie der Wissenschaften, München, Germany, 1996.
- Kovacs, A., A. Gow, and R. Morey, The in-situ dielectric constant of polar firn revisited, *Cold Regions Science and Technology*, *23*, 245–256, 1985.
- Lythe, M., D. Vaughan, and the BEDMAP Consortium, A new thickness and subglacial topographic model of Antarctica, *J. Geophys. Res.*, *106*(B6), 11,335–11,352, 2001.
- Matsuoka, K., T. Furukawa, S. Fujita, H. Maeno, S. Uratsuka, R. Naruse, and O. Watanabe, Crystal orientation fabrics within the Antarctic ice sheet revealed by a multipolarization plane and dual-frequency radar survey, *J. Geophys. Res.*, *108*(B10), 2499, 2003.
- McMorrow, A., T. van Ommen, V. Morgan, and M. Curran, Ultra-high-resolution seasonality of trace-ion species and oxygen isotope ratios in Antarctic firn over four annual cycles, *Ann. Glaciol.*, *39*, 34–40, 2004.
- Melvold, K., J. Hagen, J. Pinglot, and N. Gundestrup, Large spatial variations in accumulation rate in Jutulstraumen ice stream, Dronning Maud Land, Antarctica, *Ann. Glaciol.*, *27*, 231–238, 1998.
- Meyer, U., D. Steinhage, U. Nixdorf, and H. Miller, Airborne radio echo sounding in central Dronning Maud Land, *Geol. Jb.*, *B97*, 129–140, 2005.
- Miners, W., E. Wolff, J. Moore, R. Jacobel, and L. Hempel, Modeling the radio echo reflections inside the ice sheet at Summit, Greenland, *J. Geophys. Res.*, *107*(B8), 2172, 2002.
- Monaghan, A., D. Bromwich, R. Fogt, S. Wang, P. Mayewski, D. Dixon, A. Ekaykin, M. Frezzotti, I. Goodwin, E. Isaksson, S. Kaspari, V. Morgan, H. Oerter, T. van Ommen, C. van der Veen, and J. Wen, Insignificant Change in Antarctic Snowfall Since the International Geophysical Year, *Science*, *313*, 827–831, 2006a.

- Monaghan, A., D. Bromwich, and S. Wang, Recent trends in Antarctic snow accumulation from Polar MM5 simulations, *Phil. Trans. R. Soc. A*, 363, 1683–1708, 2006b.
- Näslund, J., Ice sheet, climate, and landscape interactions in Dronning Maud Land, Antarctica, Ph. D. thesis, Stockholm University, Sweden, 1998.
- Nishio, F., and H. Ohmae, Internal radio-echo reflections of polar snow covers in relation to acidic layers and density fluctuations, *Ann. Glaciol.*, 6, 289–291, 1985.
- Noone, D., J. Turner, and R. Mulvaney, Atmospheric signals and characteristics of accumulation in Dronning Maud Land, Antarctica, *J. Geophys. Res.*, 104(D16), 19,191–19,212, 1999.
- Oerter, H., W. Graf, F. Wilhelms, A. Minikin, and H. Miller, Accumulation studies on Amundsenisen, Dronning Maud Land, Antarctica, by means of dielectric profiling and stable-isotope measurements: first results from the 1995-96 and 1996-97 field seasons, *Ann. Glaciol.*, 29, 1–9, 1999.
- Oerter, H., F. Wilhelms, F. Jung-Rothenhäusler, F. Göktas, H. Miller, and W. Graf, Accumulation rates in Dronning Maud Land, Antarctica, as revealed by dielectric-profiling measurements of shallow firn cores, *Ann. Glaciol.*, 30, 27–34, 2000.
- Parish, T., and D. Bromwich, Continental-scale simulation of the Antarctic katabatic wind regime, *J. Climate*, 4, 135–146, 1991.
- Paterson, W., *The physics of glaciers*, Pergamon Press, Oxford, UK, 1994.
- Piciotto, E., G. Grozaz, and W. de Breuck, Accumulation on the South Pole Queen Maud Land Traverse, 1964-1968. Antarctic Snow and Ice Studies II, *Antarc. Res. Ser.*, 16, 257–315, 1971.
- Ramillien, G., A. Lombard, A. Cazenave, E. Ivins, M. Llues, F. Remy, and R. Biancale, Interannual variations of the mass balance of the Antarctica and Greenland ice sheets from GRACE, *Global and Planetary Change*, 53, 198–208, 2006.
- Richardson, C., E. Aarholt, S. Hamran, P. Holmlund, and E. Isaksson, Spatial distribution of snow in western Dronning Maud Land, East Antarctica, mapped by a ground-based snow radar, *J. Geophys. Res.*, 102(B9), 20,343–20,353, 1997.
- Richardson-Näslund, C., Spatial distribution of snow in Antarctica and other glacier studies using ground-penetrating radar, Ph. D. thesis, Stockholm University, Sweden, 2001.
- Richardson-Näslund, C., Spatial characteristics of snow accumulation in western Dronning Maud Land, Antarctica, *Global and Planetary Change*, 42, 31–43, 2004.

- Rignot, E., and R. Thomas, Mass balance of polar ice sheets, *Science*, 297, 1502–1506, 2002.
- Rotschky, G., O. Eisen, U. Nixdorf, and H. Oerter, Spatial distribution of surface mass balance on Amundsenisen plateau, Antarctica, derived from ice-penetrating radar studies, *Ann. Glaciol.*, 39, 265–270, 2004.
- Rotschky, G., P. Holmlund, E. Isaksson, R. Mulvaney, H. Oerter, M. van den Broeke, and J. Winther, A new surface accumulation map for western Dronning Maud Land, Antarctica, from interpolation of point measurements, *submitted to J. Glaciol.*, 2006.
- Scheinert, M., L. Eberlein, W. Rack, H. Anschütz, B. Bayer, M. Horwath, J. Müller, S. Roemer, S. Riedel, D. Steinhage, R. Dietrich, W. Jokat, and H. Miller, Validation and interpretation of satellite data in Dronning Maud Land, East Antarctica, with the help of geodetic, geophysical and glaciological methods - observation campaigns 2003-2005 and first results, Poster presentation at the 22nd International Polar Meeting. Jena, Germany, September 18-24, 2005.
- Schlosser, E., H. Oerter, and W. Graf, *Snow accumulation on Ekströmsisen, Antarctica*, vol. 313 of *Berichte zur Polarforschung*, Alfred-Wegener-Institut, Bremerhaven, Germany, 1999.
- Spikes, V., G. Hamilton, S. Arcone, S. Kaspari, and P. Mayewski, Variability in accumulation rates from GPR profiling on the West Antarctic plateau, *Ann. Glaciol.*, 39, 238–244, 2004.
- Steinhage, D., U. Nixdorf, U. Meyer, and H. Miller, New maps of the ice thickness and subglacial topography in Dronning Maud Land, Antarctica, determined by means of airborne radio echo sounding, *Ann. Glaciol.*, 29, 267–272, 1999.
- Steinhage, D., U. Nixdorf, U. Meyer, and H. Miller, Subglacial topography and internal structure of central and western Dronning Maud Land, Antarctica, determined from airborne radio echo sounding, *J. Applied Geophys.*, 47, 183–189, 2001.
- Swenson, S., and J. Wahr, Methods for inferring regional surface-mass anomalies from Gravity Recovery and Climate Experiment (GRACE) measurements of time-variable gravity, *J. Geophys. Res.*, 107(B9), 2193, 2002.
- Tapley, B., S. Bettadpur, M. Watkins, and C. Reigber, The gravity recovery and climate experiment: Mission overview and early results, *Geophys. Res. Lett.*, 31, L09607, 2004a.
- Tapley, B., S. Bettadpur, J. Ries, P. Thompson, and M. Watkins, GRACE Measurements of Mass Variability in the Earth System, *Science*, 305, 503–505, 2004b.

- Thomas, R., E. Rignot, G. Casassa, P. Kanagaratnam, C. Acuna, T. Akins, H. Brecher, E. Frederick, P. Gogineni, W. Krabill, S. Manizade, H. Ramamoorthy, A. Rivera, R. Russell, J. Sonntag, R. Swift, J. Yungel, and J. Zwally, Accelerated sea-level rise from West Antarctica, *Science*, 306, 255–258, 2004.
- Torinesi, O., M. Fily, and C. Genthon, Variability and trends of the summer melt period of Antarctic ice margins since 1980 from microwave sensors, *J. Climate*, 16, 1047–1060, 2003.
- Tregoning, P., B. Twilley, M. Hendy, and D. Zwartz, Monitoring isostatic rebound in Antarctica with the use of continuous remote GPS observations, *GPS Solutions*, 2(3), 70–75, 1999.
- Ulaby, F., R. Moore, and A. Fung, *Microwave remote sensing*, vol. 1-3, ARTECH House, Norwood, USA, 1982.
- Urbini, S., L. Vittuari, and S. Gandolfi, GPR and GPS data integration: examples of application in Antarctica, *Annali di Geofisica*, 44(4), 687–702, 2001.
- van de Berg, W., M. van den Broeke, C. Reijmer, and E. van Meijgaard, Characteristics of the Antarctic surface mass balance, 1958–2002, using a regional atmospheric climate model, *Ann. Glaciol.*, 41, 97–104, 2005.
- van de Berg, W., M. van den Broeke, C. Reijmer, and E. van Meijgaard, Reassessment of the Antarctic surface mass balance using calibrated output of a regional atmospheric climate model, *J. Geophys. Res.*, 111, D11104, 2006.
- van den Broeke, M., and N. van Lipzig, Factors controlling the near-surface wind field in Antarctica, *Mon. Weather Rev.*, 131, 733–743, 2003.
- van den Broeke, M., and N. van Lipzig, Changes in Antarctic temperature, wind and precipitation in response to the Antarctic Oscillation, *Ann. Glaciol.*, 39, 119–126, 2004.
- van den Broeke, M., W. van de Berg, and E. van Meijgaard, Snowfall in coastal West Antarctica much greater than previously assumed, *Geophys. Res. Lett.*, 33, L02505, 2006.
- van der Veen, C., Polar ice sheet and global sea level: how well can we predict the future?, *Global and Planetary Change*, 32, 165–194, 2002.
- Vaughan, D., How does the Antarctic ice sheet affect sea level rise?, *Science*, 308, 1877–1878, 2005.
- Vaughan, D., J. Bamber, M. Giovinetto, J. Russell, and A. Cooper, Reassessment of net surface mass balance in Antarctica, *J. Climate*, 45, 933–946, 1999.

- Vaughan, D., P. Anderson, J. King, G. Mann, S. Mobbs, and R. Ladkin, Imaging of firn isochrones across an Antarctic ice rise and implications for patterns of snow accumulation rate, *J. Glaciol.*, 50(170), 413–418, 2004.
- Velicogna, I., and J. Wahr, A method for separating Antarctic postglacial rebound and ice mass balance using future ICESat Geoscience Laser Altimeter System, Gravity Recovery and Climate Experiment, and GPS satellite data, *J. Geophys. Res.*, 107(B10), 2263, 2002.
- Velicogna, I., and J. Wahr, Measurements of time-variable gravity show mass loss in Antarctica, *Science*, 311, 1754–1756, 2006.
- Wahr, J., D. Wingham, and C. Bentley, A method of combining ICESat and GRACE satellite data to constrain Antarctic mass balance, *J. Geophys. Res.*, 105, 16,279–16,294, 2000.
- Welch, B., and R. Jacobel, Bedrock topography and wind erosion sites in East Antarctica: observations from the 2002 US-ITASE traverse, *Ann. Glaciol.*, 41, 92–96, 2005.
- Wilhelms, F., *Leitfähigkeits- und Dichtemessung an Eisbohrkernen / Measuring the Conductivity and Density of Ice Cores (in German)*, vol. 191 of *Berichte zur Polarforschung*, Alfred-Wegener-Institut, Bremerhaven, Germany, 1996.
- Wilhelms, F., J. Kipfstuhl, H. Miller, J. Firestone, and K. Heinloth, Precise dielectric profiling of ice cores: a new device with improved guarding and theory, *J. Glaciol.*, 44(146), 171–174, 1998.
- Wilhelms, F., Explaining the dielectric properties of firn as a density-and-conductivity mixed permittivity (decomp), *Geophys. Res. Lett.*, 32, L16501, 2005.
- Wingham, D., A. Ridout, R. Scharroo, R. Arthern, and C. Shum, Antarctic elevation change from 1992 to 1996, *Science*, 282, 456–458, 1998.
- Wingham, D., C. Francis, S. Baker, C. Bouzinac, D. Brockley, R. Cullen, P. de Chateau-Thierry, S. Laxon, U. Mallow, C. Mavrocordatos, L. Phalippou, G. Ratier, L. Rey, F. Rostan, P. Viau, and D. Wallis, CryoSat: A mission to determine the fluctuations in Earth's land and marine ice fields, *Advances in Space Research*, 37, 841–871, 2006.
- Zwally, J., B. Schutz, W. Abdalati, J. Abshire, C. Bentley, A. Brenner, J. Bufton, J. Dezio, D. Hancock, D. Harding, T. Herring, B. Minster, K. Quinn, S. Palm, J. Spinhirne, and R. Thomas, ICESat's laser measurements of polar ice, atmosphere, ocean, and land, *Journal of Geodynamics*, 34, 405–445, 2002.
- Zwally, J., and S. Fiegles, Extent and duration of Antarctic surface melt, *J. Glaciol.*, 40(136), 463–476, 1994.

Zwally, J., and J. Li, Seasonal and interannual variations of firn densification and ice-sheet surface elevation at the Greenland summit, *J. Glaciol.*, 48(161), 199–207, 2002.

Zwally, J., M. Giovinetto, J. Li., H. Cornejo, M. Beckley, A. Brenner, J. Saba, and D. Yi, Mass changes of the Greenland and Antarctic ice sheets and shelves and contribution to sea-level rise: 1992-2002, *J. Glaciol.*, 51(175), 509–527, 2005.